SURFACE FUNCTIONALIZATION OF MAGNETITE NANOPARTICLES WITH NATURAL AND MULTIPOTENT ANTIOXIDANTS AS POTENTIAL NANOANTIOXIDANTS AND ANTIMICROBIAL AGENTS

SYED TAWAB SHAH

INSTITUTE FOR ADVANCED STUDIES
UNIVERSITY OF MALAYA
KUALA LUMPUR

2022

SURFACE FUNCTIONALIZATION OF MAGNETITE NANOPARTICLES WITH NATURAL AND MULTIPOTENT ANTIOXIDANTS AS POTENTIAL NANOANTIOXIDANTS AND ANTIMICROBIAL AGENTS

SYED TAWAB SHAH

THESIS SUBMITTED IN FULFILLMENT OF THE REQUIREMENTS FOR THE DEGREE OF DOCTOR OF PHILOSOPHY

INSTITUTE FOR ADVANCED STUDIES
UNIVERSITY OF MALAYA
KUALA LUMPUR

2022

UNIVERSITY OF MALAYA

ORIGINAL LITERARY WORK DECLARATION

Name of Candidate: **Syed Tawab Shah**

Matric No: **17019871/1**

Name of Degree: **Doctor of Philosophy (PhD)**

Thesis ("this Work"): **Surface Functionalization of Magnetite nanoparticles with Natural and Multipotent Antioxidants as Potential Nanoantioxidants and Antimicrobial Agents**

Field of Study: **Science (Chemistry)**

I do solemnly and sincerely declare that:

(1) I am the sole author/writer of this Work;
(2) This Work is original;
(3) Any use of any work in which copyright exists was done by way of fair dealing and for permitted purposes and any excerpt or extract from, or reference to or reproduction of any copyright work has been disclosed expressly and sufficiently and the title of the Work and its authorship have been acknowledged in this Work;
(4) I do not have any actual knowledge nor do I ought reasonably to know that the making of this work constitutes an infringement of any copyright work;
(5) I hereby assign all and every rights in the copyright to this Work to the University of Malaya ("UM"), who henceforth shall be owner of the copyright in this Work and that any reproduction or use in any form or by any means whatsoever is prohibited without the written consent of UM having been first had and obtained;
(6) I am fully aware that if in the course of making this Work I have infringed any copyright whether intentionally or otherwise, I may be subject to legal action or any other action as may be determined by UM.

Candidate's Signature Date:

Subscribed and solemnly declared before,

Witness's Signature Date:

Name:

Designation:

Surface Functionalization of Magnetite Nanoparticles with Natural and Multipotent Antioxidants as Potential Nanoantioxidants and Antimicrobial Agents

ABSTRACT

Nanoparticles of Fe_3O_4 with enhanced hydrophilic/lipophilic properties were synthesized using a co-precipitation approach of Fe^{2+} and Fe^{3+} ions in a basified aqueous solution followed by a surface functionalization. Two surfacing strategies (in-situ and post-synthesis methods) were used to coat nanoparticles with natural antioxidants and synthetic multipotent antioxidants (MPAO). MPAO were synthesized and characterized by NMR. The functionalized nanoparticles (IONP@AOx) were characterized by FTIR, XRD, Raman, HRTEM, FESEM, VSM and EDX. IONP@A have average particles size 6-8 nm for in-situ synthesis, which are ultra-small particles as compared to unfunctionalized magnetite (IONP) and post functionalized magnetite with average size of 10 and 11 nm respectively. The nanoparticles also showed high saturation magnetization of about 45−59 emu/g. Prior to commencement of experimental lab work, Prediction Activity Spectra of Substances (PASS) software was used to predict the biological activities of antioxidants and it is found that experimental antioxidant activity using 2,2-diphenyl-1-picrylhydrazyl (DPPH) assay are in good agreement with the simulated results. Furthermore, the half maximal inhibitory concentration (IC50) values of DPPH antioxidant assay revealed a 2–4 fold decrease as compared to unfunctionalized IONP. The functionalization has enhanced the free radical scavenging properties of IONPs up two to four times. In addition to antioxidant activity, functionalized IONP proved outstanding antimicrobial activity while testing on different bacterial and fungal strains. The advantage of the developed nanoantioxidants is that (because of their high hydrophilicity/lipophilicity) they could interact with biological species such as enzymes, proteins, amino acids and DNA. The results reveal that the synthesized nanoparticles can be successfully used for the development of biomedicines which can be subsequently applied as antioxidant, anti-inflammatory, antibacterial and anticancer agent.

Key Words: Magnetite, Multipotent Antioxidants, DPPH, Functionalization, Antimicrobial activity

Sintesis Nanopartikel Magnetite yang Difungsionalisasikan yang Berpotensi sebagai Ejen Antioksidan dan Antimikrobial

ABSTRAK

Nanopartikel Fe_3O_4 dipertingkatkan telah disintesis menggunakan pendekatan pemendakan bersama ion Fe^{2+} dan Fe^{3+} dalam larutan asas diikuti dengan fungsionalisasi permukaan. Dua strategi fungsionalisasi permukaan (kaedah in-situ dan pasca-sintesis) telah digunakan untuk melapisi nanopartikel dengan antioksidan semula jadi dan antioksidan multipoten sintetik (MPAO). MPAO disintesis dan dicirikan oleh FTIR, NMR dan spektrometri jisim resolusi tinggi. Nanopartikel yang berfungsi (IONP @ A) dicirikan oleh FTIR, XRD, Raman, HRTEM, FESEM, VSM dan EDX. IONP @ A mempunyai saiz partikel purata dengan ukuran 6-8 nm untuk sintesis in-situ, yang merupakan partikel ultra kecil dibandingkan dengan magnetite tidak difungsionalisasikan (IONP) dan magnetite pasca fungsionalisasi dengan ukuran purata 10 dan 11 nm masing-masing. Nanopartikel juga menunjukkan ketepuan kemagnetan yang tinggi sekitar 45−59 emu / g. Sebelum memulakan kerja makmal eksperimen, satu perisian bernama Prediction Activity Spectra of Substances (PASS) digunakan untuk meramalkan aktiviti biologi bagi antioksidan dan didapati bahawa aktiviti antioksidan eksperimental menggunakan 2,2-diphenyl-1-picrylhydrazyl (DPPH) menunjukkan persetujuan yang baik dengan hasil simulasi. Tambahan pula, nilai konsentrasi penghambatan setengah maksimum (IC50) untuk antioksidan DPPH menunjukkan penurunan 2-4 kali ganda dibandingkan dengan IONP yang tidak difungsionalisasikan. Fungsionalisasi tersebut telah meningkatkan sifat 'memerangkap' radikal bebas IONP hingga empat kali. Sebagai tambahan kepada aktiviti antioksidan, kedua IONP@A membuktikan aktiviti antimikroba yang luar biasa semasa menguji pelbagai jenis bakteria dan kulat. Kelebihan nanoantioksidan yang dibangunkan dalam penyelidikan ini ialah sifat hidrofilik / lipofilik yang tinggi yang menyebabkan ianya dapat berinteraksi dengan pelbagai spesies biologi

seperti enzim, protein, asid amino dan DNA. Hasil kajian menunjukkan bahawa nanopartikel yang disintesis dapat digunakan dengan baik untuk pengembangan ubat biomedik yang boleh juga digunakan sebagai antioksidan, anti-inflamasi, antibakteria dan agen antikanker.

Kata Kunci: Antioksidan Multipoten sintetik, DPPH, Fungsionalisasi, Antimikroba

ACKNOWLEDGEMENTS

All glory to Allah, The omnipotent, who empowers us in our great exploits, the impassionate that created man and gave him the knowledge of what he was ignorant of.

I have put in my best efforts to complete this dissertation; however, human efforts are always bound to be erroneous. If there is anything extraordinary, the credit goes to my teachers and supervisors. Any deficiency and flaws have solely been attributed to the lapses on my part.

In work of my enterprising task, I have all along been guided and coached by my reverend supervisors, Dr Zaira Zaman Chowdhury and Dr. Wageeh A. Yehya and Late Prof. Sharifah, who have gone beyond mere supervision by providing me with intellectual discussions, constant encouragement, excellent learning environment and their friendliness behavior. The compassionate help and guidance of my uncle Dr. Amir Ayub, Principal Geoscientist, PETRONAS, enabled me to tread up to the apex of my work. He always guided and encouraged me like a godfather.

I would also thank all my group mates, Dr. Ibrahim Khalil, Dr. Amit Ranjin, Dr. Hafiz, Sybella Sazeli, and Cheryl, for their help, providing a friendly lab environment, and for rescuing me whenever I needed help. I would also like to pay my humble gratitude to UM fellows Dr. Shahid Mehmood and Dr. Numan Arshid for their fantastic discussions and enjoying quality fun time with them during my stay at UM. I am also immensely indebted and very grateful for the support of my family members, to whom I dedicated this thesis.

TABLE OF CONTENTS

LIST OF FIGURES

LIST OF TABLES

LIST OF SYMBOLS AND ABBREVIATIONS

AAPH	2,2-azobis(2-amidinopropane) dihydrochloride
ABTS	2,2′-Azino-bis(3-ethylbenzthiazoline-6-sulfonic acid)
ADME	Adsorption Distribution Metabolism and Excretion
ADMET	Adsorption Distribution Metabolism, Excretion and Toxicity
APTES	Aminopropyl-Triethoxysilane
BHA	butylated hydroxyanisole
BHT	butylated hydroxytoluene
CDC	The Centers for Disease Control and Prevention
CNP	Cerium nanoparticles
CNT	Carbon Nanotubes
CONP	Cerium oxide nanoparticles
DI	Deionized water
DNA	deoxyribonucleic acid
DPPH	2,2-diphenyl-1-picrylhydrazyl
EDX	Energy Dispersive X-Ray Analysis
EG	Ethylene Glycol
EPR	Electron paramagnetic resonance
FESEM	Field Emission Scanning Electron Microscope
FTIR	Fourier-Transform Infrared Spectroscopy
GPX	Glutathione Peroxidase
GSH	Glutathione
HAT	Hydrogen atom transfer
HRTEM	High Resolution Transmission Electron Microscopy
IC50	50% inhibition

IONP	Iron oxide nanoparticles
MDEG	Diethylene glycol monoethyl ether
MIC	Minimum Inhibition Concentration
MLP	Molecular Lipophilicity Potential
MPAO	Multipotent Antioxidants
MRI	Magnetic resonance imaging
MSN	SiO_2NPs
NMR	Nuclear magnetic resonance
NP	Nanoparticles
PAPM	Polyaspartic acid-based polymer micelles
PASS	Prediction Activity Spectra of Substances
PDA	Potato Dextrose agar
PEG	Polyethylene Glycol
PIDG	percentage inhibition of diameter growth
PTSA	p-Toluenesulfonic acid
RNS	Reactive Nitrogen Species
RT	Room Temperature
SOD	superoxide dismutase
TEM	Transmission electron microscopy
UV	Ultra Violet
VSM	Vibrating Sample Magnetometer
XRD	X-ray Crystallographic Data

LIST OF APPENDICES

CHAPTER 1: INTRODUCTION

1.1 Background of the Study

Age-related disorders have emerged as a major public health concern around the world in the twenty-first century. For modern society, population aging is becoming an increasingly significant social and economic burden. As people live longer, their healthspan does not necessarily rise at the same rate. Over the last few decades, the burden of age-related illnesses has grown progressively in most developed countries (Seals, Justice, & LaRocca, 2016; Yabluchanskiy, Ungvari, Csiszar, & Tarantini, 2018). The process of aging is one that occurs throughout time that results due to the degeneration of vital organ structures and functions. It increases the chance of developing a wide array of chronic diseases and contributes to the high death rate (C. H. Chang, Lee, & Shim, 2017; Dabhade & Kotwal, 2013). The free radical theory is unmatched among the several ideas that explain and uncover the aging process (Harman, 1956). According to this view, Reactive oxygen species (ROS) damage to cells and tissues is exacerbated with age because the body's defense mechanisms repeatedly fail to heal it (Islam, 2017).

Degenerative aging is well understood to be a result of oxidative stress, which plays an important part in the process. A variety of biological processes have their pathophysiology altered by the presence of reactive oxygen species (ROS), and they have also been linked to a variety of diseases like heart disease, cancer, neurological illness, and pulmonary disease, as shown in Figure 1.1 (Valentao et al., 2002). The accumulation of reactive oxygen species (ROS) in cells has also been linked to the progression of aging; nevertheless, this cannot be regarded as the sole component responsible for the progression of aging. Furthermore, increased levels of ROS are associated with mitochondrial dysfunction and cellular oxidative damage in age-related disorders (K.-H. Chang & Chen, 2020; López-Otín, Blasco, Partridge, Serrano, & Kroemer, 2013).

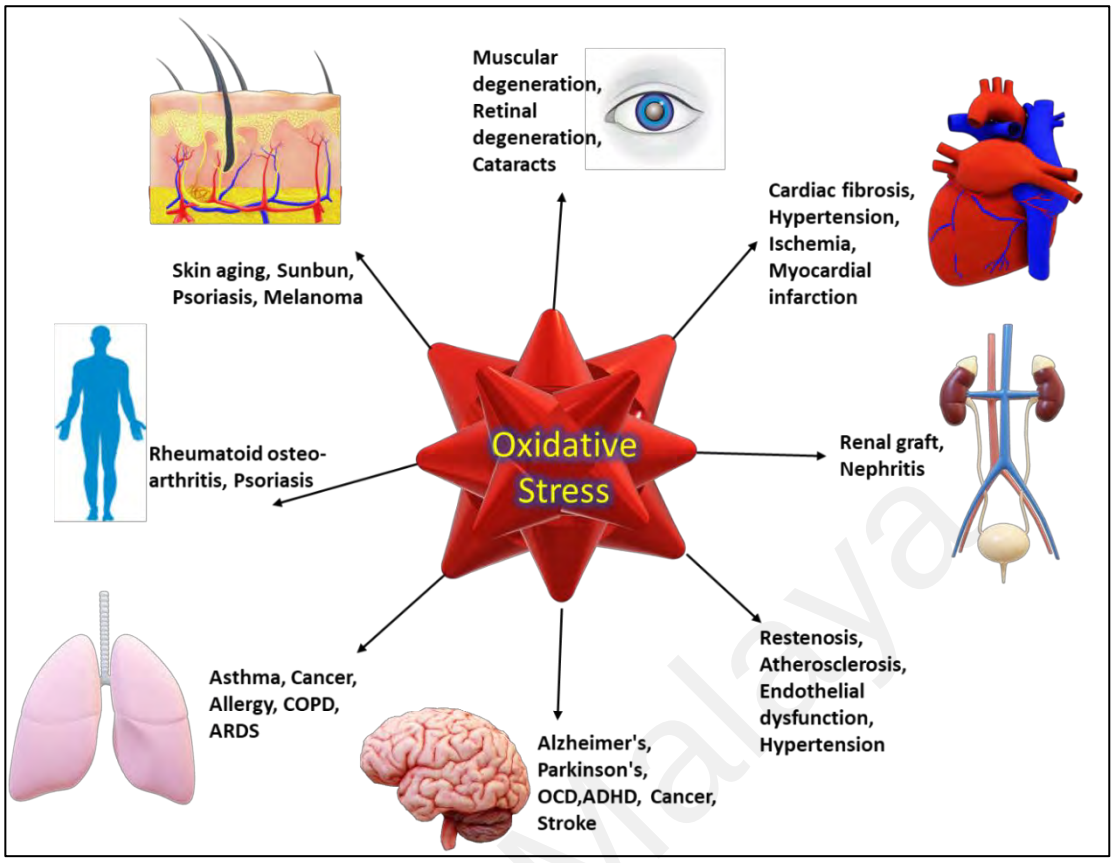

Figure 1.1 Oxidative Stress Adverse Impacts on Human Health

Organic materials, such as biological components like proteins and lipids, also include dietary supplements and cosmetics, oxidize owing to a radical-chain mechanism in which atmospheric O_2 converts alkyl radicals into peroxyl radicals (ROO•) that perpetuate the oxidative chain. This process is referred to as autoxidation or peroxidation because hydroperoxides (alkyl hydroperoxides and H_2O_2) are the primary first-formed products (Ingold & Pratt, 2014). Due to their unstable nature, hydroperoxides are capable of generating highly reactive hydroxyl (HO•) and alkoxyl (RO•) radicals, two types of radicals that can damage even generally stable molecules like DNA bases (Cadet & Wagner, 2014). The production of reactive carbonyl species (such as 4-hydroxynonenal) due to alkyl hydro-peroxide cleavage exacerbates the oxidative damage (Zhang & Forman, 2017). When a cell's ability to produce reactive oxygen species (ROS) exceeds its ability to mount an efficient antioxidant response, it experiences oxidative stress,

which leads to cell death and mutation. Oxidative stress causes irreversible damage to proteins, lipids, and DNA, as well as mutation and cell death (Morry, Ngamcherdtrakul, & Yantasee, 2017).

Research into bioactive antioxidants that lower oxidative stress and promote immunity is ongoing (Ricordi, Garcia-Contreras, & Farnetti, 2015). To promote healthy ageing and prevent oxidative stress, researchers are always searching for new antioxidant molecules.

Further study is being done to better understand antioxidants' involvement in the redox biological pathway, and to strengthen their ability to protect cells from reactive oxygen species (ROS). The phrase oxidative stress refers to an imbalance between the production of ROS and the body's response to these ROS. Internally generated ROS damage proteins, DNA, and lipids permanently to cause genetic mutations and ultimately lead to cell death (Nita & Grzybowski, 2016). Parkinson's disease, malignancies, Alzheimer's disease, and diabetes are all linked to the overproduction of reactive oxygen species (Liguori et al., 2018; Masoudkabir et al., 2017). Redox balance between pro- and antioxidants is critical in the treatment and prevention of many diseases. The use of antioxidants is generally restricted by their sensitivity to light, oxygen, and pH, as well as their poor solubility in physiological fluid, low bioavailability, and ineffective transport to undesirable cellular compartments, even if their potential is tremendous (Milinčić et al., 2019; Souto, Severino, Basso, & Santana, 2013; Valgimigli, Baschieri, & Amorati, 2018). To promote healthy aging and prevent oxidative stress, researchers are always searching for new antioxidant species.

Nanoparticles can act as smart nanocarriers and have various applications such drug delivery. Combinatorial effects of material science with nanotechnology and engineering lead to important developments that decrease free radicals' production (Eftekhari, Ahmadian, Panahi-Azar, et al., 2018). 'Nanoantioxidants' are smart nanocarriers with

antioxidant capabilities that have been developed in recent years through nanotechnology application (Khalil et al., 2020). Using nanoantioxidant systems could overcome many of the limitations of standard antioxidant molecules and increase their efficiency, thanks to their prolonged stability, improved bioavailability, the capacity to evade quick metabolic clearance, and the potential to give a regulated and targeted delivery (Deligiannakis, Sotiriou, & Pratsinis, 2012).

Smart nanocarriers surface can be functionalized with antioxidant molecules to transform nanoparticles into nanoantioxidants. In recent years, surface functionalization of nanoparticles with antioxidants has been used, improving their biostability, biocompatibility, and ability to boost the immune system (Marrazzo & O'Leary, 2020). Specifically, the simultaneous loading and functionalization of nanocarriers with antioxidants provide the advantage of delivering high antioxidant amounts and the possibility for the co-delivery of other drugs and, thus, for the use of these devices to exploit any synergic effects (Marina Massaro et al., 2016). Surface functionalization of nanoparticles with natural antioxidants also imparts specific biological activity, which mainly depends upon the material used for functionalization, such as anticancer, antimicrobial, anti-Alzheimer's and antidiabetic.

Among the most commonly used synthetic antioxidants is butylated hydroxytoluene (BHT), with many reports confirming the potent antioxidant activity in various industrial applications such as food, oil, and cosmetics industries (Ariffin, Rahman, Yehye, Alhadi, & Kadir, 2014). In addition, this synthetic phenolic antioxidant has also been applied in therapeutic fields; however, certain features of volatility and high-temperature instability, as well as toxicities and safety concerns, have greatly limited the effective therapeutic application (Elmadfa & Meyer, 2008).

The global natural antioxidants market is anticipated to grow on account of its increasing demand in food & beverages and other industries as shown in Figure 1.2.

Figure 1.2 Antioxidants Market: Product Segment Analysis

1.2 Problem Statement and Research Scope:

Despite the large number of antioxidants currently recognized, specific applications, such as food technology, cosmetics and pharmaceutical technology, or biological applications, still face significant hurdles. Traditional small-molecule antioxidants have a number of drawbacks, including possible toxicity, leaching or migration into undesirable compartments, vulnerability to ambient oxygen or oxidase enzymes, and a loss of efficacy with time. Grafting small-molecule antioxidants onto nanomaterials has recently been proposed as a novel method of improving their properties. Pure nanomaterials should be free of toxicity, have a low cost, and be easy to functionalize.

1.3 Objectives:

After conducting a thorough literature review, the following goals have been set for the current project:

- To design and synthesize novel EG-attached MPAO aimed at retarding the effects of free radicals and oxidants
- To investigate the role of natural antioxidants on particle size
- To improve the dispersion stability of IONPs
- To improve oxidative stability and maintain the magnetic properties of IONPs

1.4 Thesis Organization

This thesis consists of eight chapters: The contents of each chapter are described below:

Chapter 1 (Introduction): An overview of the study's history, problem description, objectives, and scope is provided in this chapter. To sum up, it briefly explains why this work is so important, with a brief explanation of how it differs from past studies and addresses the inadequacies of those studies.

Chapter 2 (Literature Review): Nanoantioxidants, the functionalization of nanomaterials with various antioxidants, and their antioxidant and antimicrobial effects are reviewed in this chapter.

The experimental section is covered in Chapter 3. The synthesis of IONP and MPAO is described, the functionalization of IONPs, antioxidant assay, and antimicrobial activities are explained.

Natural antioxidants are discussed in Chapters 4 and 5; multipotent antioxidants are discussed in Chapters 6 and 7. Chapter four, five, six and seven deals with results and discussion of the four main projects:

i. Design and Synthesis of Multipotent Antioxidants for Functionalization of Iron Oxide Nanoparticles
ii. Surface Functionalization of Magnetite Nanoparticles with Multipotent Antioxidant as Potential Magnetic Nanoantioxidants and Antimicrobial Agents
iii. Design and Synthesis of Multipotent Antioxidants for Functionalization of Iron Oxide Nanoparticles
iv. Surface Functionalization of Magnetite Nanoparticles with Multipotent Antioxidant as Potential Magnetic Nanoantioxidants and Antimicrobial Agents

In Chapter 8 of the thesis, the findings and future directions based on this research are summarized.

CHAPTER 2: LITERATURE REVIEW

2.1 Antioxidants

Antioxidants are substances or chemicals that, even at low concentrations, can inhibit the oxidation of a useful substrate (Ingold & Pratt, 2014; Young & Woodside, 2001). The discovery of antioxidants sparked a boom in the late 19th and early 20th centuries, thanks to their use in various industrial processes such as corrosion prevention, fuel polymerization, combustion engine fouling, and rubber vulcanization (Mattill, 1947). Antioxidants were formerly used only to protect unsaturated fats from oxidizing, resulting in the rancidity of fats (German, 1999). Any compound's antioxidant properties can be determined by measuring the rate at which fat consumes oxygen when stored oxygen-filled container within a sealed environment. The discovery of vitamins A, C, and E as antioxidants revolutionized the discipline and the vital significance of antioxidants in biochemistry of living organisms was clearly proven (Jacob, 1996; Knight, 1998). The antioxidant is a stable molecule that donates an electron to harmful free radicals, neutralizing the resulting radical, and reduces the amount of damage that it may do. Generally speaking, these antioxidants either stop or delay cellular damage from occurring (Halliwell, 1995). Antioxidants with a low molecular weight can swiftly and effectively interact with reactive oxygen species (ROS), limiting damage to essential molecules from the chain reaction, as shown in Figure 2.1.

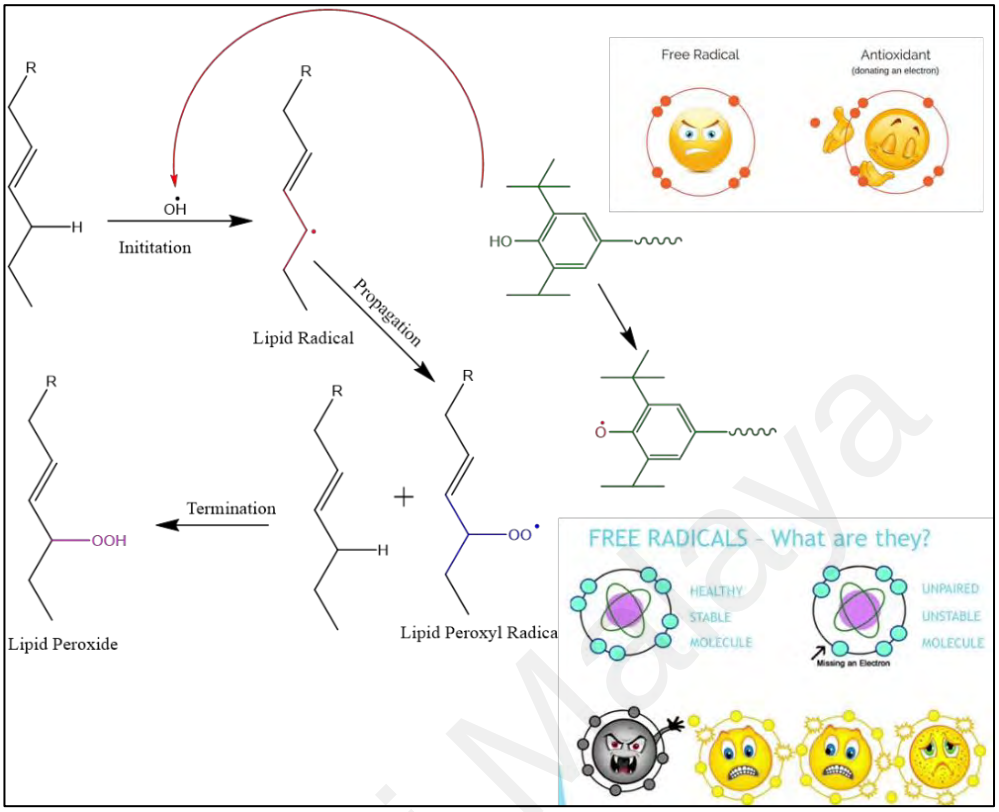

Figure 2.1 Antioxidant and Free Radical

Our bodies naturally produce antioxidant molecules such as glutathione, uric acid, and ubiquinol during regular metabolic activities (Shi, Noguchi, & Niki, 1999). Ascorbic acid (vitamin C), β-carotene, and α-tocopherol (vitamin E) are micronutrients and enzymes found in human bodies that can combat free radicals (Levine, Rumsey, Daruwala, Park, & Wang, 1999). Because the body cannot produce these molecules, they must be taken from the food we consume. There are two types of antioxidants: endogenous (found in the body) and exogenous (found in foods, such as glutathione and uric acid) (M. I. Khan & Giridhar, 2011). The graphic (Figure 2.2) summarizes the classification of antioxidants. Antioxidants found in nature may help protect against the damage caused by oxidative stress. Antioxidants like polyphenols (3,6-dihydroxyflavone), carotenoids (lutein), vitamins (ascorbic acid), and metabolic sensitizers (selenium methyl selenocysteine) have been found in a wide variety of fruits, vegetables, and fruit byproducts, and they've all

been shown to reduce the amount of harmful free radicals in the human body (Anagnostopoulou, Kefalas, Papageorgiou, Assimopoulou, & Boskou, 2006; Fleuriet & Macheix, 2003; Lim, Lim, & Tee, 2007; Medhe, Bansal, & Srivastava, 2014).

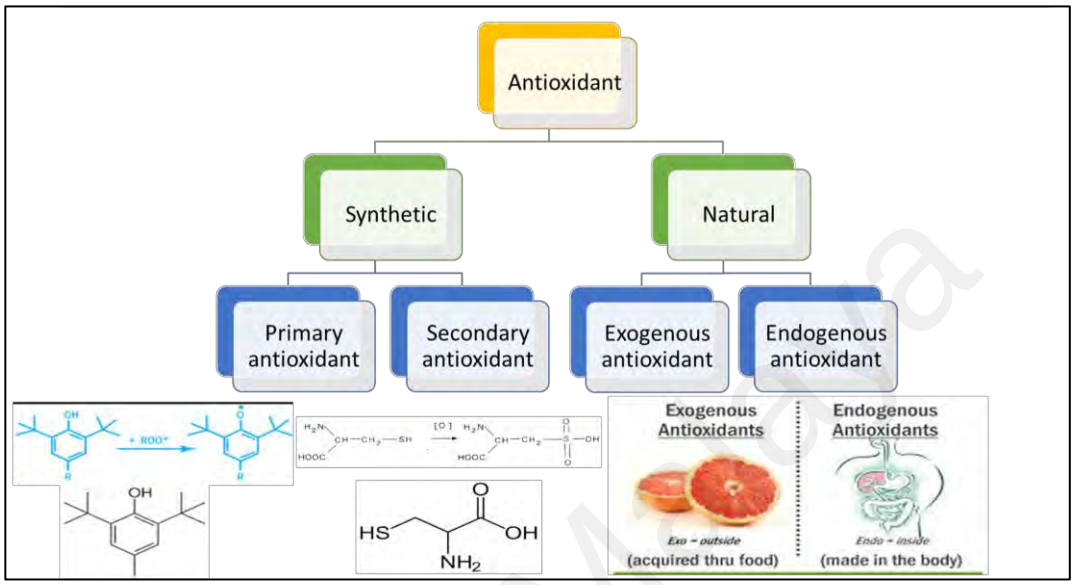

Figure 2.2 Classification of Antioxidants

Bioactive substances from various sources, such as antioxidants obtained from natural resources (such as Rosa rugosa dried flower extracts), are discovered to scavenge active oxygen species and electrophiles, block nitrosation processes, and reduce lipid peroxidation levels (Tułodziecka & Szydłowska-Czerniak, 2016). On the other hand, natural antioxidants are prone to deterioration and have low bioavailability due to low absorption and degradation during delivery (A. K. Verma, 2014). Antioxidants include synthetic substances such as butylated hydroxytoluene (BHT) and butylated hydroxyanisole (BHA), BHT analogues, GA esters, and other derivatives (Medhe et al., 2014; Pratt & Hudson, 1990). Nanotechnology has opened up new possibilities in a variety of fields. Nanoparticles are ideal for medication and drug delivery because of their small size and versatility. As a result of the integration of nanotechnology with material science and engineering, significant progress has been made in the reduction of free

radical production in a variety of fields (Eftekhari, Ahmadian, Panahi-Azar, et al., 2018). Antioxidant nanoparticles or nano-antioxidants are the nanoparticles designed for this purpose. Some of these nano-antioxidants have recently shown promise in nanomedicine studies (Hasanzadeh et al., 2017; Hasanzadeh et al., 2018).

2.2 Nanoantioxidants

Antioxidants have been proven to be helpful therapeutic and preventative agents for a variety of ailments. Most antioxidants have a few drawbacks, such as low permeability, poor water solubility, instability during storage, and digestive tract degradability (Hu, Liu, Zhang, & Zeng, 2017). The free radical generation has been minimized in several fields by developing nanoparticles and synthesized nanoparticles are known as nano-antioxidants due to the integration of material sciences and nanotechnology (Eftekhari, Ahmadian, Panahi-Azar, et al., 2018; Eftekhari, Dizaj, et al., 2018).

Nanoantioxidants are nanomaterials that capture chain-carrying radicals or reduce the number of initiation processes to lower the overall rate of autoxidation. Vitamin E (3-carotene, selenium, glutathione and polyphenols) is one of the most studied dietary antioxidants as a potential pharmacological strategy to reduce ROS levels and combat disorders caused by oxidative stress. However, there have been no conclusive results from clinical trials on the benefits of α-tocopherol, selenium, or (3-carotene supplementation) for lowering cancer risk. (Morry et al., 2017). One of the most likely explanations for these surprising outcomes is that most antioxidants fail to reach biologically relevant targets. Nanoantioxidants give a unique possibility in this context since they may be tailored to have longer stability than small molecules, escape metabolic clearance quickly and target specific locations (Morry et al., 2017).

Nanomaterials can either act as passive delivery systems for small-molecule antioxidants or have their own built-in antioxidant capabilities. A critical step in creating

new nano-antioxidants is to conduct in vitro chemical tests to assess their antioxidative activity.

Different forms of antioxidants have been discovered as a result of recent research trends. Nano-antioxidants have been made with a variety of materials until now. It has been observed that metal and metal oxide nanoparticles, carbon nanotubes and other carbon-based nanomaterials, similarly, several types of polymer-loaded antioxidant nanoparticles, have antioxidant properties. Different forms of antioxidants have been discovered as a result of recent research trends. Biodegradable nanoparticles have recently received great attention due to their high encapsulation efficiency, controlled release properties, and lack of toxicity, among other factors. As a carrier for various forms of nano-antioxidants throughout history, biodegradable polymers have proven to be the most essential materials to be explored (Eftekhari, Ahmadian, Azami, Johari-Ahar, & Eghbal, 2018; Pohlmann, Schaffazick, Creczynski-Pasa, & Guterres, 2010). Metal-based nanoparticles with high antioxidant activity are being used to develop new antioxidant materials.

For example, The antioxidant enzymes GSH-Px and thioredoxin reductase use selenium in selenoproteins to regulate hemostasis and the redox system (Mohammed & Safwat, 2013). Furthermore, as documented in several studies, selenium nanoparticles activate selenoproteins and display antioxidant activity in both the in vivo and in vitro environments (G. S. Kumar, Kulkarni, Khurana, Kaur, & Tikoo, 2014). When administered to rats, nanoselenium has been found to significantly diminish nicotine-induced nephrotoxicity by inhibiting the production of reactive oxygen species and inflammation. This impact has been attributed to the small size of nanoselenium, which has a greater surface-to-volume ratio and, as a result, has a better bioavailability than larger particles (Zahran, Elsonbaty, & Moawed, 2017).

A dose-dependent antioxidant activity has been demonstrated for ZnO nanoparticles produced from Polygala tenuifolia root extract (Baranwal, Mahato, Srivastava, Maurya, & Chandra, 2016). Antibacterial and anticancer characteristics of silver nanoparticles have made them a popular choice for medical applications. They are used in a variety of applications. The use of plant-based silver nanoparticles, on the other hand, has the advantage of having free radical scavenging action, which is becoming increasingly important in the treatment of oxidative stress-mediated toxicities (Abdel-Aziz, Shaheen, El-Nekeety, & Abdel-Wahhab, 2014).

Additionally, carbon-based nanoparticles have the potential to perform a radical cleaning up activity. Carbon nanotubes, for example, have antioxidant properties due to their strong affinity for electrons (Watts et al., 2003). Specifically, single-walled carbon nanotubes exhibit significant antioxidant effects in the oxygen radical absorbance capacity assay, which has been validated (Lucente-Schultz et al., 2009).

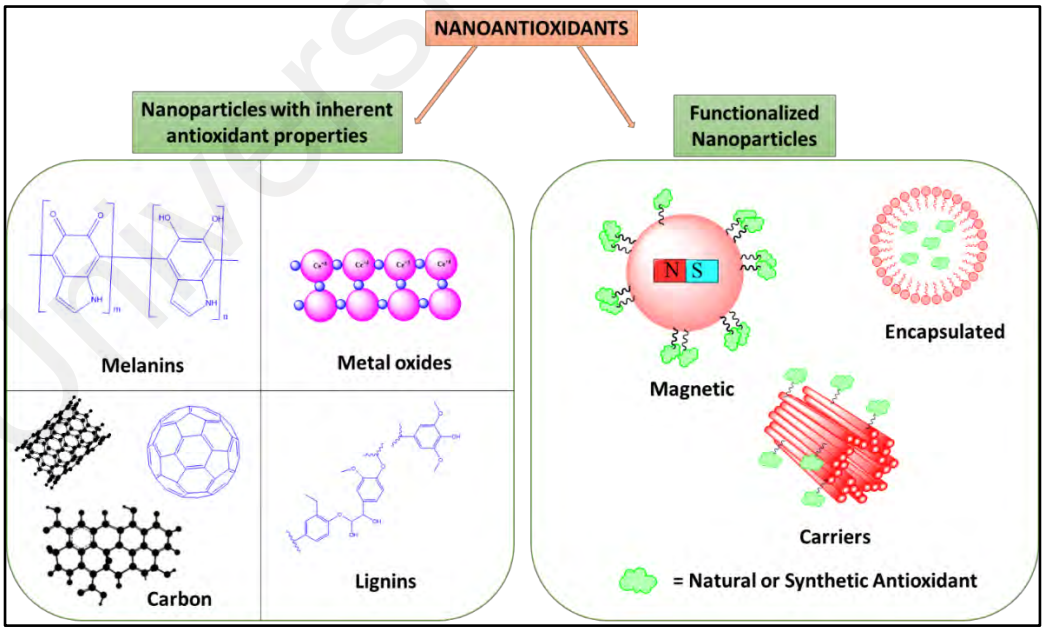

Figure 2.3 Nanoparticles with Antioxidant Activity: "Nanoantioxidants"

A variety of nanoparticles coated with antioxidant CNTs and metal or metal oxide nanoparticles have antioxidative properties (Eftekhari, Dizaj, et al., 2018). Nano-oxidant

synthesis has used various preparation strategies over the last few decades, including emulsion/solvent drying, supercritical fluid technology, solvent displacement, templating and nanoprecipitation methods (Eftekhari, Dizaj, et al., 2018).

Due to their intrinsic physicochemical features, reactive nitrogen and oxygen species can be cleaned up by using oxide nanoparticles, which mimic the antioxidant molecule (Nelson, Johnson, Walker, Riley, & Sims, 2016). There has been a great deal of interest in the biomedical field for cerium oxide nanoparticles (CONPs) because of their multi-enzymatic ROS scavenging abilities (Eriksson et al., 2018). In addition to coexisting in both oxidation states, these CONPs also exhibit a reduction potential of 1.52 V and can flip between both oxidation states (S. Das et al., 2013). However, Cerium dioxide in the form of a bulk crystal consists of $Ce^{4+,}$ whereas when it is reduced to nano-size it considerably increases the relative proportion of Ce^{3+}, resulting in improved catalytic activity. After three weeks of intravenous administration, researchers found that nanoceria dramatically reduced lipoperoxidation, demonstrating that CONPs effectively treat oxidative stress in an in vivo test on mice conducted by Hirst et al. (2013) (Hirst et al., 2013). Caputo et al. (2015) compared the antioxidant capacity of CONPs with NAC (N-acetyl-cysteine) and Trolox (soluble analogues of vitamin E) in a study (Caputo et al., 2015).

Additionally, liposomes are used to deliver antioxidants to their intended areas. Since these liposomes are both amphiphilic and biocompatible, they can hold a variety of chemicals, including antioxidant enzymes, both water-soluble and water insoluble (L. Du, Li, Chen, & Liu, 2014). The most commonly used substance to make nanoparticles is chitosan, whether as a stand-alone substance or in combination with another (Hans & Lowman, 2002). Chitosan has mucoadhesive characteristics, making it better at delivering drugs to mucosal surfaces, including the intestinal and nasal epithelium (Vila, Sánchez, Tobío, Calvo, & Alonso, 2002). It has been found that curcumin coated with

chitosan, which protects it from free radicals, is more effective in scavenging free radicals than curcumin alone (B. R. Shah, Zhang, Li, & Li, 2016). By adjusting the pH and oxidative stress levels of inflamed tissues, Pu et al. (2014) found that curcumin-based nanocarriers can encapsulate curcumin antioxidant molecules and regulate their release, which in turn increases the generation of Reactive Nitrogen Species (RNS) and ROS by lipopolysaccharide-stimulated macrophages (Pu et al., 2014).

2.3 Classification of Antioxidant Action

2.3.1 Preventive Antioxidants

Preventive antioxidants work by lowering the rate of initiation (Amorati & Valgimigli, 2015). This is a heterogeneous class of compounds that comprise scavengers (Barajas-Carmona, Francisco-Aldana, & Morales-Narv ez, 2017), metal chelators (Perron & Brumaghim, 2009), agents capable of degrading hydroperoxide (Lu & Holmgren, 2014), both smaller molecules and enzymes such as superoxide dismutase (SOD) and glutathione peroxidase (GPX) or their analogues (Brand et al., 2004).

2.3.2 Chain-Breaking Antioxidants

An antioxidant (AH) and a peroxyl radical can create a hydroperoxide and a radical of the antioxidant (A•), that also trap a second ROO• and results in the production of non-radical end products if a formal H-atom transfer occurs between them (Ingold & Pratt, 2014). Antioxidants that break chains are destroyed during the reaction, therefore, they function stoichiometrically when regeneration mechanisms are absent. Here, it is vital to note that chain-breaking antioxidants only react with peroxyl radicals, while the reactions with other radical species formed during autoxidation are of secondary consequence. Because R• interacts so quickly with oxygen, an antioxidant's chances of catching it are minimal to none. With regard to the OH• and RO• initiating radicals, these radicals have extremely high reactivity toward all organic molecules, making it impossible for the

antioxidant to compete with these reactions because the antioxidant, which, by definition, is only found in trace quantities, is unable to compete with these reactions (Amorati & Valgimigli, 2015). Figure 2.4 shows characteristics of a molecule (AH) that makes it a chain-breaking antioxidant:

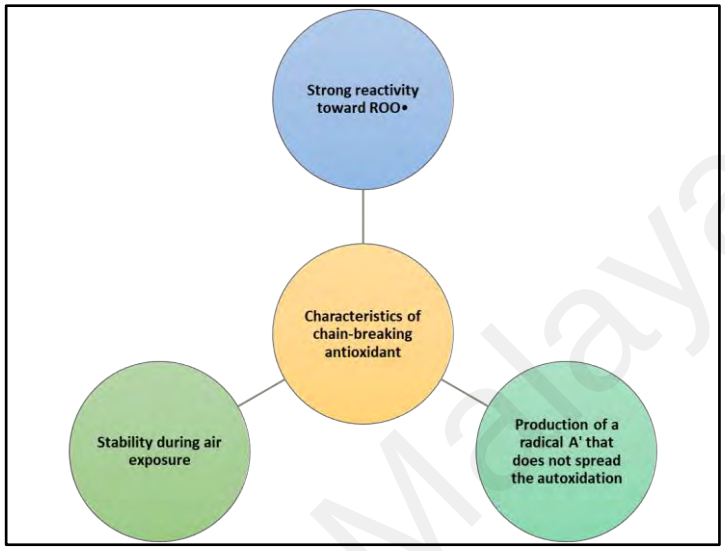

Figure 2.4 Characteristics of a Chain-Breaking Antioxidant

The most effective examples of this family of antioxidants may be phenols (such as resveratrol) and ascorbate (vitamin C), whereas synthetic equivalents include aromatic amines, BHT, BHA, and the compound nitroxide.

Besides direct antioxidants, substances that do not themselves have antioxidant activity but can promote and enhance the effectiveness of biological systems' endogenous antioxidant defenses are usually classed as indirect antioxidants.

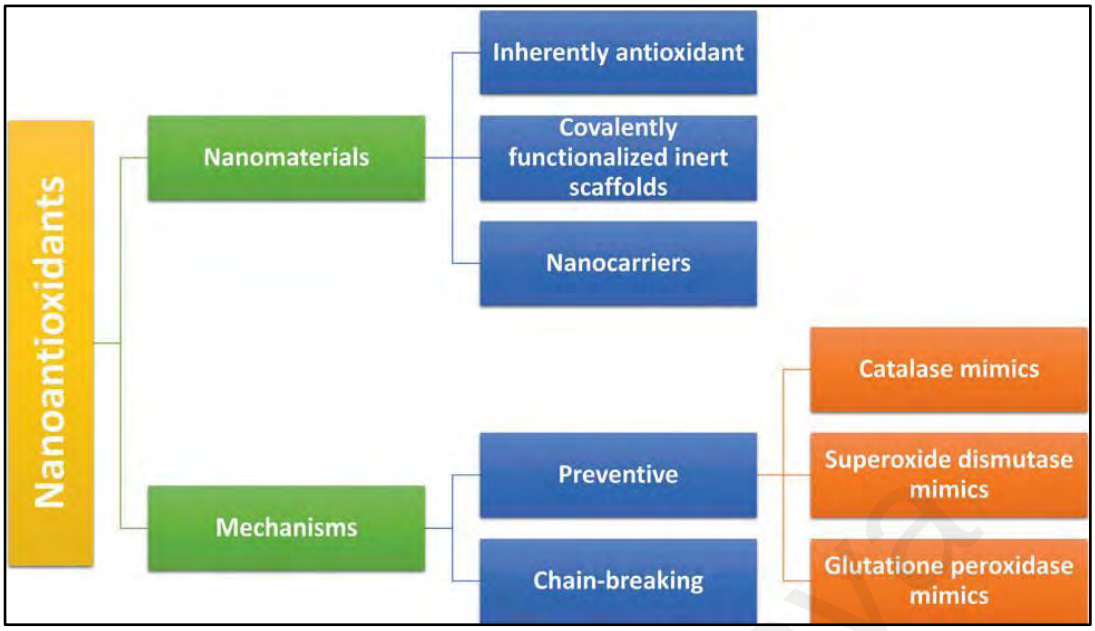

Figure 2.5 System for Classifying Nanoantioxidants Based on Structural and Mode of Action.

2.1 Nanomaterials with Inherent Antioxidant Capabilities

There are a variety of nanomaterials with inherent antioxidant capabilities that don't need to be functionalized with antioxidants; instead, their properties come from the surface features of the nanomaterials. Nanoparticles of inorganic metal are the most common type of such materials. On the other hand, organic nanoparticles are becoming increasingly essential, with a few examples below.

Metals such as silver, gold, platinum and palladium, as well as metal oxide, examples can be found throughout the literature (Z. Chen et al., 2012; Dong et al., 2014; Mu, Zhang, Zhao, & Wang, 2013; Nelson et al., 2016; Pirmohamed et al., 2010; Silvestri et al., 2017; N. Singh, Savanur, Srivastava, D'Silva, & Mugesh, 2017). NPs that act as catalase substitutes but only at neutral or basic pH levels does this activity occur; at acidic pH values, on the other hand, a prooxidant impact starts to develop. The production of HO• radicals causes the prooxidant activity of the nanoparticle as a result of the occurrence of the Fenton reaction on the nanoparticle's surface (Nosaka & Nosaka, 2017).

$$H_2O_2 + e– \rightarrow HO\bullet + HO^- \quad (1)$$

Colorimetric glucose or DNA sensing uses this reaction for nanomaterials with peroxidase activity (Wei & Wang, 2013). These nanoantioxidants have a two-sided activity, restricting their effectiveness while also providing an exciting opportunity to build pH-responsive redox modulators of the cell's oxidative stress (Wason et al., 2013).

There is still some debate about the mechanisms that underlie catalase activity in cerium oxide nanoparticles (Cafun, Kvashnina, Casals, Puntes, & Glatzel, 2013; Celardo, Pedersen, Traversa, & Ghibelli, 2011) although it appears that very stable surface peroxo/hydroperoxo species are at play (Cafun et al., 2013). In addition, nanomaterial oxidation status can affect CAT-like activity.

Although the processes behind catalase activity are still a mystery, (Cafun et al., 2013; Celardo et al., 2011), highly stable surface peroxo/hydroperoxo species are implicated in the case of cerium oxide nanoparticles. (Cafun et al., 2013) a nanomaterial's degree of oxidation has an effect on whether it behaves like a CAT.

The material with a higher $Mn^{3+/}Mn^{2+}$ ratio, generated by oxidation with $NaIO_4$, showed improved catalase (CAT) activity in comparison to material with a lower $Mn^{3+/}Mn^{2}$ ratio in Mn_3O_4 NPs with flower-like morphology ("nanoflowers") (N. Singh et al., 2017).

When it comes to Co_3O_4 nanomaterials, nanoplates were the most common, followed by nanorods and nanocubes. For three distinct Co_3O_4 nanomaterials, the amount of CAT-like activity reduced inversely as a function of their redox potential. In order to explain this result, it was found that the rate-determining step in the CAT catalytic cycles is the cleavage of the O-O bond that occurs during the nanomaterial's reduction of H_2O_2 (Mu, Zhang, Zhao, & Wang, 2014). In low-pH environments, switching from Fenton chemistry

to catalase activity is controlled by the pH of the environment (high pH). A possible explanation for this unusual behaviour is the pH dependency of the interaction between $HO^{\bullet}$ and HOOH (equation 2), which is predicted to be aided by the partial deprotonation of H_2O_2 (pKa=11.6; see equation 2) (Nosaka & Nosaka, 2017).

$$H_2O_2 + HO^{\bullet} \rightarrow O_2^{\bullet -} + H_2O + H^+ \qquad (2)$$

Theoretically, the pH switch in gold nanorods, core-shell gold-platinum nanorods, and gold-palladium nanorods is caused by the metal surface absorbing either H^+ or $HO^{\bullet}$ (J. Li, Liu, Wu, & Gao, 2015).

GPX is a clone. Glutathione peroxidase (GPX) activity, in contrast to catalase activity, has only been discovered in the case of vanadium (Vernekar et al., 2014) and manganese (N. Singh et al., 2017) oxides (see Table 2.1).

Table 2.1 Intrinsically Antioxidant Nanoparticles: Mechanisms of Action and Chemical Assays used to Evaluate their Activity

Nanoantioxidant	Assay	Ref.
Catalase mimic (pH>7		
Polyvinylpyrrolidone coated	H_2O_2 decrease (spectrophotometric), O_2 evolution	(W. He et al., 2013)
Au NPs	(EPR)	
Cerium oxide NPs	H_2O_2 disappearance (spectrophotometric), O2 generation from $_{H2O2}$ (Clark electrode)	(Pirmohamed et al., 2010)
Co_3O_4 NPs	O_2 generation from H_2O_2 (Clark electrode)	(Mu et al., 2013)
Au nanorods; core-shell	H_2O_2 decrease (spectrophotometric), O_2 evolution	(J. Li et al., 2015)
Au@Pt nanorods; core-shell	(Clark electrode)	
Au@Pd nanorods		
Apoferritin coated Pt NPs	H_2O_2 consumption, formation of bubbles attributed to	(Fan et al., 2011)
	O_2	
Pt nanopowder	O_2 detection by EPR line broadening	(Y. Liu, Wu, Li, Yin, & Nie, 2014)
Mn_3O_4 “nanoflowers”	H_2O_2 decrease (spectrophotometric)	(N. Singh et al., 2017)

Nanoantioxidant	Assay	Ref.
Dimercaptosuccinic acid coated Fe_3O_4 NPs	O_2 evolution (Clark electrode)	(Z. Chen et al., 2012)
Eumelanin-silica NPs	H_2O_2 decrease (Ferrous xylenol orange assay)	(Silvestri et al., 2017)
GPX mimic		
V_2O_5 nanowires	Glutathione reductase coupled assay (spectrophotometric), change in absorbance of coenzyme NADPH at 340 nm	(Vernekar et al., 2014)
Graphene oxide supported selenium NPs	Glutathione reductase coupled assay (spectrophotometric)	(Huang et al., 2017)
Mn_3O_4 "nanoflowers"	Glutathione reductase coupled assay (spectrophotometric)	(N. Singh et al., 2017)
Chain-breaking		
Polyacrylic acid (PAA)-protected Pt NPs	Inhibit linoleic acid peroxidation (O_2 consumption by Clark electrode), DPPH (spectrophotometric), AAPH-derived radicals scavenging (EPR detection)	(Watanabe et al., 2009)
Oleic acid coated cerium oxide NPs	AAPH-derived radicals scavenging (ORAC assay)	(S. S. Lee et al., 2013)
ZrO2 NPs	DPPH (spectrophotometric)	(Balaji, Mandal, Ranjan, Dasgupta, & Chidambaram, 2017)
PEG coated melanin NPs	DPPH (spectrophotometric and EPR)	(K.-Y. Ju, Lee, Lee, Park, & Lee, 2011)
SOD mimic		
PEG coated melanin NPs	EPR study of the reaction with $^1O_2$ with 5-diethoxyphosphoryl-5-methyl-1-pyrroline N oxide (DEPMPO), O_2 evolution (Clark electrode)	(Y. Liu et al., 2017)
Polyvinylpyrrolidone coated Au NPs	Xanthine/xanthine oxidase and a spin-trap with EPR detection	(W. He et al., 2013)
Glycine coated Cu(OH)2 NPs	Xanthine/xanthine oxidase and iodonitrotetrazolium chloride (spectrophotometric)	(Korschelt et al., 2017)
PEG coated MnO NPs	Xanthine/xanthine oxidase and cytochrome C (spectrophotometric)	(Ragg, Tahir, & Tremel, 2016)
PEG coated carbon nanoclusters	EPR study of the reaction with O_2	(E. L. Samuel et al., 2015)
Pd nanocrystals	Xanthine/xanthine oxidase and a spin-trap with EPR detection	(C. Ge et al., 2016)
Pt nanopowder	Xanthine/xanthine oxidase and a spin-trap with EPR detection	(Y. Liu et al., 2014)
Mn_3O_4 "nanoflowers"	Xanthine/xanthine oxidase and iodonitrotetrazolium chloride (spectrophotometric)	(N. Singh et al., 2017)
Dimercapto succinic acid coated Co_3O_4 NPs	Xanthine/xanthine oxidase and a spin-trap with EPR detection	(Dong et al., 2014)
Multiwalled carbon nanotubes	Xanthine/xanthine oxidase and cytochrome c (spectrophotometric)	(G. F. Liu et al., 2008)
Functionalized fullerene	Reaction with $^1O_2$ (spectrophotometric)	(G. F. Liu et al., 2008)

GPX Mimics: For the first time, GPX activity has only been found in vanadium (Vernekar et al., 2014) and manganese (N. Singh et al., 2017) oxides, as opposed to the widespread catalase activity found in many metals and metal oxides.

Glutathione (GSH) is sacrificed when V_2O_5 nanowires are used in physiological settings to mediate the H_2O_2 to H_2O reduction because of V_2O_5's unique ability instead to produce polar peroxido species instead of HO• radicals (equation 3) (Ragg et al., 2016).

$$2\ GSH + H_2O_2 —* GS\text{-}SG + 2\ H_2O \qquad (3)$$

Compounds with heavy chalcogen atoms, such as selenium and tellurium, are more likely to exhibit GPX-like activity. Due to their large surface area and rapid reactivity, graphene oxide-supported selenium nanoparticles showed GPX-like activity (Huang et al., 2017).

SOD Mimics: Due to the fact that although the superoxide radical is a member of the peroxyl radical family, its unique chemistry distinguishes it from other radicals such as the alkylperoxyl radical, antioxidants that trap the radical must be taken into consideration independently.

When it comes to superoxide, the predominant form is $O_2^{\bullet}$ since the conjugated acid ($HOO^{\bullet}$) has a pKa value of 4.5. In the protonated state (neutral, $HOO^{\bullet}$), superoxide has a dual behaviour, as it may both abstract and donate a H atom to create HOOH and O_2 (Cedrowski, Litwinienko, Baschieri, & Amorati, 2016). when the superoxide is protonated (in the neutral state). On the other hand, deprotonated $O_2^{\bullet}$ has the majority of the properties of a reducing agent.

A diverse variety of nanomaterials, including noble metals (gold, platinum, palladium) as well as metal oxides (cerium, cobalt, manganese oxides), carbon clusters (carbon nanotubes, fullerenes), and melanin, have been shown to have SOD-like activity.

SOD- and GPX-like activity were concurrently achieved by a "multi nanozyme" based on MnO_2 nano-nanoparticles deposited on V_2O_5 nanowires by polydopamine (E. Ju et al., 2016)

Instead of chain-breaking antioxidant activity, a given nanomaterial must be capable of quenching alkylperoxyl radicals by converting them to hydroperoxides (Balaji et al., 2017; K.-Y. Ju et al., 2011; S. S. Lee et al., 2013; Watanabe et al., 2009). Alkylperoxyl radicals (ROO•, where R is an alkyl, such as lipids) can be quenched by either an H-atom donating antioxidant AH or an electron-donating antioxidant (D) and a protic solvent SolvH as shown in Figure 2.6.

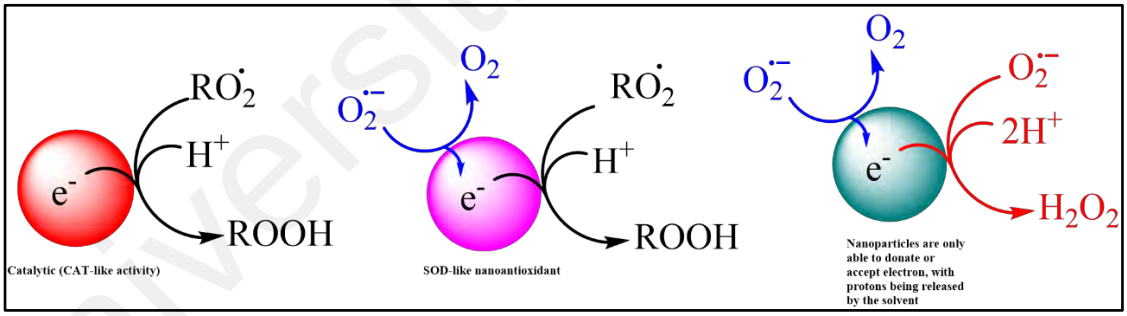

Figure 2.6 Similarities and Differences Between Sacrificial (A), Catalytic (B) SOD-like nanoantioxidants (C). Nanoparticles as Electron Donor or Accepter

In the same way, nanoparticles with cleavable O-H groups, such as lignin and melanin behave. Antioxidant activity of lignin nanoparticles has been found in apolar polymers such as natural rubber and methanol, for example (Barana et al., 2018).

2.1.1 Antioxidant Functionalized Nanoparticles

Bioactive substances such as terpenoids, alkaloids, polyphenols, and phenolic acids have been found in bacteria, algae, fungi, lichens, and plants. These bioactive chemicals could lead to better results. The antioxidative properties of these compounds have been demonstrated to decrease and stabilize metallic ions. Table 2.2 illustrates the various types of antioxidant nanoparticles with functionalized antioxidants from different sources. The evolution of nanoantioxidants is depicted in Figure 2.7.

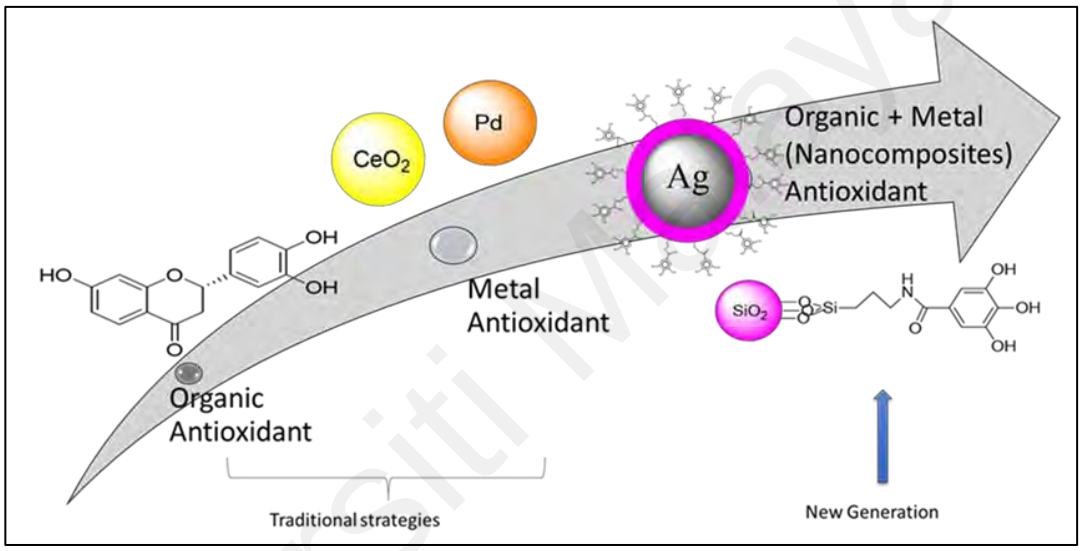

Figure 2.7 Development of Nanoantioxidants

Table 2.2 Antioxidant Functionalized Nanoparticles

Types of Nanoparticles	Biological Extract	Morphology	Size	Antioxidant Activity	Ref.
Iron	*Amaranthus dubiusleaf extract*	Spherical	43–220 nm	DPPH	(Harshiny, Iswarya, & Matheswaran, 2015)
Iron	*Amaranthus spinosus* leaf extract	Spherical	-	DPPH	(Muthukumar & Matheswaran, 2015)
Iron	*Asphodelus aestivus Brot. Extract*	Spherical	20–25 nm	DPPH, ABTS	(Tuzun et al., 2020)
Iron oxide	*tea-pruning waste*	Spherical	20–35 nm	DPPH	(Periakaruppan et al., 2021)
Iron oxide	*Phoenix dactylifera L.*	Spherical	2–30 nm	DPPH	(Abdullah et al., 2020)
Iron oxide	*curcumin*	Spherical	--	DPPH	(Mohamed, Hessen, & Mohammed, 2021)
Iron oxide	*Coriandrum sativum L. (cilantro)*	Spherical	-	DPPH	(K. Singh, Chopra, Singh, & Singh, 2020)
Iron oxide	*Blumea eriantha DC*	spherical and irregular shapes	10 - 60	DPPH, ABTS, Hydrogen peroxide scavenging activity and Reducing power assay activity	(Chavan et al., 2020)
Nickel Oxide	*Stevia rebaudiana* Bertoni leaf extract	Spherical	20–50 nm	DPPH	(Srihasam, Thyagarajan, Korivi, Lebaka, & Mallem, 2020)
Gold	*Lactobacillus kimchicus DCY51T biomass*	Spherical	13 nm	DPPH	(Markus et al., 2016)
Silver	*Streptomyces griseorubens AU2 cell free supernatant*	Spherical	5–20 nm	DPPH	(Baygar & Ugur, 2017)
Gold	*Enterococcus* species cell free extract	Sphere	8–50 nm	DPPH	(Oladipo et al., 2017)
Gold	*Snail slime*	Spherical, hexagonal, trapezoidal, and rod shape	14 ± 6 nm	DPPH, ABTS	(Rizzi et al., 2021)
Gold	*Achillea biebersteinii*	Spherical	2–30 nm	DPPH	(Mobaraki et al., 2021)
Gold	*Centaurea behen*	Spherical	50 nm	DPPH	(Abdoli, Arkan, Shekarbeygi, & Khaledian, 2021)

Types of Nanoparticles	Biological Extract	Morphology	Size	Antioxidant Activity	Ref.
Gold	*Cannabis sativa L*	Spherical	-	DPPH	(Y. Chang, Zheng, Chinnathambi, Alahmadi, & Alharbi, 2021)
Gold	*Curcumae Kwangsiensis Folium*	Spherical	8–25 nm	DPPH	(J. Chen et al., 2021)
Gold	*Kaempferia parviflora rhizome*	Spherical	20-60 nm	DPPH	(Varghese et al., 2021)
Gold	*Atriplex halimus and Chenopodium amperosidies*	Spherical	2 - 10 nm	DPPH	(Hosny, Fawzy, Abdelfatah, Fawzy, & Eltaweil, 2021)
Gold	*Brassica rapa var. pekinensis*	Spherical	25 nm	DPPH, ABTS	(Aghamirzaei, Khiabani, Hamishehkar, Mokarram, & Amjadi, 2021)
Gold	*Sambucus wightiana*	trigonal, cubic, hexagonal, and polygonal	15.96 nm	DPPH	(Khuda et al., 2021)
Gold	*Curcuma pseudomontana*	Spherical	20 nm	DPPH,Reducing power (RP) assay, Hydrogen peroxide radical scavenging (H_2O_2) assay, Nitric oxide radical scavenging (NO) assay, Cupric ion reducing antioxidant capacity (CUPRAC) assay	(Muniyappan, Pandeeswaran, & Amalraj, 2021)
Gold	*Quercetin*	Spherical	100 nm	DPPH, ABTS and nitric oxide free radical scavenging	(Milanezi et al., 2019)
Gold and Silver	*Escherichia coli* cell *protein*	Triangular, circular,hexagonal (AuNPs), Sphere (AgNPs)	10–100 nm (AuNPs), 10–50 nm (AgNPs)	EC75 (for scavenging 75% effective	(Veeraapandian, Sawant, & Doble, 2012)
Gold and Silver	*Crassocephalum rubens*	spherical	15–25 nm for AgNPs, 10 – 20 nm for AuNPs	DPPH, lipid peroxidation	(Adewale et al., 2020)

Types of Nanoparticles	Biological Extract	Morphology	Size	Antioxidant Activity	Ref.
Silver	*Streptomyces griseorubens AU2 cell free supernatant biomass*	Sphere	5–50 nm	DPPH	(Shanmugasundaram, Radhakrishnan, Gopikrishnan, Pazhanimurugan, & Balagurunathan, 2013)
Silver	*Cuscuta japonica*	oval-spherical	30-50 nm	DPPH	(Prakash Patil, Seong, Kim, Bae Seo, & Kim, 2021)
Silver	*Striga angustifolia*	nanoflakes	106.40 nm	DPPH	(Raja, Balamurugan, Selvakumar, & Vasanth, 2021)
Silver	*Olea europaea*	Spherical	10.47 ± 9.19 nm	DPPH	(Ragunathan & K, 2021)
Silver	*Galphimia glauca*	Spherical	19 - 37 nm	DPPH	(Chakraborty et al., 2021)
Silver	*Cannabis sativa*	Spherical	10–50 nm	DPPH	(Kong, Paray, Al-Sadoon, & Fahad Albeshr, 2021)
Silver	*polyphenol-rich kiwi peel*	Spherical	200−300 nm	ABTS	(X. Sun et al., 2021)
Silver	*Tilia cordata*	Spherical	50 nm	FRAP	(Saygi & Cacan, 2021)
Silver	*Cissampelous pairera*	Spherical	60 nm to 118 nm	DPPH	(Gauthami, Vinitha, Philip Anthony, & Sundaram Muthuraman, 2021)
Silver	*Rhus javanica, Rumex hastatus, and Callistemon viminalis*	-	1 - 100 nm	DPPH, ABTS	(W. Khan et al., 2021)
Silver	*Annona muricata*	Spherical	35 nm	DPPH, ABTS	(Badmus et al., 2020)
Selenium	*Streptomycesminutiscleroticus RT M10A62 biomass*	Spherical	10–250 nm	DPPH	(Ramya, Shanmugasundaram, & Balagurunathan, 2015)
Selenium	Pantoea agglomerans UC-32	Spherical	100 nm	High antioxidant activity in human umbilical	(S. K. Torres et al., 2012)
Gold and Silver	*Gordonia amicalis* HS-11 cell free supernatant	Grain	5–25 nm	CFS synthesized AgNPs and AuNPs	(Sowani et al., 2016)
Silver	*Streptomyces violaceus MM72 exopolysaccharides*	-	30 nm	DPPH	(Sivasankar et al., 2018)
Silver doped zinc oxide	*Morinda citrifolia*	Spherical	-	DPPH	(Shreema et al., 2021)
Zinc Oxide	*Pichia kudriavzevii cell free extract*	Hexagonal	10–61 nm	DPPH	(Moghaddam et al., 2017)
Silver	*Pestalotiopsis microspora* filtrate	Sphere	2–10 nm	-	(Netala, Bethu, et al., 2016)
Gold	*Cladosporium cladosporioides* filtrate	Cubic	100 nm	DPPH	(M et al., 2017)

Types of Nanoparticles	Biological Extract	Morphology	Size	Antioxidant Activity	Ref.
Silver	*Cladosporium*	Sphere	100 nm	-DPPH	(Manjunath Hulikere & Joshi, 2019)
Copper	Cissus arnotiana	Sphere	60-90 nm	DPPH	
Copper oxide	*Sargassum longifolium*	Sphere	40 and 60 nm	DPPH	(Rajeshkumar et al., 2021)
Copper	*Blumea balsamifera*	Sphere	30-55 nm	DPPH	(Ginting, Maulana, & Karnila, 2020)
Copper	*Borreria hispida*	Sphere	121 ± 37 nm	DPPH	(Venugopalan, Pitchai, Devarayan, & Swaminathan, 2020)
Copper	*Fragaria ananassa*	Sphere	10–30 nm	DPPH	(Hemmati, Ahmeda, Salehabadi, Zangeneh, & Zangeneh, 2020)
Copper	*Persea americana*	Sphere	42 - 90 nm	DPPH	(Rajeshkumar & Rinitha, 2018)
Copper	*Falcaria vulgaris*	Sphere	20–25 nm	DPPH	(Zangeneh et al., 2019)
Copper Oxide	*Cissus arnotiana* leaf extract	Spherical	80–90 nm	DPPH	(Netala, Kotakadi, Bobbu, Gaddam, & Tartte, 2016)

2.1.2 Inert Scaffold with Antioxidant Functionalities

Approximately fifteen years ago, Liu and colleagues published a proof-of-concept study demonstrating the efficiency of antioxidants grafted onto a nanomaterial (Nie et al., 2007), who connected Trolox, a synthetic a-tocopherol analogue, or salvianic acid (Libo Du et al., 2013) to gold nanoparticles encapsulated with thiol.to gold nanoparticles encapsulated with thiol. The radical trapping ability of Au@Trolox was shown to be superior to that of Trolox itself, indicating that this technique will not decrease the antioxidant characteristics of the compound. The food-grade antioxidants caffeic acid (Ebabe Elle, Rahmani, Lauret, Morena, Bidel, Boulahtouf, Balaguer, Cristol, Durand, & Charnay, 2016) and gallic acid (Sotiriou, Blattmann, & Deligiannakis, 2016b) were covalently attached to SiO_2 NPs of different sizes by using aminopropyl-triethoxysilane (APTES) as the linker. Due to the fact that silica is regarded biochemically inert, it is used as a flowing aid in the production of nutraceutical and pharmaceutical products. Gallic acid coupled to SiO_2 demonstrated excellent radical trapping capabilities and was capable of being reused without losing its activity. For the first time, the authors demonstrated that, following the reaction with free radicals, these nanoparticles exhibited considerable agglomeration, which they attributed to the presence of cross coupling between free radicals on the surface (Deligiannakis et al., 2012).

Similarly, the phenolic antioxidants, Trolox or curcumin were covalently linked to graphite-coated cobalt magnetic nanoparticles using a similar technique (Viglianisi et al., 2014). Alternatively, on the outside of halloysite nanotubes(Marina Massaro et al., 2016). Inorganic alumino-silicate clay halloysite (HNTs) has a tubular hollow structure (up to 800 nm in length and 80 nm in external diameter) consisting of siloxane groups (moderate acidity) on the outer surface and aluminol (basicity) on the inner surface, allowing for variable selectivity of molecules grafted onto either surface.Using a disulfide bridge,

Halloysite nanotubes were used to covalently link curcumin to the surface, allowing for thiol-dependent release while maintaining curcumin's free radical trapping ability (M Massaro et al., 2016). To create a bi-functional nanoantioxidant, a synthetic tocopherol (Trolox) was grafted onto the HNT's external surface using APTES as a linker (HNT-Trolox). This was combined with quercetin, a naturally occurring polyphenolic antioxidant, to create a hybrid nanoantioxidant (Marina Massaro et al., 2016) (Figure 2.8). With regards to model substrate peroxidation, this material demonstrated good antioxidant capabilities due to Trolox acting as the primary radical quencher and quercetin serving as a co-antioxidant.

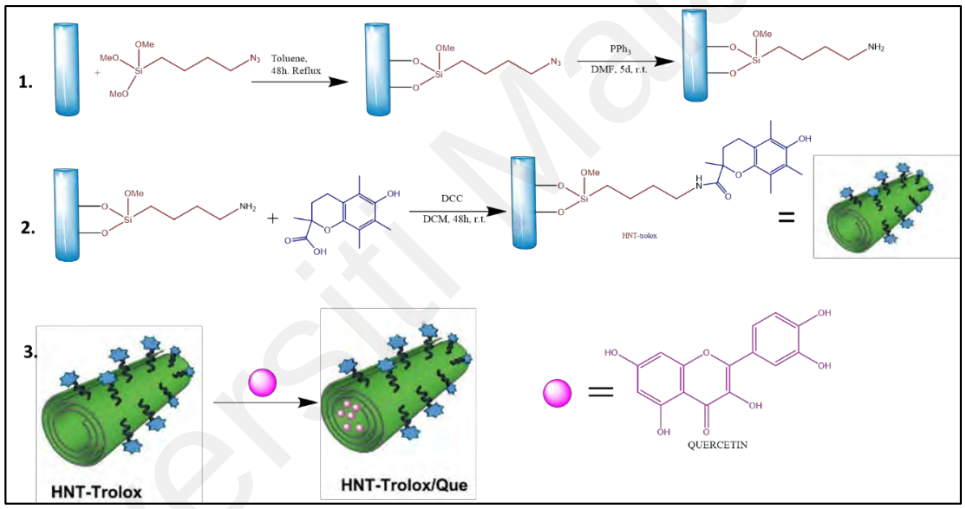

Figure 2.8 Trolox Grafting Procedure on Halloysite Nanotubes; The Incorporation of the Antioxidant Quercetin in the Nanotubes' Interior

Cerium nanoparticles can act as antioxidant enzyme mimics in addition to scavenging ability of ROS and RNS. This is due to the material's inherent physicochemical features at the nanoscale level, its oxygen absorption and release capability, and the relative thermodynamic efficiency of redox cycling between Ce^{3+} and Ce^{4+} ions on the ceria nanoparticle surface (Kalashnikova et al., 2017; Nelson et al., 2016). Combining CNPs with curcumin in a single formulation may result in increased physiological activity due

to curcumin's anticancer properties. Curcumin-loaded nanoceria (CNP-Cur) and dextran-laden nanoceria (Dex-CNP-Cur) were studied in MYCN-amplified and non-amplified cells for their anticancer effects (Kalashnikova et al., 2017).

Table 2.3 Antioxidants Supported by Nanoparticles: Mechanisms of Action and Chemical Assays used to Evaluate their Activity

Nanomaterial	Antioxidant	Method to determine Activity	Ref
Halloysite nanotubes	Curcumin	Inhibited autoxidation O_2 consumption (pressure sensor), DPPH (spectrophotometric)	(M Massaro et al., 2016)
Halloysite nanotubes	Trolox	Inhibited autoxidation O_2 consumption (pressure sensor), DPPH (spectrophotometric)	(Marina Massaro et al., 2016)
Graphite coated cobalt nanoparticles	Trolox	Inhibited autoxidation O_2 consumption (pressure sensor)	(Viglianisi et al., 2014)
Silica	Caffeic acid or rutin	ORAC	(Ebabe Elle, Rahmani, Lauret, Morena, Bidel, Boulahtouf, Balaguer, Cristol, Durand, & Charnay, 2016)
Gold Nanoparticles	Trolox	DPPH• (EPR detection)	(Nie et al., 2007)
Gold Nanoparticles	Salvianic acid	DPPH• (EPR detection)	(Libo Du et al., 2013)
Silica coated Silver nanoparticles	Gallic acid	DPPH• (spectrophotometric and EPR)	(Sotiriou et al., 2016b)
Silica nanoparticles	Gallic acid	DPPH• (spectrophotometric and EPR)	(Deligiannakis et al., 2012)
Single walled CNTs	BHT	ORAC	(Lucente-Schultz et al., 2009)
Fullerene	BHT	Inhibited autoxidation, O_2 consumption (pressure sensor)	(Enes et al., 2006)
Fullerene	Flavonoids	Inhibited autoxidation, O_2 consumption (pressure sensor)	(Enes et al., 2006)
double hydroxide NPs	SOD	Xanthine and xanthine oxidase, nitroblue tetrazolium (spectrophotometric)	(Czochara, Kusio, & Litwinienko, 2017)
Cerium nanoparticles	SOD	Xanthine and xanthine oxidase, hydrosoluble tetrazolium salt (spectrophotometric)	(Gil et al., 2017)
Cerium nanoparticles	CAT	Amplex red assay	(Gil et al., 2017)
MSN	Morin (2',3,4',5,7-pentahydroxyflavone); surface functionalization	Potent HO• scavenger and $^1O_2$ quencher	(Arriagada et al., 2016)

Nanomaterial	Antioxidant	Method to determine Activity	Ref
MSN	Poly Tannic acid; crossing linking	Trolox equivalency antioxidant capacity (TEAC)	(Sahiner, Sagbas, & Aktas, 2016)
MSN	Caffeic acid and Rutin; covalent grafting	Antiradical functions, cellular toxicity alleviation and effective against oxidative stress	(Ebabe Elle, Rahmani, Lauret, Morena, Bidel, Boulahtouf, Balaguer, Cristol, Durand, & Charnay, 2016)
MSN	3,5-di-tert-butyl-4-hydroxybenzoic acid; grafting	oxidation induction time (OIT) determined by DSC	[(P. Liu et al., 2017)
MSN	Curcumin; loaded	Quantification of cellular ROS	(Kotcherlakota et al., 2016)
PEG coated AuNPs	Salvianic acid; Surface functionalization	Thiobarbituric acid reactive substance (TBARS) DPPH(spectrophotometric)	(Libo Du et al., 2013)
AuNPs	Trolox; Self-assembly	DPPH• radical scavenging assay (spectrophotometric)	(Nie et al., 2007)
AuNPs	3,6-dihydroxyflavone, lutein and selenium methyl selenocysteine; embedded	DPPH (2,2-diphenyl-l-picrylhydrazyl), OH (hydroxyl), H_2O_2 (hydrogen peroxide) and NO (nitric oxide) radical scavenging assays	(M. I. Khan & Giridhar, 2011)
AgNPs	Lignin capped	Potent antioxidant DPPH(spectrophotometric); antifungal and antibacterial agents against human pathogens *S. aureus*, *E. coli*, and *A. niger*	(Marulasiddeshwara et al., 2017)
Fe_3O_4NPs	GA;surface functionalization	Magnetically separable; greater antioxidant activity; outstanding antibacterial and antifungal activity	(S. T. Shah et al., 2017)
Fe_2O_3NPs	Carboxymethyl-inulin; coated	non-cytotoxic to the immortalized human cancer cell lines	(Santiago-Rodríguez et al., 2013)
Fe_2O_3NPs	Carbon; coated	Potential antioxidant, exhibited compatibility with the peripheral blood mononuclear cells	(Bhattacharya, Gogoi, Buragohain, & Deb, 2014)
Fe_2O_3NPs	Poly GA, coated	Significantly reduce the oxidative stress; biocompatible and bioactive	(Márta Szekeres et al., 2015)
Magnetic-silk core-shell nanoparticle	Curcumin, loaded	Greater cellular uptake and cytotoxicity in human breast cancer cell line	(Song et al., 2017).

Nanomaterial	Antioxidant	Method to determine Activity	Ref
Ceria nanoparticles	Dextran coated and curcumin loaded	Anti-cancer properties	(Kalashnikova et al., 2017)
Ceria nanoparticles	Phospholipid-PEG; coated	Biocompatible; reduce oxidative stress, cytotoxicity, and effective agent for intracerebral hemorrhage patient	(K. Liu, Xiao, Wang, Chen, & Hu, 2017)
PLGA-PEG	Curcumin; loaded	Ensures neuroprotection in neonatal with hypoxic-ischemic encephalopathy	(Joseph et al., 2018)
Ag-Se bimetal	Quercetin and GA	Antioxidant, antimicrobial and antitumor potentials	(Mittal, Kumar, & Banerjee, 2014)

2.1.3 Gold Nanoparticles (AuNPs)

Recently, there has been a lot of interest in gold nanoparticles (AuNPs) because of size, shape, and optical properties, which are biocompatible (H. Kumar et al., 2020). In the medical field, gold nanoparticles of various sizes and shapes have been used for cancer detection and drug delivery (e.g., Paclitaxel) (H. Kumar et al., 2020). Table 2.3 reveals that antioxidant AuNPs are typically obtained from plant parts such as leaves and fruits, and that they are particularly effective in combating free radicals. Markus et al. (2016) employed an internal membrane-bound technique to identify Kimchi-isolated probiotic strain Lactobacillus kimchicus DCY51T and then used this bacteria to produce antioxidant functionalized AuNPs (Markus et al., 2016). When exposed to malignant cell types, such as human colorectal adenocarcinoma (HT29) and murine macrophages, the AuNPs developed an amino acid capping layer, as well as the fact that proteins attached to their surface rendered them harmless (RAW264.7). It has been discovered that biologically synthesised gold nanoparticles are superior scavengers of free radicals, notably DPPH, when compared to gold salts. In this study, techniques such as FT-IR, UV-visible spectra HRTEM were used to confirm the identification and usage of an Enterococcus species that lives in food for the synthesis of gold nanoparticles (Oladipo

et al., 2017). Extracellular proteins from Escherichia coli were employed to create anisotropic gold nanoparticles by Veeraapandian et al. (2012) (Veeraapandian et al., 2012). When it comes to the size and structure of AuNPs, the amount of protein present has a significant impact. Extracellular proteins operate as a capping agent for nanoparticles, increasing their shelf life and improving their stability. When it comes to the size and structure of AuNPs, the amount of protein present has a significant impact. Extracellular proteins operate as a capping agent for nanoparticles, increasing their shelf life and improving their stability. Manjunath et al. (2017) produced gold nanoparticles using a fungal endophyte, *Cladosporium cladosporioides*, isolated from the seaweed Sargassum wightii (M et al., 2017). For the reduction of gold metal salts into gold nanoparticles, it was found that the NADPH-dependent reductase enzyme was responsible for the utilisation of phenolic compounds. AuNPs were synthesized by Lee et al. (2015) utilizing extracts from the mushroom Inonotus obliquus, which did not require the use of hazardous chemicals (K. D. Lee, Nagajyothi, Sreekanth, & Park, 2015). Researchers made AuNPs from extracts of Gracilaria corticate, a marine red alga as reducing agents (Naveena & Prakash, 2013). Sharma et al. (2014) reduced and stabilized AuNPs using the dried biomass of *Lemanea fluviatilis* (Sharma et al., 2014). Debnath et al. (2016) synthesized gold nanoparticles from dried biomass of lichens found in the alpine region of the Eastern Himalayas (India) at high altitudes, without the use of foreign stabilizing and reducing agents (Arriagada et al., 2016). To compare the antioxidant properties of the two gold nanoparticles, those produced from Acroscyphus sp. lichen possessed prismatic and multiplied twinned quasi-spherical shapes, while those made from Sticta sp. algae were only multiply twinned.

DPPH radical-induced free radical scavenging was investigated in both light and dark settings using a gold nanoparticle (AuNP) attached to cellulose fiber (UKP), which is an

unbleached kraft paper (Bumbudsanpharoke, Choi, Park, & Ko, 2015). Surface functionalization of AuNPs coated with polyethylene glycol PEG and the antioxidant salvianic acid A (Au@PEG3SA) (Figure 2.9) was successfully performed and their antioxidant activities were evaluated. With the addition of Au@PEG3SA, the Radical scavenging activity rate was nine times higher than with the pure salvianic acid. In vitro and in vivo studies used stopped-flow analysis, laser scanning confocal microscopic inspection, and the thiobarbituric acid reactive substance assay to study the kinetic behaviour of radical-scavenging activity primarily exerted by scavenging oxygen-centered free radicals and other ROS based on the findings, antioxidant-functionalized AuNPs have a more potent ROS scavenging impact that can be used in living cells (Libo Du et al., 2013).

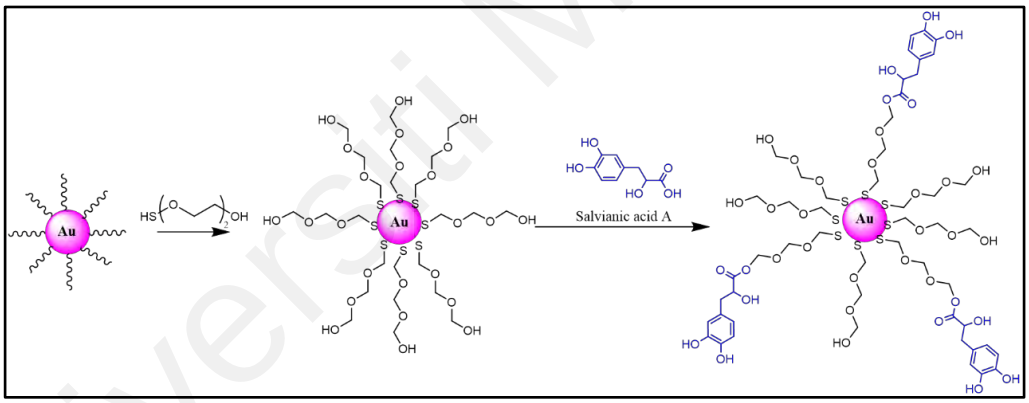

Figure 2.9 AuNPs (Au@- PEG3SA) Functionalized with Salvianic Acid A

Trolox, a vitamin E analogue, was used to produce functionalized AuNPs (Au@Trolox) via Au-S bonding aided by Trolox's thiol (SH) ligand in combination with AuNPs (Figure 2.10) (Nie et al., 2007). Additionally, the inclusion of AuNPs embedded in 3,6-dihydroxyflavone along with other nutrients such as lutein and selenium methly selenocysteine increased maximum inhibition by 87.13% for the reduction of DPPH, 85.11% for the reduction of OH, and 84.02% for the reduction of NO, with an overall

increase in antioxidant activity of 29.53%, 26.61%, 25.45%, and 26.07%, respectively (Medhe et al., 2014).

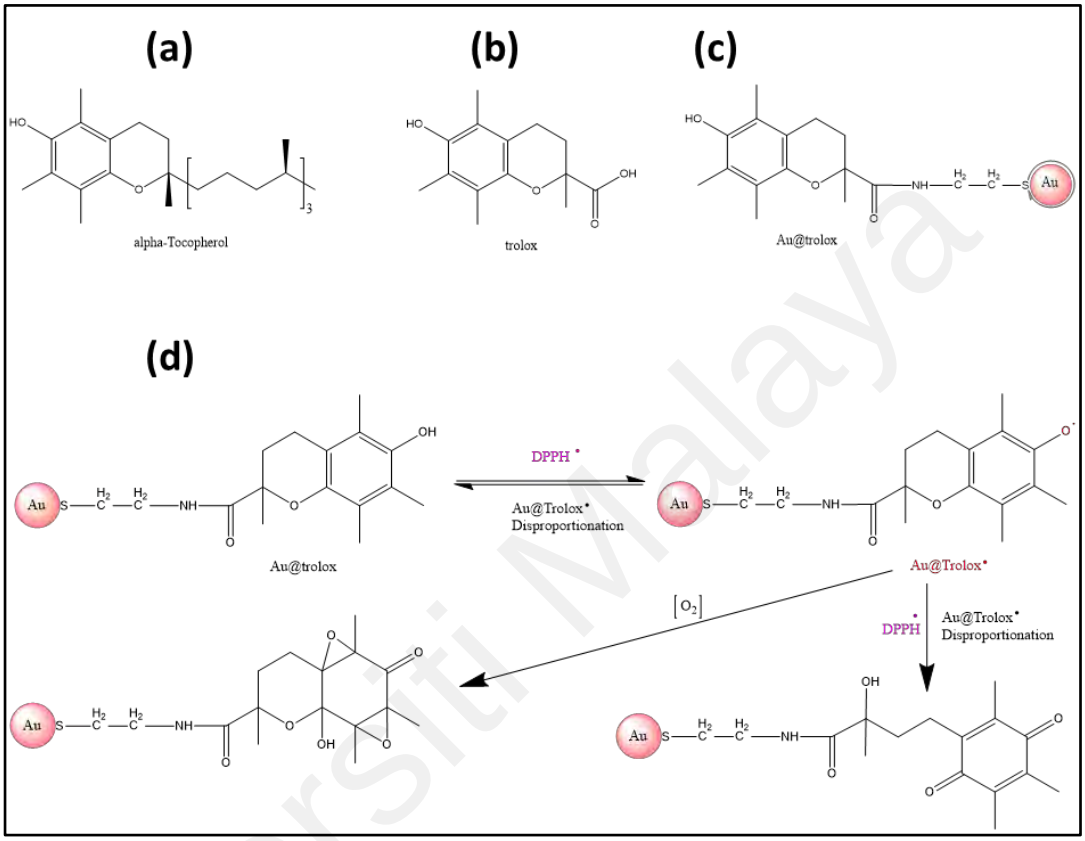

Figure 2.10 Molecular Structure of (a) Alpha-Tocopherol, (b) Trolox, (c) Trolox functionalized AuNPs, and (d) Reactions of Au@Trolox with DPPH• Radicals

2.1.4 SiO_2 Nanoparticles

Due to their mechanical stability. optical and chemical transparency, biocompatibility, and scalability, silica (SiO_2) nanoparticles have numerous applications in chemistry, medicine, pharmaceuticals, and biomedical research (Arriagada et al., 2016; Libo Du et al., 2013; Liberman, Mendez, Trogler, & Kummel, 2014). Nanosized SiO_2 particles can be immobilised with antioxidants to produce high-value hybrid nanocomposites. Nano-antioxidants were developed by Natural antioxidants, such as GA, were covalently

grafted onto the surface of commercially available well-characterized SiO_2NPs (8–30 nm in diameter).The ability of these nano-antioxidants to neutralise DPPH radicals was tested in a single assay (Figure 2.11). The SiO_2-GA nanoparticles execute quick H-atom transfer (HAT) and secondary/slow radical-radical coupling processes, which are two different types of scavenging reactions. The rapid HAT reactions of all SiO_2NPs can be compared to those of pure GA at stoichiometry ratios of 2 (nfast) (Deligiannakis et al., 2012). Morin (2′,3, 4′,5,7-pentahydroxyflavone, a flavonoid) functionalized mesoporous SiO_2NPs (MSN) were also tested for their antioxidant properties as HO• scavengers and O_2 quenchers. In homogeneous fluids and lipid membranes, the nanoantioxidant composite demonstrated a one-order-of-magnitude lower O_2 deactivation than morin, which, on the other hand, displayed a synergic effect on the antioxidant property. In homogeneous solvents and lipid membranes, compared to morin, the nanoantioxidant composite showed a one-order-of-magnitude lower inactivation of O_2 and a synergistic effect on the antioxidant property against HO•, with the effect being proportional to the amount of morin adsorbed. Mesoporous poly(tannic acid) (TA) crosslinked SiO_2NPs composites were tested for their antioxidant activities in the same way, with concentrations ranging from 50 mg to 1000 mg of TA, and reaction durations from 2 to 24 hours The composite's thermal stability decreased as the TA concentration and reaction time increased, resulting in particle sizes ranging from 237 to 445 nm.. After 12 and 2 h of reaction, the highest (1000 mg) TA contents and the largest surface area (872 m^2/g), respectively, were obtained for the highest TA contents, which was also proven to be the most effective antioxidant materials activity, with 14 ± 0.3 μg mL^{-1} GA equivalent total phenol content, and 68 ± 6 mM Trolox (a vitamin E analogue) equivalent (Sahiner et al., 2016).

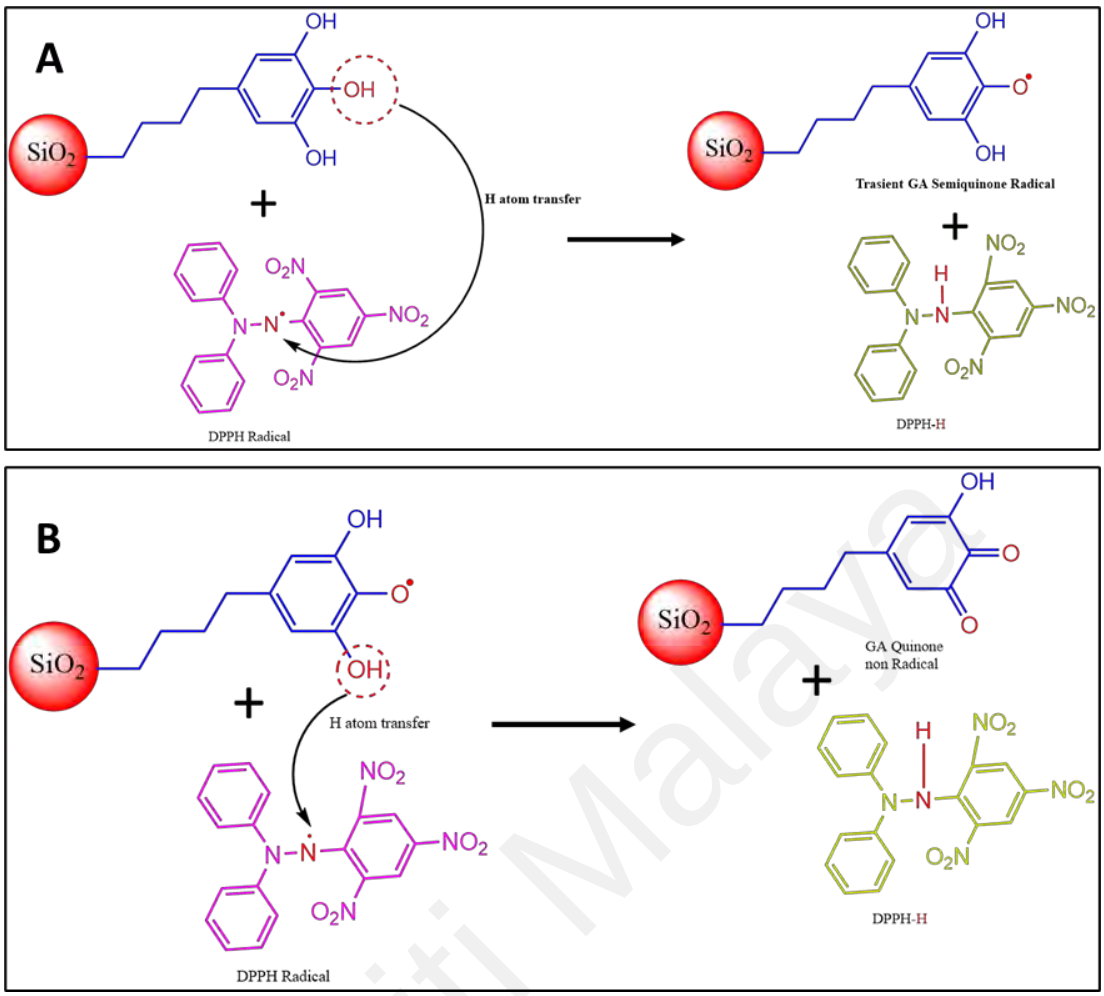

Figure 2.11 (A) Through the H atom Transfer (HAT) Process from the GA (Gallic acid) molecule, one DPPH Radical is Scavenged by Two SiO_2-GA nanoparticles, Resulting in the Formation of a Transitory GA radical. (B) HAT from the GA Semiquinone Results in the Formation of a Nonradical GA Quinone, which is Scavenged by SiO_2-GA nanoparticles.

However, MSN coated with caffeic acid (MSN-CAF) or rutin (quercetin 3-O-[-l-rhamnosyl-(1-6)-d-glucopyranoside]) was examined for its antioxidative stress properties. To prevent ROS generation and biological harm, these phenolic antioxidants can scavenge or donate hydrogen atom to free radicals because of the ortho- and meta-hydroxyl groups in the catechol structure they possess. Caco-2 and HaCaT cell lines were employed to evaluate ROS generation, activation of the Keap1-Nrf2 pathway and cell death induced by free and functionalized MSNs in two cellular models, respectively (Figure 2). The antiradical test (oxygen radical absorbance capacity (ORAC)) was also

used to investigate the antiradical characteristics of free or grafted antioxidant compounds. At 30.3 g/mL, the ORAC test shows that MSN-CAF and MSN-RUT had a Trolox equivalent level substantially higher than that of naked nanoparticles or amino-propyl functionalized silica nanoparticles ($MSNNH_2$), and the antiradical function of MSN-RUT was found to be 3.7 times more than that of MSN. However, MSN coated with caffeic acid (MSN-CAF) or rutin (quercetin 3-O-[-l-rhamnosyl-(1-6)-d-glucopyranoside]) was examined for its antioxidative stress properties. To prevent ROS generation and biological harm, these phenolic antioxidants can scavenge or donate hydrogen atom to free radicals because of the ortho- and meta-hydroxyl groups in the catechol structure they possess. Caco-2 and HaCaT cell lines were employed to evaluate ROS generation, activation of the Keap1-Nrf2 pathway and cell death induced by free and functionalized MSNs in two cellular models, respectively (Figure 2.12). The antiradical test (oxygen radical absorbance capacity (ORAC)) was also used to investigate the antiradical characteristics of free or grafted antioxidant compounds. At 30.3 g/mL, Antiradical activity of MSN-RUT was found to be 3.7 times greater than that of MSN-CAF, according to the ORAC test, which found that the Trolox equivalent level of MSN-CAF and MSN-RUT was significantly higher than that for naked nanoparticles or amino-propyl functionalized silica nanoparticles ($MSNNH_2$) (Ebabe Elle, Rahmani, Lauret, Morena, Bidel, Boulahtouf, Balaguer, Cristol, Durand, Charnay, et al., 2016).

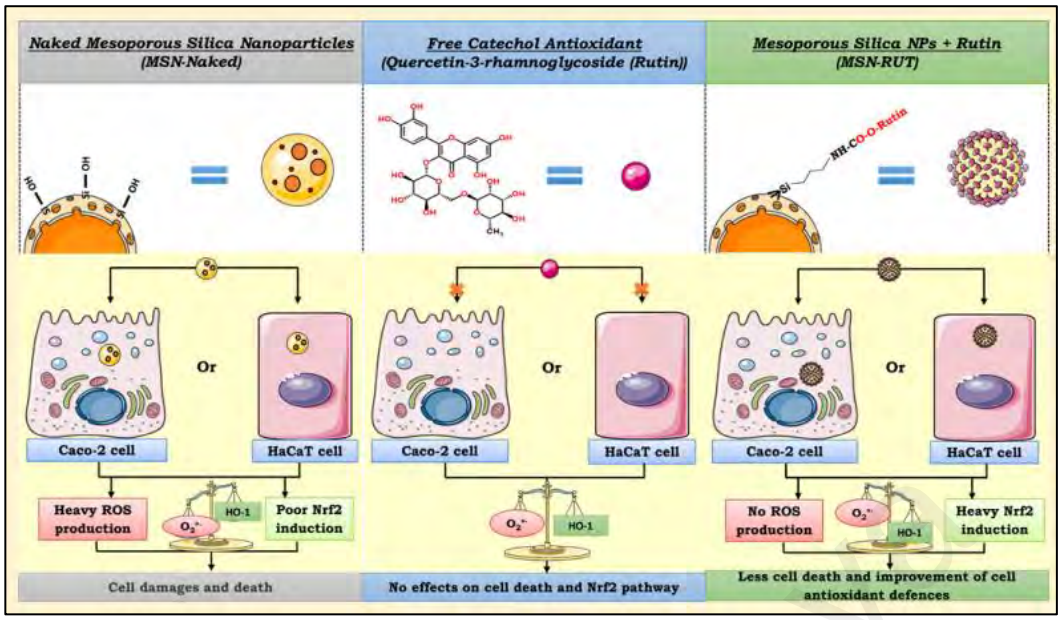

Figure 2.12 Effects of naked MSNs, free catechol antioxidant (Rutin), and MSNs-RUT on ROS generation, Nrf2 activation, and cell death

2.1.5 Silver Nanoparticles (AgNPs)

Silver nanoparticles (AgNPs) have a significantly greater surface area when compared to chemically identical particles, which is due to their outstanding biochemical and catalytic activity (H. Kumar et al., 2020). Colloidal silver nanoparticles are agglomerated to create oligomeric clusters, which are then stabilized, in order to make AgNPs (H. Kumar et al., 2020). It is necessary to use biological catalysts (enzymes) in order to reduce the Ag+ ions, and various plant extracts can be used to create AgNPs with various antioxidant properties.It is necessary to use biological catalysts (enzymes) in order to reduce the Ag+ ions, and various plant extracts can be used to create AgNPs with various antioxidant properties as shown in Table 2.2. Patra et al. (2016) synthesized AgNPs at room temperature under light-exposed conditions using the aqueous watermelon rind component. Silver nanoparticles with potential antioxidant capabilities have been discovered in actinobacteria, and whole-cell biomass and cell free extract of *Streptomyces naganishii* MA7 and *Streptomyces griseorubens* AU2 have been used to create silver

nanoparticles with potential antioxidant characteristics (Baygar & Ugur, 2017; Shanmugasundaram et al., 2013). Antioxidant-functionalized AgNPs have been synthesized using fungal species such as Aspergillus versicolor ENT7, Cladosporium cladosporioides, and Pestalotiopsis microspore (Manjunath Hulikere & Joshi, 2019; Netala, Bethu, et al., 2016; Netala, Kotakadi, et al., 2016). Researchers have also discovered that *Ganoderma lucidium* is an important plant source of antioxidant functionalized AgNPs (Aygün, Özdemir, Gülcan, Cellat, & Şen, 2020; Poudel, Pokharel, K.C, Awal, & Pradhananga, 2017; Sriramulu & Sumathi, 2017). Venkatesan et al. (2016) synthesised silver nanoparticles using Ecklonia cava extracts (Venkatesan, Kim, & Shim, 2016). Ecklonia cava is a marine alga that has been identified as a source of phenolic compounds capable of acting as capping and reducing agents. AgNPs were synthesised using extracts of Parmeliopsis ambigua, Punctelia subrudecta, Evernia mesomorpha, and Xanthoparmelia plitti (Dasari et al., 2013). AgNPs produced from Clerodendrum phlomidis leaves extract have a ferric reducing potential of 1.63 AU, which is higher than the leaves extract alone (Sriranjani et al., 2016). The AgNPs produced from Clerodendrum phlomidis leaves had a higher scavenging activity (55.86 g/mL) than the extract (which had a higher IC50 value of 1920 g/mL). The DPPH radical scavenging activity of AgNPs was likewise discovered to be dose-dependent, with the highest inhibition (85.74 percent) being higher than that of the extract alone. AgNPs had a lower IC50 value (9.12 g/mL) than the extract (388.4 g/mL) and standard ferulic acid (182.8 g/mL), showing that they had good antioxidant properties. Das and colleagues discovered that AgNPs produced from Morus alba leaves extract improved DPPH scavenging activity to 47.81 percent, compared to 56 percent for conventional ascorbic acid at the same dose, in a study published in 2019. AgNPs mediated by plant extracts, on the other hand, demonstrated 95.08 percent ABTS+ scavenging activity, which is equivalent to the

95.51 percent at 100g/mL reported for the BHT standard, showing that they have a high scavenging capacity. AgNPs scavenged 64.04 percent of nitric oxide at 100 g/mL, compared to 45.72 percent and 88.62 percent for plant extract and gallic acid standard, respectively. On the other hand, when applied at a 100g/mL concentration, AgNPs demonstrated statistically significant superoxide scavenging activity of 81.92 percent, which was equivalent to 85.35 percent when applied to the tocopherol standard (D. Das, Ghosh, & Mandal, 2019).

Due to their extensive properties, AgNPs offer a plethora of medical science applications. When synthesizing AgNPs, numerous methods are used, including new green approaches, which can give environmentally friendly capping agents that aren't harmful and toxic (Vilas, Philip, & Mathew, 2016). Different green synthesis techniques were used, including lignin-capped silver nanoparticles (LCSN) (grafted on lignin with a spherical shape and a size range of 10–15 nm) (Marulasiddeshwara et al., 2017), In the presence of sunlight, *Sida cordifolia* leaf extract stimulated biogenic production of AgNPs (Srinithya et al., 2016), aqueous extract of *Clerodendrum phlomidis* L. leaves (Sriranjani et al., 2016), Seabuckthorn (SBT) leaves extracts employed AgNPs (SBT@AgNPs) (Kalaiyarasan, Bharti, & Chaurasia, 2017) and poly(vinyl alcohol) embedded AgNPs (PVA-AgNPs) (Teerasong, Jinnarak, Chaneam, Wilairat, & Nacapricha, 2017) have been found to have antioxidant activity.

2.1.6 Copper Oxide Nanoparticles

For nanoparticle synthesis, copper has lately caught interest because of its availability and desirable properties like as catalysis, electrical, and optical properties (Guajardo-Pacheco, Morales-Sánchez, González-Hernández, & Ruiz, 2010; Y. He, 2007; Xi et al., 2010). In modern technology, an important inorganic substance, copper oxide is widely

employed, especially for ceramics, catalysis, and superconducting applications. This material can also operate as electrode to degrade nitrous oxide with ammonia and oxidize carbon monoxide, hydrocarbon, and phenol to produce supercritical water (Motoyoshi et al., 2010). Cu_2ONPs with antioxidant properties synthesized by plant derived synthesis are summarized in theCu_2ONPs with antioxidant properties synthesized by plant-derived synthesis are summarised in the Table 2.2. Using leaf extract from *Cissus arnotiana*, Rajeshkumar and colleagues found that copper nanoparticles have similar radical scavenging properties as ascorbic acid (Rajeshkumar et al., 2019).

2.1.7 Iron Nanoparticles (IONPs)

The unique physiochemical properties of iron, such as its low toxicity, good magnetic properties, microwave absorption capabilities, and high catalytic activity make it crucial for nanoparticle synthesis (Guo, Wang, Tjiu, Pan, & Liu, 2012; Herlekar, Barve, & Kumar, 2014; Huber, 2005). The three types of iron nanoparticles are: Iron oxide nanoparticles (IONPs), Iron hydroxide nanoparticles (FeOOH), and zero-valent iron nanoparticles (INPs) (Babay, Mhiri, & Toumi, 2015; H. J. Kim et al., 2015; Saleh et al., 2008; Yang et al., 2008). These new technologies include hyperthermia, bio-separation and bioprocess intensification, ferrofluids for medication delivery and environmental remediation, food preservation and gene therapy, pigments, and thermal-ablation using lithium-ion batteries (Ebrahiminezhad et al., 2018). Table 2.2 indicates the antioxidant capacity of plant mediated INPs. Muthukumar and Manickam discovered in 2015 that As a capping agent, amaranthine and phenolic compounds present in the Amaranthus spinosus leaf extract mediated Iron nanoparticles have a high antioxidant activity (Muthukumar & Matheswaran, 2015).

The antioxidant properties of Fe_2O_3 nanoparticles have already been studied, and the theory behind it is based on the neutralization of free radicals by the transfer of an electron (Alves, Mainardes, & Khalil, 2016). Although numerous techniques, such as carbon coating, carboxymethyl-inulin, and poly(GA), modifying surface with gallic acid and incorporation of curcumin in magnetic-silk core-shell nanoparticles, were successful in tailoring Fe_2O_3 nanoparticles. The composites shown improved dispersibility and stability; they were examined for their efficient antioxidant characteristics, antibacterial activities, and targeted drug administration to specific organs, as well as their cytotoxicity and biocompatibility/hemocompatibility (Santiago-Rodríguez et al., 2013; Song et al., 2017; Márta Szekeres et al., 2015). Magnetically separable ligand-functionalized magnetite with the natural antioxidant gallic acid (GA) displayed antimicrobial and antioxidant activities (Figure 2.13).

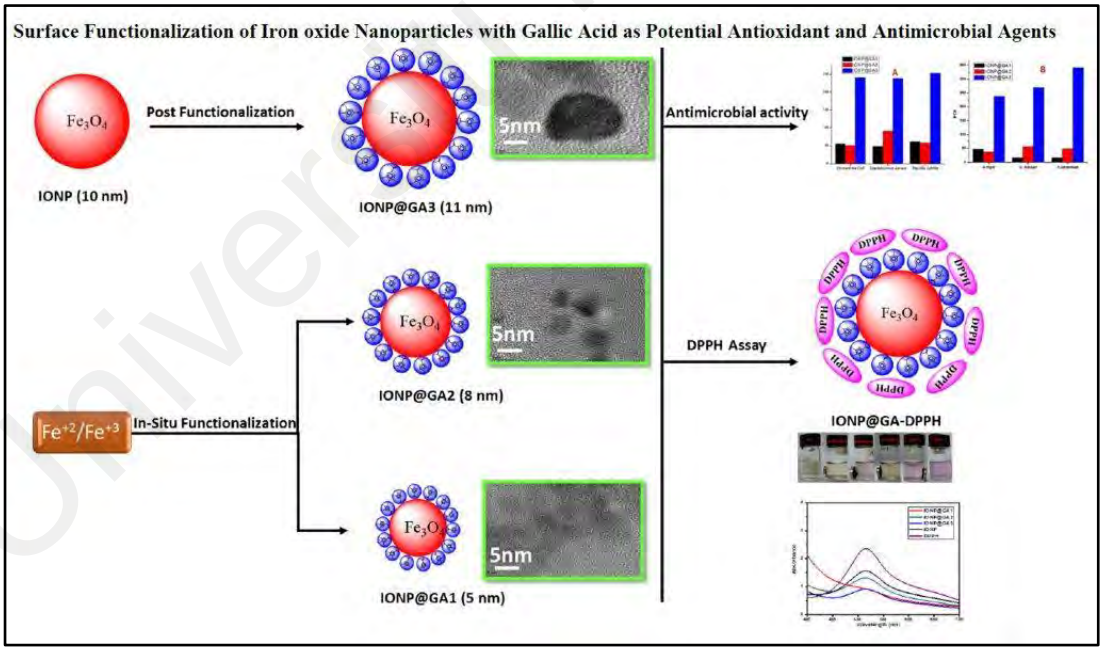

Figure 2.13 Surface Functionalization of IONP with Gallic Acid

2.1.8 Selenium Nanoparticles (SeNP)

As part of their research in 2013, Li and his colleagues developed 6-hydroxy-2,5,7,8-tetramethylchroman-2-carboxylic acid (Trolox) coated surface-functionalized selenium nanoparticles (Se@Trolox) with antioxidant activity (Morry et al., 2017). Furthermore, Se@Trolox was discovered to inhibit the activation of the AKT and MAPK signalling pathways, the buildup of reactive oxygen species (ROS) generated by cisplatin, and the phosphorylation of the p53 gene in HK-2 cells after DNA damage (Morry et al., 2017).

The antioxidant capability of plant-derived nickel oxide nanoparticles is demonstrated in Table 2.2.

2.1.9 Bimetallic Nanoanyioxidants

The ability to scavenge ROS or RNS was studied in various combinations of bimetallic nanocomposites in addition to antioxidant functionalized materials. The antioxidant activity of the stabilized, mono-dispersed Ag-Se bimetallic nanoparticles (Ag-Se) was examined in vitro using the 2,2′ azino-bis-ethyl benzthiazoline-sulfonic acid (ABTS), 3-(4,5-dimethylthiazol-2-yl)-2,5-diphenyltetrazolium bromide (MTT), and 2,2-diphenyl-1-picrylhydrazyl (DPPH) assays (Mittal et al., 2014). Gallic acid functionalized GA-SiO2@Ag particles demonstrated significantly increased proton-coupled electron transport at near-IR wavelengths (700–1100 nm) when seen at 700–1100 nm (PCET) (Sotiriou et al., 2016b).

It was found that silica-coated AuNPs (Si@AuNP) and PAPM (polyaspartic acid-based polymer micelles) were both glucose sensitive and efficient in targeting the cell. The nanocomposites were made in two steps: First, the primary amine-terminated nanoparticle (either Si@AuNP or PAPM) was functionalized with phenylboronic acid, and then vitamin C was chelated to the nanoparticle via chelation (Figure 2.14). The

resulting Si@AuNP and PAPM have hydrodynamic sizes of 40–50 nm and 40–80 nm, respectively, and contain vitamin C concentrations of 4–8 weight percent and 10–13 weight percent. At micromolar concentrations, vitamin C protects the cell, whereas at millimolar concentrations, Inducing oxidative stress and ultimately cell death through the production of H_2O_2.

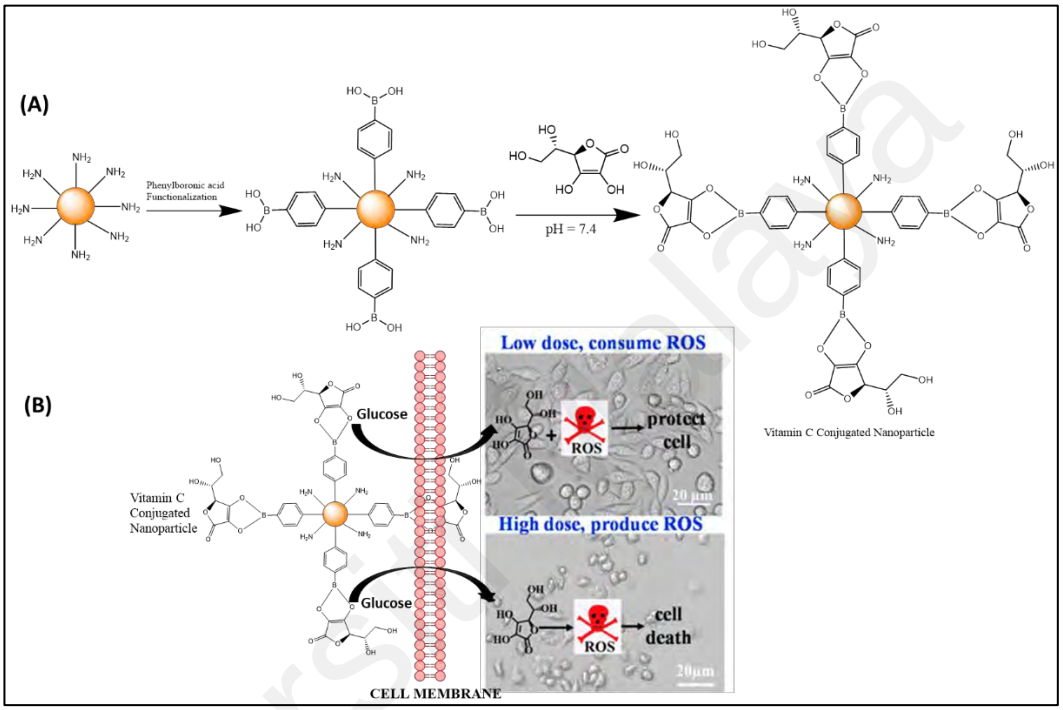

Figure 2.14 (A) Synthesis of Vitamin C Coupled Nanoparticles (Si@AuNP or PAPM): (B) Cellular Oxidative Stress at Concentrations of Micro and Millimolar Vitamin C

2.2 Antimicrobial Properties of Metal Based Nanoparticles

Over the last decade, numerous studies have been conducted to develop metal-based nanomaterials with antibacterial, antiviral, and antifungal properties to address pathogen-related disorders. Bacteria and other microbes pose a threat to humans, resulting in thousands of cases of pathogen-related diseases and illnesses each year. According to (Vos et al., 2017), given the fact that the last new class of antibiotics was introduced in 2003.

Many infectious infections, particularly those caused by multidrug-resistant bacteria, remain challenging to treat (Geisinger & Isberg, 2017). In the United States, The Centers for Disease Control and Prevention (CDC) estimates that antibiotic-resistant ESKAPE pathogens cause over 2 million infections and close to 23 000 deaths annually (Prevention, 2013), a group of pestilential bacterial pathogens that includes *Entercoccus faecium, Staphylococcus aureus, Klebsiella pneumoniae, Acinetobacter baumannii, Pseudomonas aeruginosa,* and *Enterobacter* species (Santajit & Indrawattana, 2016).

In the post-antibiotic era, where previously antibiotic-responsive illnesses become resistant to two or more classes of even the most effective medications, new ways for battling microbial diseases are urgently required (S. J. Lam et al., 2016).

Antimicrobial metal nanostructures in biomedical devices have gained substantial attention in both academia and the pharmaceutical industry as a possible microbicidal method for treating these extensively drug-resistant diseases (Jiang, Lin, Taggart, Bengoechea, & Scott, 2018).

In terms of antimicrobial nanomaterials, they can be categorized into those that are inherently antimicrobial, those that serve as carriers for antimicrobial compounds, and those that have both functional qualities.

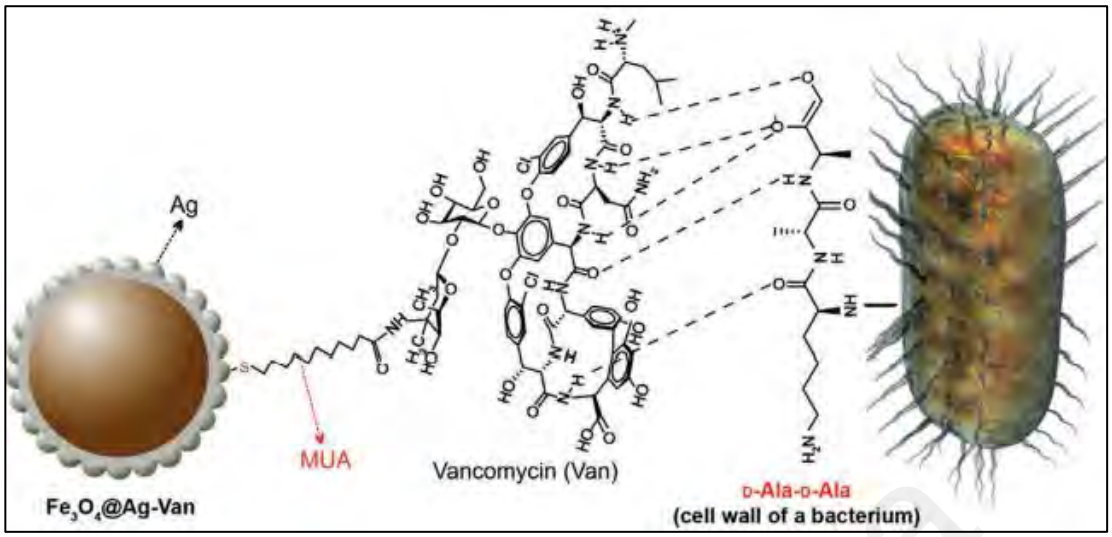

Figure 2.15 Fe_3O_4@Ag-Van Nanoparticle Attachment to Bacterial Cell Wall via Vancomycin-d-alanine-d-alanine (d-Ala-d-Ala) Interaction

As nanoparticles are increasingly used for antimicrobial applications, human exposure to them is unavoidable. A large proportion of the population are concerned about cytotoxicity as a result. In order to avoid harmful side effects in humans, these nanomaterials have been specifically designed to interact with cells.

Figure 2.16 Potential of Antimicrobial Nanomaterials in Combating Infections in Different Parts of the Human Body

Biomedical applications of nanotechnology for antimicrobial therapeutics are mainly academic research and at best preclinical; there are few examples of nanoparticle-containing wound-dressing, catheters, bone cements and cardiovascular implants and dental restorative materials that are currently available for clinical use. Although nanometals could have a huge impact on the fight against human infectious illnesses, they are still in their infancy. There are numerous uses for Ag nanoparticles, which have a long history in treating local infections on a topical basis (L. Ge et al., 2014).

But there are ways to change the biological activity of nanometals so that they can introduce new features or enhance the properties of present medicines. Since their constituent parts work well together, antimicrobial compounds based on metal-oxide

nanoparticles, alloys, and metal-doped and nanocomposites have received a great deal of attention as possible antimicrobial agents (Stankic, Suman, Haque, & Vidic, 2016). [352] These metal-based nanoparticles have the potential to overcome the cytotoxicity and agglomeration issues associated with pure metal and metal oxide nanoparticles. The antibacterial and poisonous properties of metal alloys vary with the composition of the alloy (Varkey, 2010).

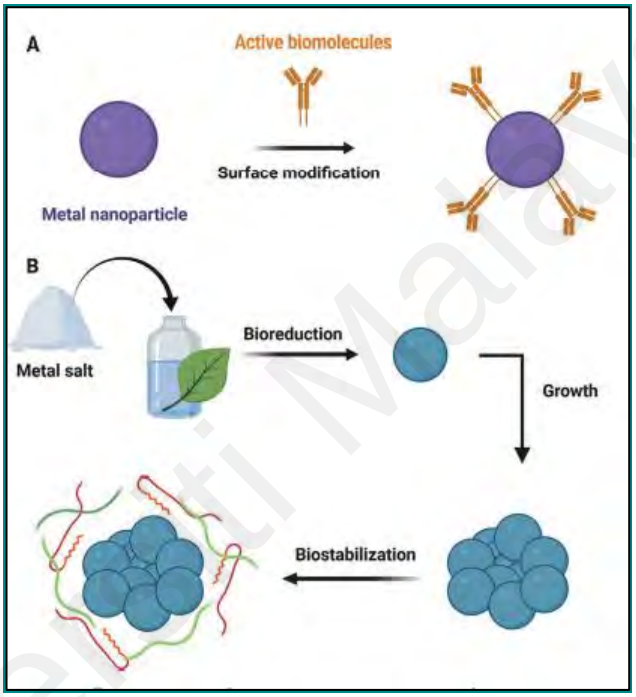

Figure 2.17 Different Ways to Change the Biological Activity of Nanosized Metals. Nanoparticles A) Surfaces are Altered by Biological Substances. B) The Production of Metal Nanoparticles employing Green Synthesis

In the field of biomedicine, iron oxide nanoparticles are particularly popular for their biocompatibility, colloidal stability, and surface engineering capabilities For in vivo applications, iron oxide is an excellent choice. Maghemite (Fe_2O_3) and hematite (hexavalent Fe_2O_3) are the most common types of magnetite (Wu, Jiang, & Roy, 2016). Additionally, iron oxide nanoparticles can be coated with synthetic or natural polymers,

organic surfactants, inorganic substances (e.g., silica), or bioactive molecules (e.g., bovine serum albumin) to improve their stability, biocompatibility, or antimicrobial properties, as well as their biocompatibility and antimicrobial properties. [260] Hybrid nanoparticles such as Ag–iron oxide, (Ebrahimi et al., 2016) Co–iron oxide, (Ahamed, Akhtar, Khan, Alhadlaq, & Alshamsan, 2016) Au–iron oxide, (Hoskins et al., 2012) Mn–zircon oxide, (Lopez-Abarrategui et al., 2016) and Cu–iron oxide have recently been used to improve functional properties (Liakos et al., 2016). Iron oxide nanoparticles' antibacterial and antifungal capabilities have been widely studied over the last decade.

CHAPTER 3: MATERIALS AND METHODS

3.1 Materials

Ferrous chloride tetrahydrate ($FeCl_2 \cdot 4H_2O$, Merck, Mendota Heights, MN, USA), ferric chloride hexahydrate ($FeCl_3 \cdot 6H_2O$, Sigma ≥ 97%, (Saint Louis, MO, USA)), Gallic acid (R and M), Quercetin (R & M) and ammonia solution (R and M, 28%) (Shanghai, China) were used as received without further purification. Analytical grade reagents were used during all experiments. Deionized water was used throughout the entire study.

The surface morphological features with a particle size of IONP@Q samples were studied using a JEOL JEM-2100F High-Resolution Transmission Electron Microscope with a field emission gun operating at 200 kV. Samples for TEM measurements were prepared by evaporating a drop of the colloid onto a carbon-coated copper grid. The mean particle size of the was calculated as from the HRTEM image from an observation of 100 particles using Gatan Digital MicroGraph software.

The identity of the phase and the degree of crystallinity of the magnetite samples were investigated using a PANalytical X-ray diffractometer (model EMPYREAN) with a primary monochromatic high-intensity Cu-Kα (λ =1.54060 A°) radiation. A range of 2θ (from 10.00 to 90.00) was scanned. FTIR of the samples was recorded using a Perkin Elmer FTIR-Spectrum 400. EDX was studied using EDX (INCA Energy 200 (Oxford Inst.)) under a vacuumed condition with a working distance of 6mm. The surface area method was employed to calculate the percentage composition. Raman spectra of the synthesized samples were analyzed using 514 nm Argon gas laser. The magnetism hysteresis loop measurement was conducted using Lake Shore vibrational sample magnetometer (VSM) in the solid state. The measurement was carried out under room

temperature where the magnetic field range was kept at −10 to +10 kOe. LaboGene's coolsafe freeze dryer was used for Lyophilization.

3.2 Synthesis

3.2.1 Synthesis of Magnetite Nanoparticles (IONP)

IONP was synthesized by combining ferrous and ferric chlorides at a 1:1.5 ratio. In 100 ml of deionized water, the salt mixture was dissolved, and ammonium hydroxide solution (3M) was added at a 5 ml/min rate until the pH reached 11. The mixture was continuously stirred at 600 rpm by using a mechanical stirrer, as shown in Figure 3.1. The reaction mixture was kept at 80 °C for 90 minutes with continuous stirring. The resultant black precipitate was isolated by magnetic decantation. The precipitates were thoroughly washed with DI water and ethanol and finally, it was freeze dried. The process of lyophilization or freeze drying involves the removal of water from a product after it has been frozen in order to allow it to transform directly from solid state into gaseous state (Libo Du et al., 2013). sample was frozen to a temperature below its "eutectic point" at -60 ºC and then freeze dried at under ultra-low pressure.

3.2.2 Synthesis of MPAO1 (2-(2-(2-hydroxyethoxy)ethoxy)ethyl 2-((3,5-di-tert-butyl-4-hydroxybenzyl)thio)acetate)

Triethylene glycol was added to a solution of 2-((3,5-di-tert-butyl-4-hydroxybenzyl)thio)acetic acid (2 g) in dry toluene (5 ml), p-Toluenesulfonic acid **(**PTSA) (0.02 g) was used as a catalyst. The reaction mixture was refluxed for 8 hours. Dean Stark apparatus was used to remove water produced during the reaction. The catalyst and unreacted materials were removed by filtration and then washed with distilled water. The mixture was dried by using anh. sodium sulphate. The precipitates obtained were filtered and dried at RT and recrystallized from the appropriate solvent.

Chemical Formula: $C_{23}H_{38}O_6S$, Molecular Weight: 442.61, ^{1}H NMR (ppm) (600 MHz, $CDCl_3$) δ 7.04 (s, 2H), 5.10 (s, 1H), 4.23 (s, 2H), 3.71 (s, 2H), 3.65 (s, 4H), 3.60 (s, 4H), 3.52 (s, 2H), 3.08 (s, 2H), 1.71 (s, 1H), 1.36 (s, 18H). ^{13}C NMR (ppm) (151 MHz, $CDCl_3$) δ 170.58, 152.74, 125.86, 72.51, 70.62, 70.36, 69.02, 64.14, 61.78, 36.82, 34.31, 32.57, 30.29.

3.2.3 Synthesis of MPAO2 (2-(2-(2-(2-hydroxyethoxy)ethoxy)ethoxy)ethyl 2-((3,5-di-tert-butyl-4-hydroxybenzyl)thio)acetate)

Tetraetylhene glycol was added to a solution of 2-((3,5-di-tert-butyl-4-hydroxybenzyl)thio)acetic acid (2 g) in dry toluene (5 ml), PTSA (0.02 g) was used as a catalyst. The reaction mixture was refluxed for 8 hours. Dean Stark apparatus was used to remove water produced during the reaction. The catalyst and unreacted materials were removed by filtration and then washed with distilled water. The mixture was dried by using anh. sodium sulphate**.** The precipitates obtained were filtered and dried at RT and recrystallized from the appropriate solvent.

Chemical Formula: $C_{25}H_{42}O_7S$, Molecular Weight: 486.66, ^{1}H NMR (ppm) (396 MHz, $CDCl_3$-D) δ = 7.16 (d), 7.10 – 7.06 (m), 5.08 (d), 4.08 (q), 3.75 (s), 2.01 (s), 2.01 (s), 1.39 (s), 1.39 (s), 1.22 (t), 1.22 (t). ^{13}C NMR (100 MHz, $CDCl_3$) (ppm) δ = 173.68, 171.27, 153.13, 136.08, 127.35, 125.95, 77.44, 77.33, 77.12, 76.80, 60.47, 36.86, 34.35, 32.44, 30.28, 21.09, 14.23, 1.06.

3.2.4 Synthesis of MPAO3 (2-(2-methoxyethoxy)ethyl 2-((3,5-di-tert-butyl-4-hydroxybenzyl)thio)acetate)

To a solution of 2-((3,5-di-tert-butyl-4-hydroxybenzyl)thio)acetic acid (2 g) in dry toluene (5 ml) was mixed with the respective Diethylene glycol monomethyl ether (MDEG). PTSA (0.02 g) was introduced with the above mixture, and the resultant

solution was refluxed for 8 hours. The water produced throughout the reaction was removed using the Dean-Stark system as shown in Figure 3.1. After cooling, the mixture was filtered and washed with distilled water to remove PTSA and unreacted EG, dried over anhydrous sodium sulphate. The precipitate was collected by filtration, dried at RT, and recrystallized from the appropriate solvent.

Molecular Formula: $C_{23}H_{38}O_5S$, Molecular Weight: 426.61, ^{1}H NMR (600 MHz, $CDCl_3$) δ 7.04, 5.09, 4.24, 4.23, 4.23, 3.71, 3.67, 3.66, 3.65, 3.59, 3.58, 3.57, 3.52, 3.51, 3.50, 3.46, 3.45, 3.44, 3.42, 3.07, 1.36, 1.13.

^{13}C NMR (151 MHz, $CDCl_3$) δ 170.60, 153.01, 135.99, 127.53, 125.86, 70.69, 69.82, 69.02, 66.70, 36.76, 34.31, 32.56, 30.30, 15.11.

3.3 Functionalization

3.3.1 Functionalization using In-Situ Technique

3.3.1.1 Synthesis of Organic IONP@GA1

Ferrous chloride and ferric chloride with a molar ratio of 1:1.5 was dissolved into 100 mL deionized water, followed by the addition of 1 g GA. 3.0 M of ammonium hydroxide solution was added 5.0 mL min^{-1} into the solution at 600 rpm stirring speed to reach a final pH 11. The reaction was conducted at 80 °C under oxidizing environment with continued stirring for another 90 min. The resultant black precipitate was isolated by magnetic decantation. Lastly, the precipitate was rinsed with deionized water and ethanol, then freeze-dried.

3.3.1.2 Synthesis of Organic IONP@GA2

Ferrous chloride and ferric chloride with a molar ratio of 1:1.5 was dissolved in 100 mL deionized water. Ammonium hydroxide solution (3.0 M) was added at a speed of 5.0 mL min^{-1} into the solution at a stirring speed of 600 rpm to reach a final volume of 100 mL. One gram of GA was added to the reaction mixture. The reaction was carried out at

80 °C under an oxidizing environment with continued stirring for another 90 min. The resultant black precipitate was isolated by magnetic decantation. Finally, the precipitate was rinsed with deionized water and ethanol, then freeze-dried.

3.3.1.3 Preparation of organic IONP@Q1

Ferrous and ferric salts with a molar ratio of 1:1.5 were dissolved in 100 ml DI. Quercetin dihydrate (1g) was dissolved in 3ml of acetone. Subsequently, the quercetin solution was added to the ferrous/ferric solution with continues stirring. NH_4OH (3.0 M) was added dropwise (5mL min^{-1}) to the ferrous/ferric solution at 600 rpm until the solution has a final pH value of 11. The reaction was carried out at 80°C with continuous stirring for 90 minutes under the oxidizing environment. The resultant magnetite nanoparticles were washed thrice with DI water and acetone collected using an external magnet and dried using freeze drier.

3.3.2 Functionalization using Post Functionalization Technique

3.3.2.1 Preparation of IONP@Q2

Quercetin functionalized IONP were synthesized by the nanoprecipitation method (S. R. Kumar et al., 2014) with some modifications. Quercetin (0.5g) was dissolved in minimum amount of acetone. Then, 1 g of IONP were dissolved in 50 ml of DI and sonicated for 30 minutes. Quercetin solution was continuously added during sonication followed by stirring for 24 hours. The resultant magnetite nanoparticles were washed thrice with DI water and acetone collected using an external magnet and dried using freeze drier.

3.3.2.2 Synthesis of IONP@GA3

One gram of GA was mixed with the IONP and was kept under stirring for 24 h. The precipitate was rinsed with deionized water and ethanol, then freeze-dried.

3.3.2.3 Synthesis of IONP@AOx

The synthesized MPAO1 was dissolved in ethanol and was mixed with the ethanolic suspension of IONPs. To obtain IONP@AO1, the reaction mixture was sonicated for 20 minutes and then stirred for 24 hours. Deionized water and ethanol (C_2H_5OH) was used to rinse the precipitates prior to freeze-drying thoroughly. To synthesize IONP@AO2, the same process was repeated with MPAO2. Figure 3.1 shows a schematic illustration of IONP functionalization.

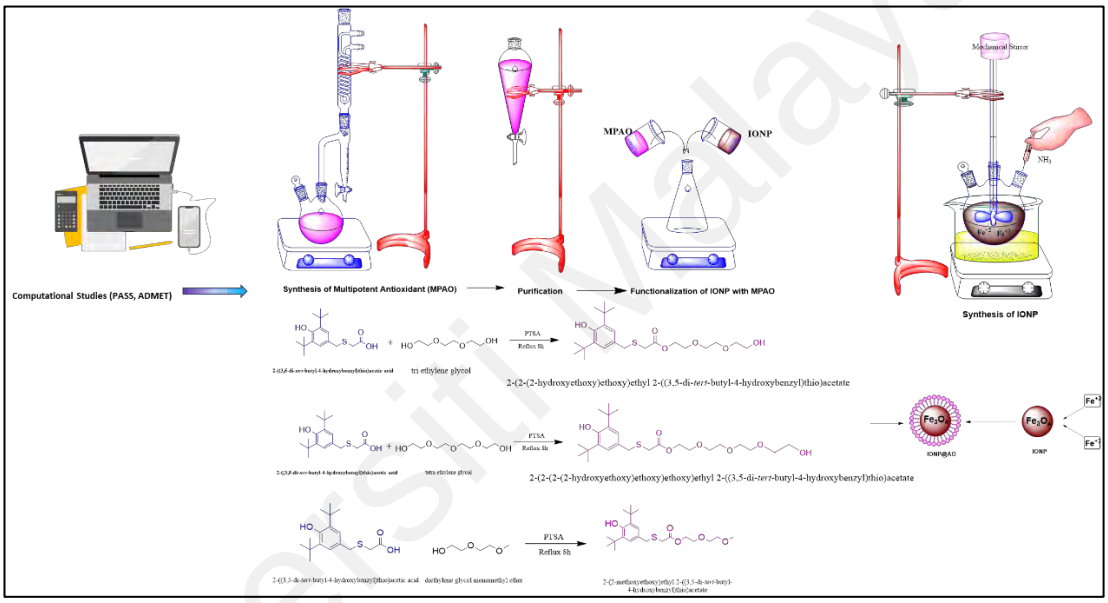

Figure 3.1 Functionalization of IONP with Multipotent Antioxidants

3.4 Antioxidant Activity

Various chemical based assays have been used to determine antioxidant activities. Based on the reaction involved, these assays can be classified into two main types. Hydrogen atom transfer (HAT) and electron transfer. In this present work, the DPPH assay involving electron transfer was selected to study the antioxidant activity of functionalized magnetite nanoparticles (Sotiriou, Blattmann, & Deligiannakis, 2016a).

The antioxidant activity was determined by using a standard DPPH method with some modification (Deligiannakis et al., 2012; Sotiriou et al., 2016a). Sample stock suspensions in methanol (300 µL) and 1 mL of methanolic solution of DPPH (0.2 mM) were mixed in a 1 cm quartz cuvettes. Absorbance measurements were taken after 30 min. The decrease in absorbance at 517 nm was observed continuously. All the experiments were duplicated. All the measurements were taken within exactly 30 min after mixing the sample with DPPH solution. The radical scavenging activity was calculated using Equation (1):

$$\text{Percentage of Inhibition (\%)} = \frac{(Ac - As)}{Ac} \times 100 \quad (1)$$

In which *As* = the absorbance of the compounds/positive control and *Ac* = the absorbance of the control (DPPH solution). To determine the concentration required to achieve 50% inhibition (IC_{50}) of the DPPH radical; the percentage of DPPH inhibition for each compound was plotted against different concentrations.

3.5 Antimicrobial Activity

3.5.1 Determination of Antibacterial Activity

The antibacterial activities of the IONP@GA were estimated using the agar well diffusion method (Sahu et al., 2013). Precultures of *Staphylococcus aureus*, *Bacillus substilis*, and *Escherichia coli* were spread on the surface of nutrient agar (NA) agar and wells (diameter = 6 mm) were filled with 100 µL of the test samples (100 mg/mL) and incubated at 37 °C for 24 h. Sterile distilled water was used as a negative control. Positive controls used were streptomycin 100 mg/disc and ampicillin 100 mg/mL for Gram-positive and Gram-negative bacteria, respectively. The formation of the halo (inhibition) zone and the diameter of inhibition zones were determined to evaluate the antibacterial properties.

3.5.2 Determination of Antifungal Properties

For antifungal properties, all IONP@GA types were tested against *Aspergillus niger*, a filamentous fungus (multicellular); *Saccharomyces cerevisiae*, a yeast (unicellular); and *Candida albicans*, a yeast using the well diffusion method. Potato Dextrose agar (PDA) plates were inoculated with fungal strains under aseptic conditions and wells (diameter = 6 mm) were filled with 100 µL of the test samples (100 mg/mL) and incubated at 25 °C for 48 h. Sterile distilled water was used as negative control. The positive control used was nystatin at 100 mg/mL. The percentage of Inhibition (POI) of mycelia growth was calculated using Equation (2):

$$POI = \frac{R1 - R2}{R1} \times 100 \quad (2)$$

where

$R1$ = radius of the pathogen away from the antagonist.

$R2$ = radius of the pathogen towards the antagonist.

3.6 Computational Studies

PASS web server was used to investigate potential biological activities of MPAO. PASS is a useful tool for exploring possible bioactivities of organic molecules based on their chemical formula (Lagunin, Stepanchikova, Filimonov, & Poroikov, 2000). It employs two-dimensional molecular fragments known as multilevel neighbours of atoms (MNA) descriptors to imply that a chemical compound's biological activity is a function of its molecular structure. It calculates the prediction score for biological attributes based on the ratio of the probability of being active (Pa) to the probability of being inactive (Pi). A higher Pa value indicates that the biological feature is more likely to occur in a compound . The bioactivity of selected compounds was assessed using the Molinspiration

Cheminformatics server (http://www.molinspiration.com). In addition, fragment-based virtual screening, bioactivity prediction, and data visualisation are all supported by this programme. Lipinski's rule of five was applied to predict Adsorption Distribution Metabolism, Excretion and Toxicity (ADMET) and physicochemical properties.

CHAPTER 4: SURFACE FUNCTIONALIZATION OF IRON OXIDE NANOPARTICLES WITH GALLIC ACID AS POTENTIAL ANTIOXIDANT AND ANTIMICROBIAL AGENTS

4.1 Introduction

The role of antioxidants in maintaining healthy cells status is well-defined, with a very large amount of research and published articles (Armstrong, Bharali, Armstrong, & Bharali, 2013; Erica, Daniel, & Silvana, 2011; Patrick-Iwuanyanwu, Onyeike, & Adhikari, 2014; Urso & Clarkson, 2003; Wageeh A. Yehye et al., 2015). The endogenous antioxidant defense system is usually sufficient in handling free radicals in the body, while in disease developing-threshold circumstances, the critical need for exogenous antioxidants rises (Armstrong et al., 2013).

The fast-growing field of nanotechnology has recently presented a remarkable resolution that can even surpass exogenous dietary antioxidant sources (Armstrong et al., 2013). Nanoantioxidants constitute the upcoming antioxidant agents for therapeutic and industrial applications (Sandhir, Yadav, Sunkaria, & Singhal, 2015). Their powerful activity is believed to present more effective dominance over various Reactive Oxygen Species (ROS) (Sandhir et al., 2015).

Of late, researchers have investigated antioxidant activity of various metal-based nanocomposites, such as gold (BarathManiKanth et al., 2010; Esumi, Takei, & Yoshimura, 2003), platinum (Kajita et al., 2007; J. Kim et al., 2008; Moglianetti et al., 2016), iron (Paul, Saikia, Samdarshi, & Konwar, 2009; Marta Szekeres et al., 2013; Toth et al., 2014), nickel oxide (Saikia, Paul, Konwar, & Samdarshi, 2010), ceria (C. K. Kim et al., 2012; Niu, Wang, & Kolattukudy, 2011), and yttria (Erica et al., 2011; Schubert, Dargusch, Raitano, & Chan, 2006), for applications as nanoantioxidants. Magnetic IONPs owe protuberant antioxidant activity against oxidative damage-related diseases

(Blanco-Andujar, Ortega, Southern, Pankhurst, & Thanh, 2015; Chorny, Hood, Levy, & Muzykantov, 2010; Dorniani et al., 2012; Gupta & Gupta, 2005; Majeed et al., 2013; Tudisco et al., 2015; Zhu et al., 2015). However, there are several factors that strongly affect nanomaterials antioxidant activity for instance chemical composition, surface charge, particle size, and coating of the surface (Cîrcu, Nan, Borodi, Liebscher, & Turcu, 2016; E. L. G. Samuel et al., 2014; Sandhir et al., 2015; Sharpe, Andreescu, & Andreescu, 2011). The surface coating could be biocompatible, nontoxic and allow targeted drug delivery (Bhattacharya et al., 2014; T. Lam et al., 2016; Nasirimoghaddam, Zeinali, & Sabbaghi, 2015; Santiago-Rodríguez et al., 2013; Sodipo & Abdul Aziz, 2015; Tancredi, Botasini, Moscoso-Londoño, Méndez, & Socolovsky, 2015).

Gallic acid (GA) is a well-known powerful natural antioxidant constituent of various herbs (L. Li et al., 2005; Prakash, Singh, Mathur, & Singh, 2007). It has versatile applications in medicine, food and pharmaceutical industries because of its unique physiochemical characteristics, such as non-toxicity, biodegradability, abundant availability, and low cost. GA possesses multi-therapeutic protecting capabilities, as well as antioxidant, anti-inflammatory, anticancer, antitumor, antimicrobial, and antidiabetic properties (Adefegha, Oboh, Ejakpovi, & Oyeleye, 2015; Akiyama, Fujii, Yamasaki, Oono, & Iwatsuki, 2001; Locatelli, Filippin-Monteiro, Centa, & Creczinsky-Pasa, 2013; Seo et al., 2013; Stanely Mainzen Prince, Kumar, & Selvakumari, 2010). Surface functionalized nanomaterials have demonstrated that attachment of antioxidants results in increased antioxidant activity and bioavailability (Deligiannakis et al., 2012; Kojima, Shiraishi, Hisamatsu, Miyamoto, & Kajita, 2008). Previous studies have reported the successful functionalization of GA on silica nanoparticles surface, which was identified as an efficient nanoantioxidant (Deligiannakis et al., 2012; Sotiriou et al., 2016a). The

bimetallic (Ag-Se) nanoparticles functionalized with quercetin and gallic acid were used as antioxidant, antimicrobial, and antitumor agents (Mittal et al., 2014).

Superparamagnetic iron oxide has numerous applications, such as in Magnetic resonance imaging (MRI) (Zhu et al., 2015), drug delivery systems (Majeed et al., 2013; Tudisco et al., 2015), hyperthermia (Blanco-Andujar et al., 2015), immunoassay and tissue repair and detoxification (Mittal et al., 2014). Magnetic nanoparticles loaded with antioxidant enzymes (such as superoxide dismutase (SOD) or catalase (CAT)) have been used as in drug delivery system through magnetic guiding. Magnetically-responsive antioxidant nanocarriers can provide therapeutic guiding of high concentrations of antioxidants to specific locations with elevated levels of ROS (Chorny et al., 2010). Catalase-loaded magnetic nanoparticles showed rapid cellular uptake and provided increased resistance to oxidative stress damage induced by hydrogen peroxide (Chorny et al., 2010; Erica et al., 2011). Magnetic nanoparticles have been used for targeted enzyme therapy, which might be used in the treatment of cardiovascular diseases (Chorny et al., 2010; Lacramioara, Diaconu, Butnaru, & Verestiuc, 2016) that are related to oxidative damage (Erica et al., 2011). Recent studies revealed that iron oxide nanoparticles exhibited antioxidant properties and their activity increased with the decrease in particle size (Paul et al., 2009).

Biomedical applications need nano-sized particles with high magnetization value and narrow particle size distribution. Furthermore, these nanoparticles require a surface coating that must be biocompatible, nontoxic, and allow targeted drug delivery to a specific area. Nanoparticles can be stabilized by various protection strategies which could be organic coating, such as poly(ethyleneglycol) (Y. Li et al., 2015), polysaccharide (Santiago-Rodríguez et al., 2013), dodecanethiol-polymethacrylic acid (Majeed et al., 2013), and chitosan (Nasirimoghaddam et al., 2015), or a coating with an inorganic

coating such as silica (Deligiannakis et al., 2012), metal or non-metal, metal oxide or sulphide (Tancredi et al., 2015). This surface coating protects nanomaterials from agglomeration while at the same time functionalizing it (Bhattacharya et al., 2014; Sodipo & Abdul Aziz, 2015). The functionalized magnetic nanoparticles can bind to drugs, proteins, enzymes, antibodies, or nucleotides and can be directed to an organ, tissues, or a tumor using an external magnetic field (Chorny et al., 2010; Gupta & Gupta, 2005; Lacramioara et al., 2016; Laurent et al., 2008; Mittal et al., 2014).

In this study, we report on IONP functionalized with GA as diverse water-soluble antioxidants which have favorable therapeutic and industrial applications. The resulted IONPs@GA nano-antioxidant has advanced biocompatibility, hydrophilicity, and further synergistic organic-inorganic hybrid antioxidant properties. We investigated the influence of GA in the size-controlled synthesis process and the surface functionalization of Fe_3O_4 nanoparticles by the in situ oxidation-precipitation of ferrous hydroxide method. Prediction of biological activities of GA molecule at IONP surface was performed with the Prediction Activity Spectra of Substances (PASS) training set. Analytical results based on antioxidant and antimicrobial activities confirmed the predictions obtained by the PASS program.

4.2 Results and Discussion

4.2.1 Fourier-Transform Infrared Spectroscopy (FTIR) Analysis

The FTIR spectra of Iron oxide nanoparticles (IONP), In situ functionalized iron oxide nanoparticles IONP@GA1, IONP@GA2 and post-functionalized IONP@GA3 are illustrated by Figure 4.1 a. The peak at 550, 551, 554, and 554 cm^{-1} represent the characteristic Fe-O stretching of for IONP, IONP@GA1, IONP@GA2 and IONP@GA3, respectively (Márta Szekeres et al., 2015). Broad peak at 3100–3200 cm^{-1} refers to OH stretching of phenol. The peak at 1079, 1089, and 1078 cm^{-1} corresponds to Fe-O-C for sample IONP@GA1, IONP@GA2 and IONP@GA3, respectively. Peak at 1633, 1611,

and 1630 cm^{-1} confirms the presence of carbonyl group in IONP@GA1, IONP@GA2, and IONP@GA3, respectively.

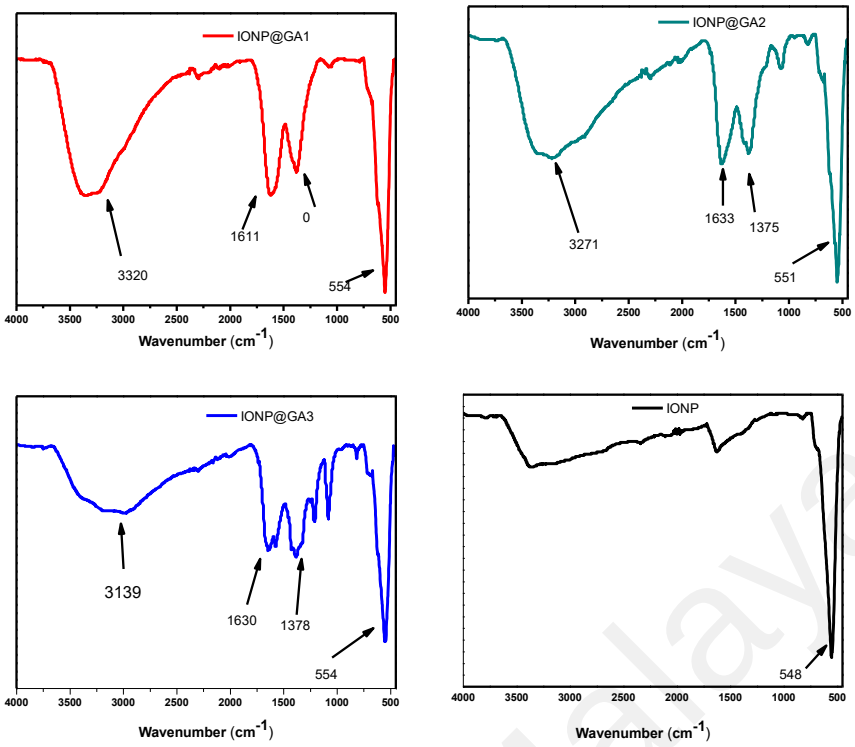

(a)

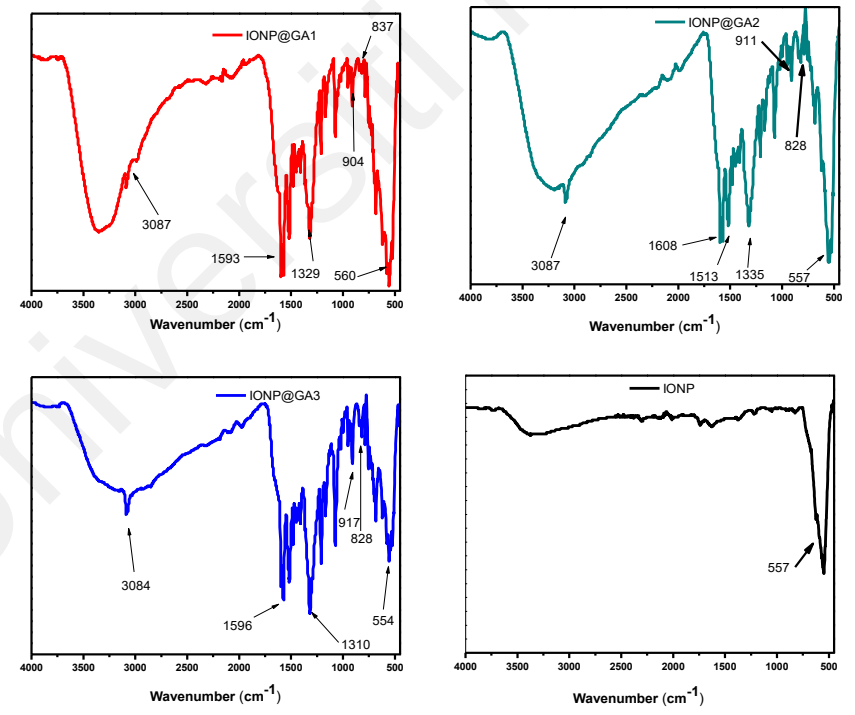

(b)

Figure 4.1. FTIR Spectra of (a) IONP@GA before DPPH Assay (b) IONP@GA after DPPH Assay

Further the surface reactivity was ascertained after 2,2-diphenyl-1-picrylhydrazyl (DPPH) assay. Figure 4.1 b shows the FTIR spectra of IONP@GA samples after DPPH assay. IONP@GA samples were mixed with the excess DPPH. The mixture was kept in the dark for 30 min and then washed thrice with ethanol. N-O stretching gave two peaks at 1530, 1310, 1513, 1335, 1530, and 1329 cm^{-1} for IONP@GA3, IONP@GA1, and IONP@GA2, respectively. This confirms the attachment of DPPH radical to the surface of IONP@GA. Not a single peak for DPPH radicals was appeared for IONP.

4.2.2 Raman Spectra

Raman spectra of IONP@GA samples are shown in Figure 4.2. The structural phase of the synthesized nanoparticles is further supported by Raman spectroscopy that shows the band absorption at 671 cm^{-1} (A1g) is for magnetite (De Faria, Venâncio Silva, & De Oliveira, 1997). In addition to main band absorption at 671 cm^{-1}, all the samples show peaks at 466 cm^{-1} (T2g) and 348 cm^{-1} (Eg) of magnetite. Moreover, the Raman spectra also confirmed the absence of maghemite (Francisco et al., 2011; Shebanova & Lazor, 2003).

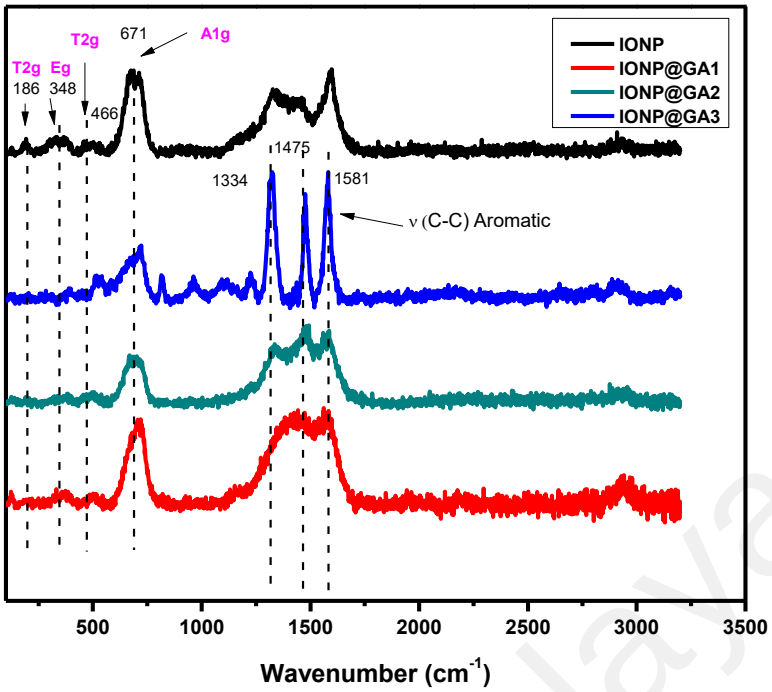

Figure 4.2 Raman Spectra of IONP@GA

4.2.3 X-ray Diffraction(XRD) Analysis

The XRD peak patterns of unfunctionalized and functionalized iron oxide nanoparticle are illustrated by Figure 4.3. XRD reflections shows pure magnetite nanoparticle with cubic inverse spinal structure in all the samples (JCPDS No. 82-1533) (Dorniani et al., 2012). Further, diffraction peaks for magnetite appeared at the 2θ value of 25°, 30°, 43°, 57°, and 63°, correspond to [311], [220], [400], [422] and [440] lattice planes, respectively. The absence of superlattice diffractions at [210], [213] and [300] confirms that maghemite is not present in any sample. Moreover, XRD data confirms that coating did not affect the phase of iron oxide.

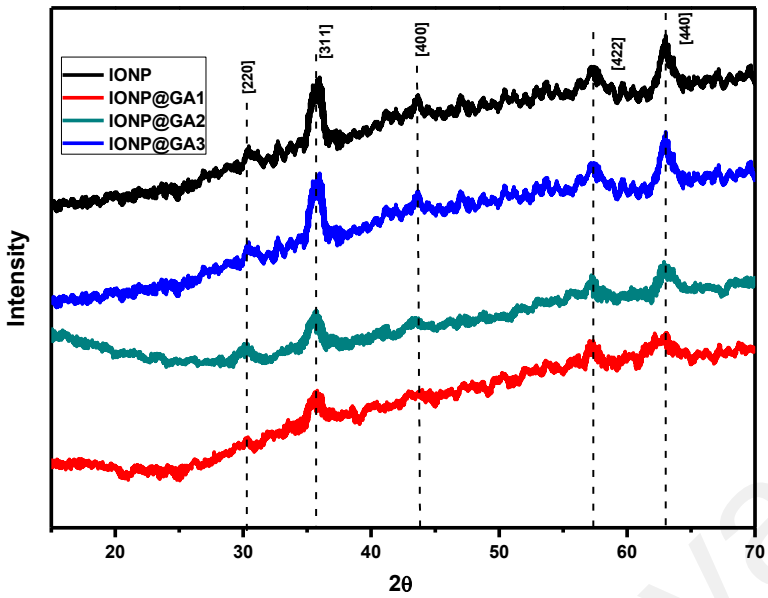

Figure 4.3 XRD spectra of Unfunctionalized and Functionalized IONP

4.2.4 Morphological Characterization

The morphology of the synthesized IONP@GA was analyzed using High Resolution Transmission Electron Microscopy (HRTEM). Figure 4.4 shows the HRTEM image with size distribution for GA functionalized magnetite nanoparticles. The average size for IONP@GA1, IONP@GA2, and IONP@GA3 and IONP are 5, 8, 10.8 and 10.0 nm, respectively (Figure 4.4 b,d,f,h). It is clear from the image that the particles have spherical shape with uniform size distribution. Crystal lattice fringe spacing of 0.26 nm, corresponding to the [220] lattice planes in cubic iron oxide nanoparticles (Iyengar et al., 2014). The agglomeration of nanoparticles occurs due to the magnetic behavior of the particles.

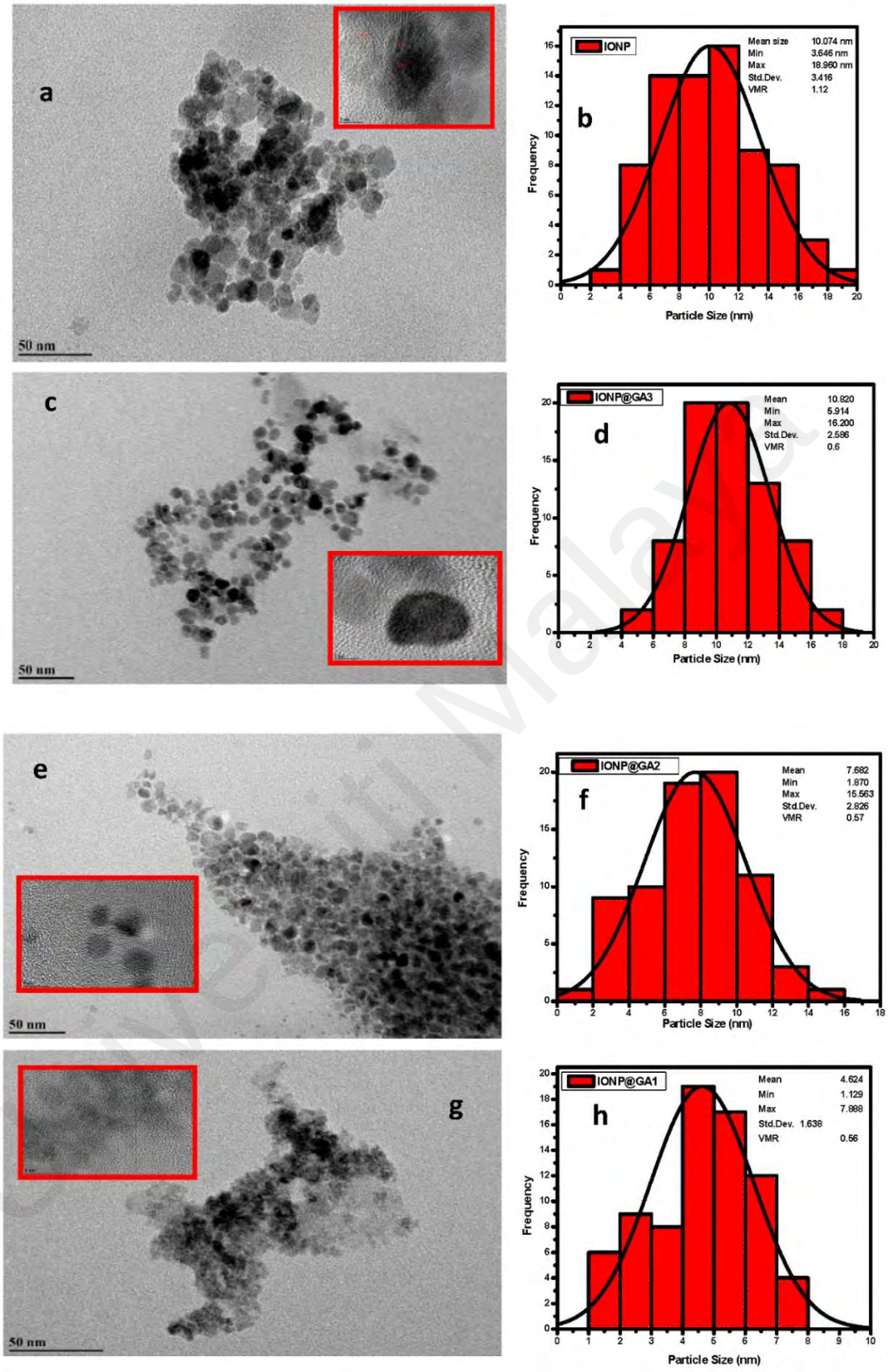

Figure 4.4 HRTEM images (a,c,e,g) and Particle Size Distribution (b,d,f,h) of IONP@GA

The in situ functionalized IONP@GA1 and IONP@GA2 have ultra-small particle size as compared to IONP and post functionalized IONP@GA3 as shown in Figure 4.4. This reveals that the in-situ functionalization process followed in this study has a strong and successful size-control effect, which is significantly lower than other synthesis routes.

The remarkable size-control effect exerted by GA on in situ-functionalized IONP, can be attributed to iron cations chelate with GA (Figure 4.5) to form blue-black ferrous/ferric gallate (Krekel, 1999; Toth et al., 2014). In the same context, GA had minimized the IONP agglomeration, which might be due to either GA bonding site, which strongly coordinates with the IONP surface by forming a monolayer on the IONP surface, which leads to a decrease in magnetic dipole-dipole interaction among the aggregates during formation of nanoparticles and/or the presence of the bulky phenyl group in GA provides sufficient steric hindrance to minimize the IONP agglomeration. Moreover, GA has hydrophilic functional groups, which improves the solubility of IONP in polar solvents and could serve as potential H-bonding sites (X. Wang, Tilley, & Watkins, 2014). Overall, GA has proved an astounding ability to control particle size, solution stability, and hydrophilicity of the IONP nano-antioxidant system.

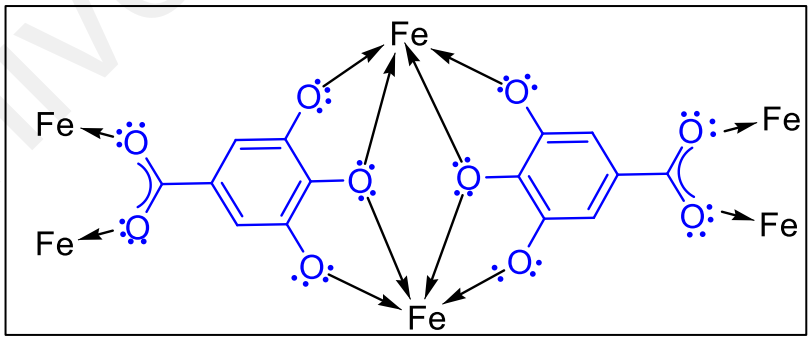

Figure 4.5 Proposed Structure of Iron Gallate

4.2.5 Magnetic Properties

Figure 4.6 shows the hysteresis loops as a function of the magnetic field at room temperature. The values of 64.19, 60.28, 53.43 and 43.92 emu g^{-1} were given for IONP, IONP@GA2, IONP@GA3, and IONP@GA1, respectively. The magnetic parameters, including saturation magnetization are shown in Table 4.1. The nanoparticles synthesized here are superparamagnetic with low magnetization values than the bulk magnetite (~92 emu g^{-1}) (Cornell & Schwertmann, 2006). Functionalized IONPs showed a decrease in saturation magnetization which was most likely due the decrease in saturation magnetization for functionalized IONPs was due to the presence of more organic contents and impurities on the surface of the magnetic nanoparticles (Dorniani et al., 2014; Dorniani et al., 2012; Ma, Qi, Maitani, & Nagai, 2007).

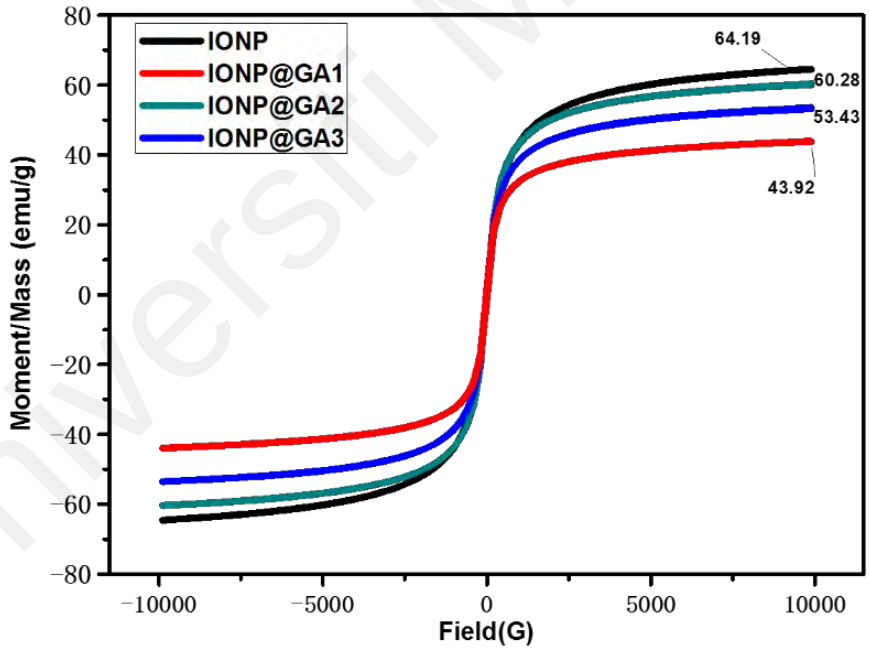

Figure 4.6 Magnetic Hysteresis Loops of IONP@GA

Table 4.1 Saturation Magnetizations of IONPs

Sample	*Ms* (emu g^{-1})
IONP	64.19
IONP@GA1	43.90

IONP@GA2	60.26
IONP@GA3	53.43

4.2.6 Energy Dispersive X-ray Spectroscopy (EDX) Analysis

Fe and O signals confirmed the presence of magnetite nanoparticles, while the C signals are derived from the organic matrix as shown in Table 4.2. N signals were also observed in sample IONP@GA1 and IONP@GA2 which might be due to formation of ferrous/ferric gallate during synthesis. The spatial distribution of the iron atoms observed from the mapping images, clearly indicates the uniform distribution of the atoms. Figure 4.7 a–d represents the EDX of IONP@GA1, IONP@GA2, IONP@GA3, and IONP, respectively, after conducting DPPH assay.

Table 4.2 EDX Elemental Composition (A) Before DPPH Assay (B) After DPPH Assay

Sample	A				B			
	Fe	O	C	N	Fe	O	C	N
IONP	69.6	39.4	-	-	77.5	21.2	1.3	-
IONP@GA1	62	30.2	7	0.6	62.6	29.5	7.2	0.8
IONP@GA2	65.6	29.1	4.8	0.4	63.7	29.7	6	0.6
IONP@GA3	58.7	30	10.8	-	61.5	26.4	11.7	0.3

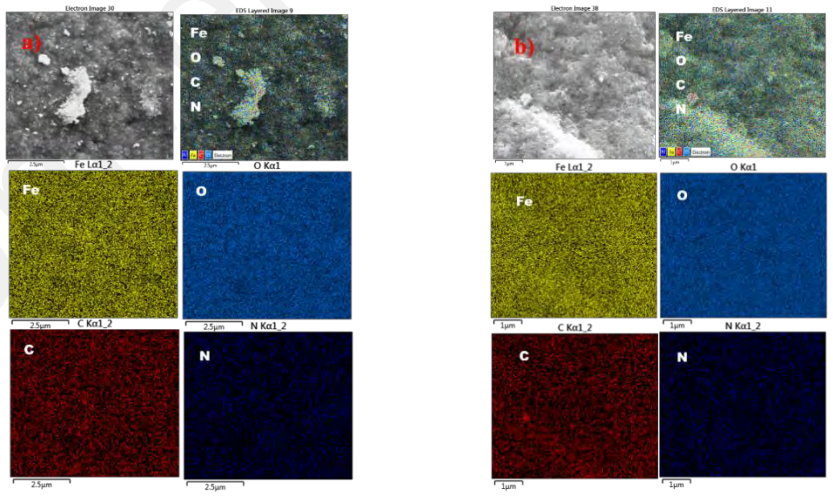

(**a**) (**b**)

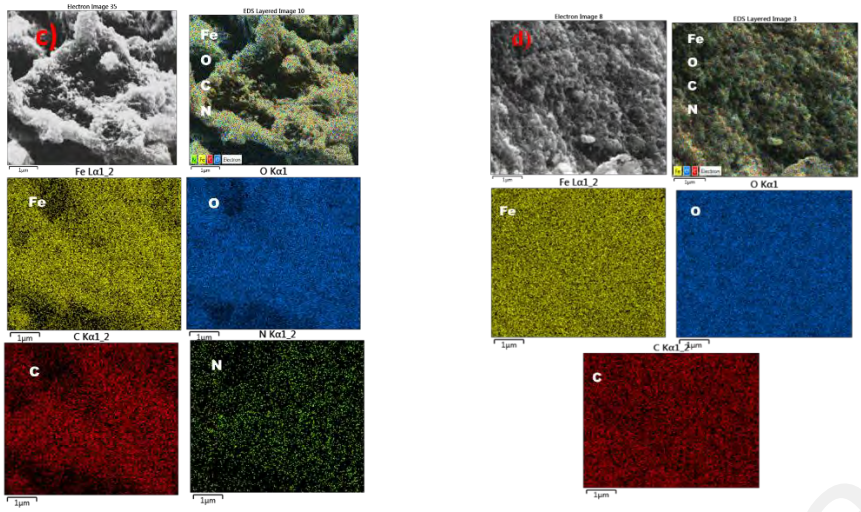

(c) (d)

Figure 4.7 FESEM image (a) IONP@GA1 (inset: EDX Elemental Map of Fe, O, C, and N); (b) IONP@GA2 (inset: EDX Elemental Map of Fe, O, C, and N); (c) IONP@GA3 (inset: EDX Elemental Map of Fe, O, C, and N); and (d) IONP (inset: EDX Elemental Map of Fe, O, C)

The EDX mapping after the DPPH assay, indicates an increase in the percentage of carbon and nitrogen, which could be strongly attributed to attachment of DPPH radicals on the surface of IONP@GA to form IONP@GA-DPPH, which is in agreement with the FTIR results. Nitrogen contents increased from 0% to 0.8%, 0.4% to 0.6%, and 0.6% to 0.3% for IONP@GA1, IONP@GA2, and IONP@GA3 respectively, while carbon contents increased from 7% to 7.2%, 4.8% to 6%, and 10.8% to 11.7% for IONP@GA1, IONP@GA2, and IONP@GA3, respectively. No change in nitrogen contents for unfunctionalized IONP was observed, which indicated that free radicals could not attach to the IONP surface.

4.2.7 Prediction Activity Spectra of Substances (PASS) of Biological Activity

PASS predictions have been applied to design of new potent free radical inhibitors in phenol series as potential antioxidant drugs (Kareem et al., 2015; Poroikov et al., 2003; Wageeh A Yehye et al., 2015). PASS provides simultaneous predictions over 4000 kinds of biological activity with mean accuracy of 95% (Anzali et al., 2001; A. Stepanchikova, A. Lagunin, D. Filimonov, & V. Poroikov, 2003). The outcome of prediction is available

Table 4.3 as list of activities with appropriate Pa (probability "to be active") to Pi (probability "to be inactive") ratio for GA. It is reasonable that only those types of activities may be revealed by the compound, which Pa > Pi (PharmaExpert., 2015).

Table 4.3 Predicted biological activity spectra of the GA on the basis of PASS prediction software

Biological Activity	Pa [a]	Pi [b]
Antioxidant	0.529	0.005
Free Radical Scavenger	0.579	0.007
Lipid Peroxidase Inhibitor	0.554	0.012
Anti-inflammatory	0.560	0.041
Antibacterial	0.420	0.026
Antibacterial, ophthalmic	0.255	0.005
Antifungal	0.255	0.050
Antifungal (Pneumocystis)	0.109	0.003

[a] Probability "to be active"; [b] Probability "to be inactive".

4.2.8 Antioxidant Activity

The color of the DPPH solution in the presence of the functionalized iron oxide changes gradually from deep violet to pale yellow, which provides the visual monitoring of the antioxidant activity of the nanoparticles. From the UV-VIS absorption curve in Figure 4.8, it can be inferred that the peak intensity of DPPH is lowering. The free radical scavenging percentage is calculated from the decrease in absorbance at 517 nm. In the DPPH scavenging assay, the IC50 value (Table 4.4) and the inhibition of stable DPPH free radicals of the compounds were found to be IONP@GA1 (2.7 ± 0.003 mg/mL; 61%), IONP@GA2 (2.2 ± 0.002 mg/mL; 59%) and IONP@GA3 (IC50 1 ± 0.003 mg/mL; 78%) at 10^{-4} M, which are 2–4 fold more than the unfunctionalized IONP (IC50 4.7 ± 0.002 mg/mL; 50%) (Table 4.4) as a reference in this assay. The DPPH scavenging of four samples was found to be in the order of IONP@GA3 > IONP@GA1 > IONP@GA2 > IONP. The free radical scavenging is most probably due to electron transfer from IONP@GA to free radicals located at the central nitrogen atom of DPPH. Enhanced free radical scavenging for IONP@GA is due to the synergistic effect of IONP and GA.

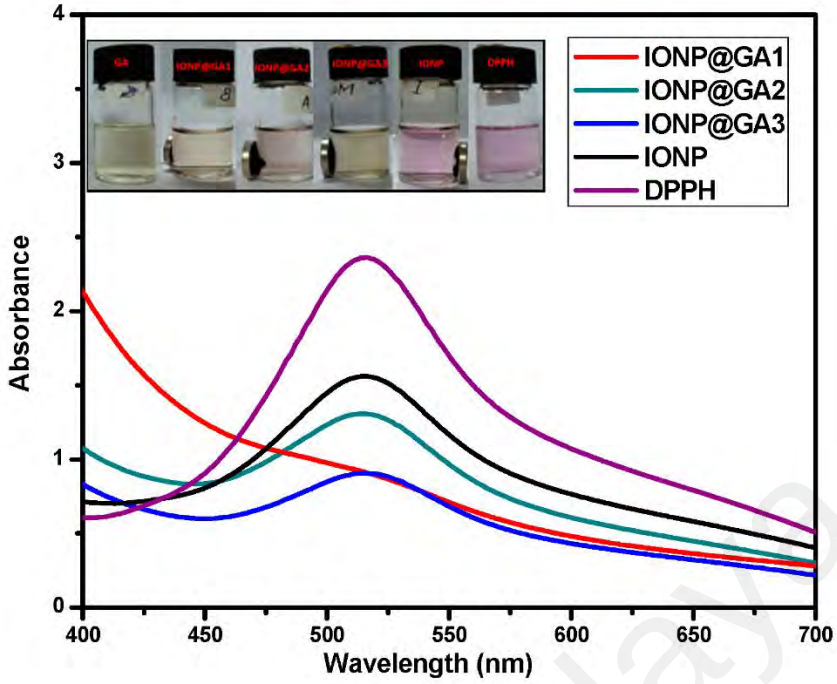

Figure 4.8 UV-VIS Spectra of IONP@GA

Table 4.4 IC50 of IONP@GA

IC50 [a] Values (mg/mL) ± S.E.M [b] and Max. Inhibition %			
Sample		**IC50 mg/mL**	**% Inhibition**
IONP@GA3	5 mg	1.00 ± 0.003	78
IONP@GA2	5 mg	2.2 ± 0.002	59
IONP@GA1	5 mg	2.7 ± 0.003	61
IONP	5 mg	4.7 ± 0.002	50

[a] IC50: 50% effective concentration; [b] S.E.M: standard error of the mean.

4.2.9 Antimicrobial Activity

4.2.9.1 Antibacterial Activity

Figure 4.9 A shows the agar well diffusion test results expressed as percentage inhibition of diameter growth (PIDG) of IONP at a concentration of 100 mg/mL. All three types of functionalized IONP@GA showed antibacterial activity on both Gram-positive and -negative strains. However, the highest growth inhibition percentages were observed upon using IONP@GA3, in which all bacterial strains scored high inhibition values. Thus, revealing its prominent and powerful bactericidal effect.

Generally, results showed a variable IONP@GA antibacterial activity among different bacterial strains. Such trend can be explained based on cell wall composition of each type. Upon administration of IONP@GA, bacterial growth inhibition is believed to occur through the penetration of functionalized IONPs into cells with subsequent cell wall damage by breaking β-1,4-glyosidic bond. Nevertheless, nano-antioxidant IONP@GA compounds were proven to exhibit antibacterial activity on both bacterial strains. In addition, nanomaterials have been demonstrated to influence bacterial metabolism through a number of mechanisms, including reactive oxygen and metal ion dissolution (Padmavathy & Vijayaraghavan, 2011; Yu et al., 2014). NPs can also affect the metabolite levels of bacterial communities (Pan et al., 2015).

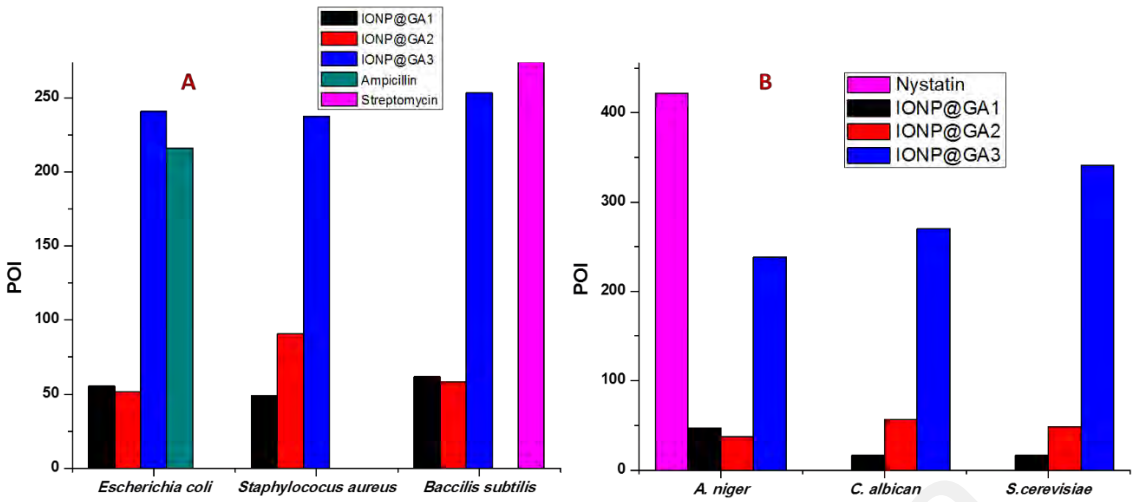

Figure 4.9 Percentage of Inhibition (POI) of (A) Bacterial Growth and (B) Mycelia Growth of Fungi, after Treatment with IONP@GA

4.2.9.2 Antifungal Activity

The antifungal activity of IONP@GA against *Aspergillus niger, Candida albicans*, and *Saccharomyces cerevisiae* was investigated using the well diffusion method. Results, as presented in Figure 4.9 B, show a potent antifungal activity of tested compounds among all fungi strains used. The highest percentage of inhibition (POI) was obtained by utilizing IONP@GA3 compound. Together with its antibacterial activity, these results confirm the higher antimicrobial activity of IONP@GA3 compared to other functionalized IONP compounds. The mechanism responsible for antifungal activity seen, can be assumed to involve the attachment of nanoparticles to the respiratory sequence, which leads to cell death (Rudramurthy, Swamy, Sinniah, & Ghasemzadeh, 2016).

With reference to the above discussed results, the synthesized nano-antioxidant IONP@GA in this study had proven to own strong antimicrobial properties, that potentiate various biomedical applications. Yet, the astonishing antioxidant activity of IONP@GA compounds may find further applications in industrial fields. The proposed potential application of nanomagnetite in industries as illustrated in Figure 4.10. We

propose that controlling the size and antioxidant activity is a promising method for improving industrial based materials. These magnetic nanoantioxidants have many advantages over conventional antioxidants. In addition to the GA functional moiety that enables less toxic, biocompatible coating with fine size-control, the mixture of IONP@GA and toxic materials (IONP@GA-ROS) formed during the reaction of nanomagnetite with ROS can be easily removed from the system by a magnet and can be recycled.

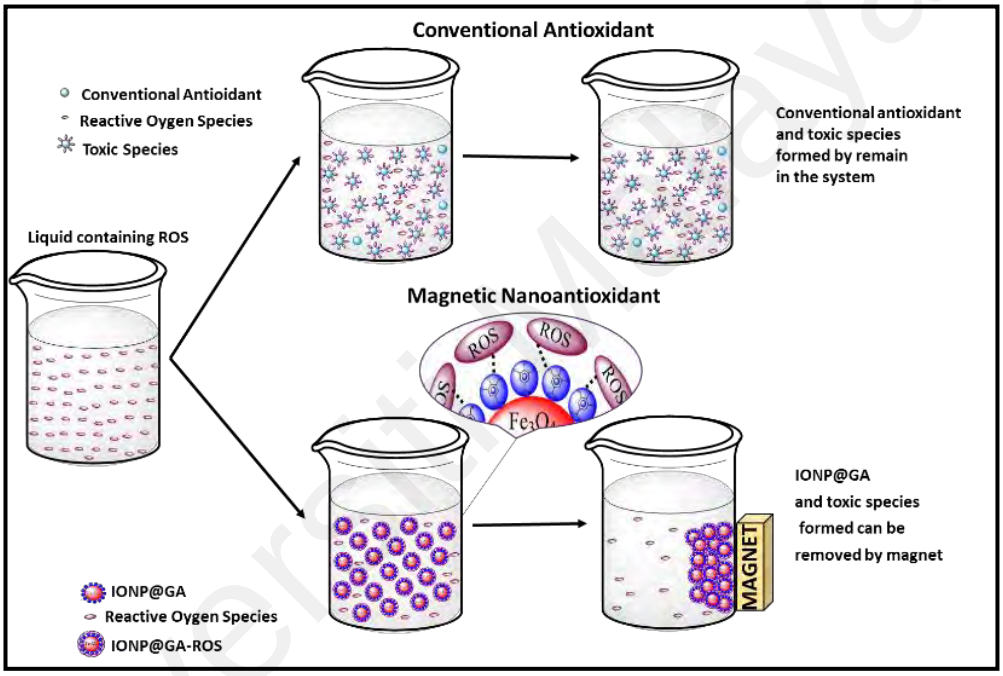

Figure 4.10. Proposed Potential Applications of IONP@GA in Industry

4.3 Discussion

GA functionalized organic nanomagnetites have been successfully synthesized via in situ and post-functionalization techniques. The average particle size is 5 and 8 nm for in situ-functionalized nanomagnetite IONP@GA1 and IONP@GA2, respectively, while it is 11 nm for post-functionalized IONP@GA3. The particle size decreases in order of IONP@GA3 > IONP > IONP@GA2 > IONP@GA1. The addition of GA during in-situ synthesis had controlled the particle size of IONP, thus efficiently overcoming a critical

obstacle in nano-antioxidant synthesis. PASS-predicted antioxidant values and other biological activities for the GA indicated that the GA-functionalized IONP surface could be likely to reveal these activities, in addition to the iron oxide activities and its biocompatibility as multi-purpose tools for guided drug delivery and bioimaging. The DPPH scavenging of the four samples is found to be in the order of IONP@GA3 > IONP@GA1 > IONP@GA2 > IONP. The in situ and post functionalization methods successfully improved the free radical scavenging of IONP to be more than 2–4 fold. The present investigation highlights the synergistic effect of the magnetite and GA, which leads to the enhancement of the free radical scavenging capacity of IONP@GA. The synthesized IONPs@GA samples are hydrophilic and exhibited greater antioxidant activity and degraded the DPPH radicals efficiently. FTIR and EDX techniques confirmed that IONP@GA is scavenged the DPPH radicals and yielding IONP@GA-DPPH composite suggesting that free radicals can be easily removed from the system by magnet and can be recycled. Finally, IONP@GA showed potential antimicrobial activity (antibacterial and antifungal) effects on strains tested, probably through the destruction of membrane integrity; therefore, it was concluded that IONP@GA has considerable antimicrobial activity, which is promising for further clinical applications. The methodology used here can be employed for synthesizing organic nanocompounds with other antioxidants that are magnetically separable, efficient, low cost and may have potential applications in polymer, cosmetics, biomedical and food industry.

CHAPTER 5: MAGNETICALLY DIRECTED ANTIOXIDANT AND ANTIMICROBIAL AGENT: SYNTHESIS AND SURFACE FUNCTIONALIZATION OF MAGNETITE WITH QUERCETIN

5.1 Introduction

The field of nanotechnology is emerging rapidly as it has elicited much interest among the research community due to a diverse range of applications in different fields such as industry, medicine, and cosmetics. Rather than the bulk materials; their nanostructured counterparts, display unique optical, physiochemical, electrical and magnetic characteristics. This attributed to their higher surface to volume ratio, size and shape effects. This innovative feature of nanoparticles enables them to be used extensively for biomedical applications. Different types of nanoparticles including metallic (Liao, Nehl, & Hafner, 2006), fluorescent (quantum dot), magnetic (Chatterjee, Gnanasammandhan, & Zhang, 2010; Corr, Rakovich, & Gun'ko, 2008), protein-based nanoparticles (Hawkins, Soon-Shiong, & Desai, 2008; Kogan et al., 2007) and polymeric (Kumari, Yadav, & Yadav, 2010; Soppimath, Aminabhavi, Kulkarni, & Rudzinski, 2001) are utilized for biomedical applications. However, most of the research has been focused to develop the magnetic nanoparticles. The dimension of the magnetic nanoparticles can be few nanometers up to tens of nanometers. Usually, they have a similar or smaller size than the protein molecule, it easier for the cells or viruses to interact or attach/infiltrate inside the biological matrix of concern (Varadan, Chen, & Xie, 2008).

The functionalized IONP can interact and bind with different types of biological molecules including enzymes, proteins, nucleotides or antibodies. Even it can interact with the drugs based on functionalization techniques. Thus, an external magnetic field can be used to release it inside the targeted tissues, organ or a tumor (Chorny et al., 2010; Gao, Gu, & Xu, 2009; Gupta & Gupta, 2005; Lacramioara et al., 2016; Laurent et al.,

2008). It can be used as a curing agent for cardiovascular diseases (Chorny et al., 2010). It has the potential to cure the oxidative damage (Erica et al., 2011). The presence of magnetic nanoparticles can ensure targeted drug delivery to the specific organs (N. K. Verma et al., 2013). The presence of reactive oxygen species (ROS) inside the body can damage several biological activities including DNA-protein cross-links, protein fragmentation/oxidation and enzyme activation/deactivation (Kareem et al., 2015). The endogenous antioxidants are naturally produced inside the human organ. Some of the anti-oxidants can be provided externally through food and termed as exogenous antioxidants (Wageeh A Yehye et al., 2015). Recently the development of biocompatible nanoparticles having antioxidant properties has gained a great deal of attention.

Among different types of IONP, Magnetite (Fe_3O_4) nanoparticles are extensively used in magnetic separation, targeted drug delivery, magnetic resonance imaging, tissue engineering, bio-separation, magnetic hyperthermia and cell tracking (Mirzajani & Ahmadi, 2015; Thomas et al., 2015; T. Torres et al., 2010; Tudisco et al., 2015). Earlier research in vivo has demonstrated that Magnetite nanoparticles are comparatively benign due to their non-accumulating tendencies inside the vital organs. It can be promptly eliminated from the body (Boyer, Whittaker, Bulmus, Liu, & Davis, 2010). Polymeric coating such as polyethylene glycol (PEG) over the IONP can reduce its' toxicity level when used for human fibroblasts (Y. Wang et al., 2008). Thus, numerous process optimization techniques have been undertaken to functionalize or coat IONPs. This has been done mainly by controlling the synthesis parameters or choosing suitable groups to incorporate with them (Barreto et al., 2011).

Flavonoids are hydrophobic substances and used as natural antioxidants in several studies. This can be classified as flavones, flavonols, flavanones, flavan-3ols,

anthocyanidins, and isoflavones (Ross & Kasum, 2002). Quercetin is a kind of natural flavonol and can be extracted from berries, tea, red wine apples, citrus fruits, and red onions. It has exhibited antioxidant (Casas-Grajales & Muriel, 2015; Gormaz, Quintremil, & Rodrigo, 2015), anti-inflammatory, anti-obesity, (Williams et al., 2013) anticancer (F. Khan et al., 2016), anti-viral and antimicrobial properties (Aziz, Farag, Mousa, & Abo-Zaid, 1998; K. Liu et al., 2017). The coplanar structure coupled with their hydrophobicity enables them to interact with phospholipid bilayer of bio-membranes. The –OH and –C_6H_5 groups of flavonol can be specific or non-specific in binding to the functional proteins (enzymes, hormone receptors, and transcription factors). However, quercetin is sparingly soluble in water and unstable in physiological systems (D. Sun et al., 2015). Thus, its direct applications are somewhat restricted. To resolve these limitations, quercetin can be used as a functionalizing agent for nanoparticles. For instance, magnetite-quercetin nanoparticles have been studied as a drug delivery system (Barreto et al., 2011). Quercetin functionalized rare earth oxides have been demonstrated to exhibit synergistic antibacterial and hydroxyl radicle scavenging properties (K. Wang et al., 2013). Quercetin and Gallic acid have been used for consecutive coating of the bimetallic nanoparticles. The coating enables it to be used successfully as antioxidant, antimicrobial and antitumor agents (Mittal et al., 2014). The coating provided by quercetin can give a protective layer over the nanoparticles to inhibit cellular damage, cytotoxicity and apoptotic death (Sarkar & Sil, 2014).

In this research, quercetin functionalized IONP has been prepared, using in-situ synthesis and post-synthesis method. Both the methods used here provided nano-particle samples with controlled particle sizes. The functionalization has been carried out successfully and the sample has shown great potential to be used as an antimicrobial and

antioxidant agent. The antioxidant activity of the synthesized sample has been checked using 2, 2-diphenyl-1-picrylhydrazyl (DPPH) assay. Some commonly available pathogens which can easily resist different types of drugs have been chosen for antibacterial studies (e. g. Gram-positive *Staphylococcus aureus*, *Bacillus subtilis,* and Gram-negative *Escherichia coli*) in vitro. The antifungal activity of IONP@Q against *Aspergillus niger, Candida albicans, Trichoderma* sp. and *Saccharomyces cerevisiae* has been investigated. The biological activity of the synthesized sample has been analyzed using the PASS program. The values of the half maximal inhibitory concentration (IC50) of the DPPH antioxidant assay was decreasing using the functionalized one and it exhibited 2–3 fold decreasing tendency than the unfunctionalized IONP. MIC values confirms that functionalized IONP@Q have excellent antibacterial against strains used and fungal strains. Our findings illustrated that the synthesized quercetin functionalized nanoparticles can be a promising candidate as nano antioxidant and an antimicrobial therapeutic agent.

5.2 Results and Discussion

5.2.1 Surface Functional Groups Analysis using FTIR Techniques

The surface functional groups over the synthesized samples were identified using the FTIR analysis and are illustrated in Figure 5.1 (A-D) illustrates the FTIR spectra of IONPs, Q, In-situ IONPs and Post situ IONPs. The sharp peak around 550, 554 and 549 cm^{-1} confirms the presence of magnetite (S. T. Shah et al., 2017). After in-situ and post situ functionalization, the peaks were shifted slightly due to IONPs-Q complex formation. The broad peak around 3000 cm^{-1} in all the samples showed the presence of –OH stretching vibration. The presences of the sharp peak for carbonyl groups were observed at 1623 and 1621 cm^{-1} IONP@Q1, and IONP@Q2, respectively (Bukhari, Memon, Mahroof-Tahir, & Bhanger, 2009). After DPPH assay was carried out, surface functional

groups for IONP@Q samples were again identified and shown by Figure 5.1 (E-H). Excess DPPH solution was added with IONP@Q samples. The resultant mixture was stored inside the dark for 30 minutes. After that, the samples were washed three times with ethanol. N-O stretching band was present, and it gave rise to peaks at 1530, 1310, 1513, 1335, 1530, 1329 cm^{-1} for IONP@Q1 and IONP@Q2 respectively. This reflected that the functionalized surface of IONPs was attached with DPPH radical. The representative peaks for DPPH radicals were absent on IONPs (S. R. Kumar et al., 2014; S. T. Shah et al., 2017).

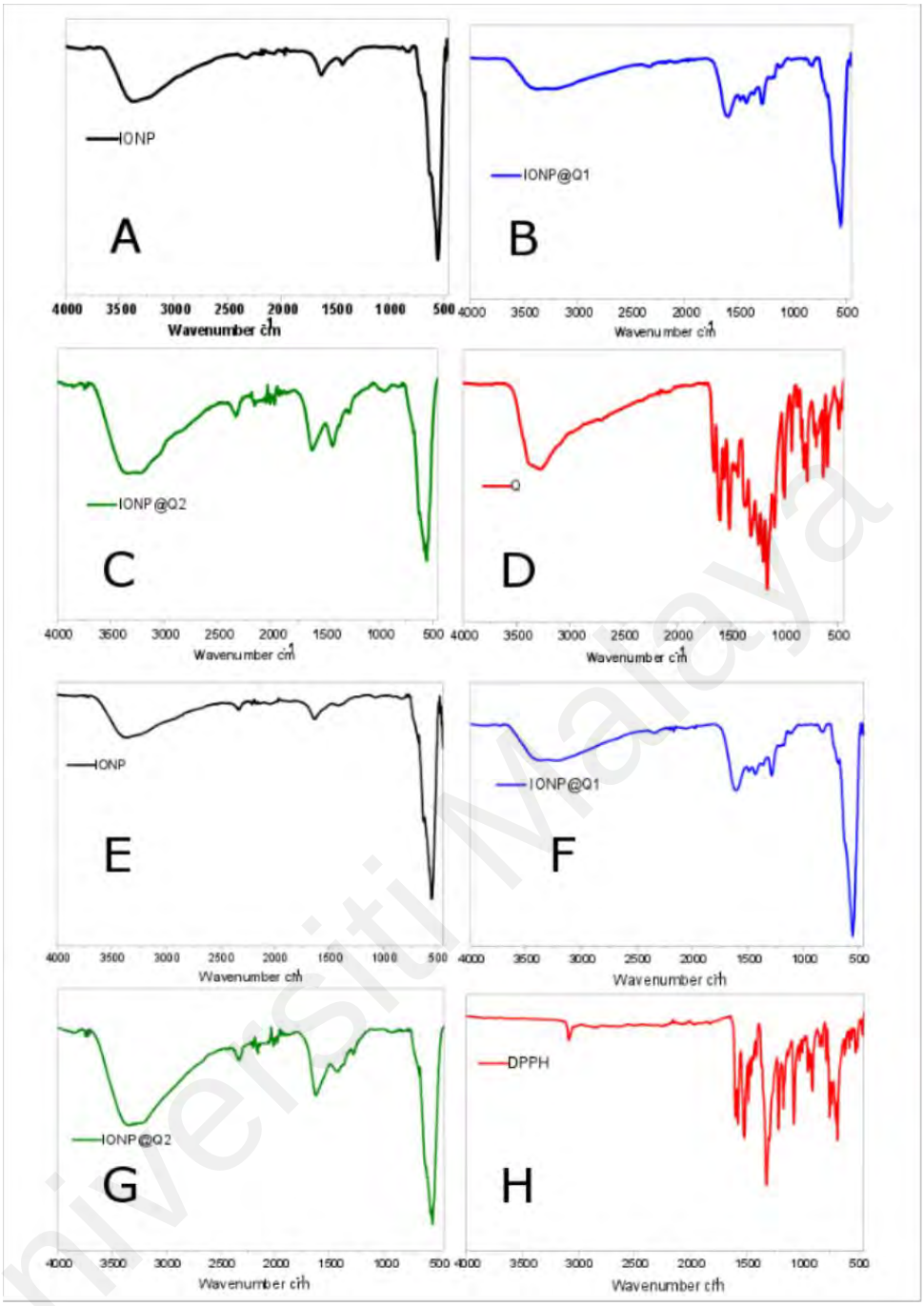

Figure 5.1. FTIR Spectra of (A-D) IONP@Q before DPPH Assay (E-H) IONP@Q after DPPH Assay

5.2.2 Raman Spectra

The structural phase of the functionalized nanoparticles has also been illustrated by Raman spectra (Figure 5.2). The Magnetite phase of IONPs is confirmed by the presence of the main vibrational mode around 671 cm^{-1} (A1g) (De Faria et al., 1997). Nevertheless,

all the samples have the main band around 671 cm^{-1}, 466 cm^{-1} and 348 cm^{-1} that have been assigned to A1g, T2g and Eg vibrations of magnetite. The absence of maghemite was also confirmed by the Raman Spectra *(Francisco et al., 2011; Shebanova & Lazor, 2003)*. The functionalized IONPs showed some additional bands around 1217 and 1337 cm^{-1} which are attributed to the aromatic ring of Q. The band around 1450 and 1519 cm^{-1} over IONP-Q are due to the OH bending band whereas the band at 1597 cm^{-1} indicates C=O stretching (Numata & Tanaka, 2011).

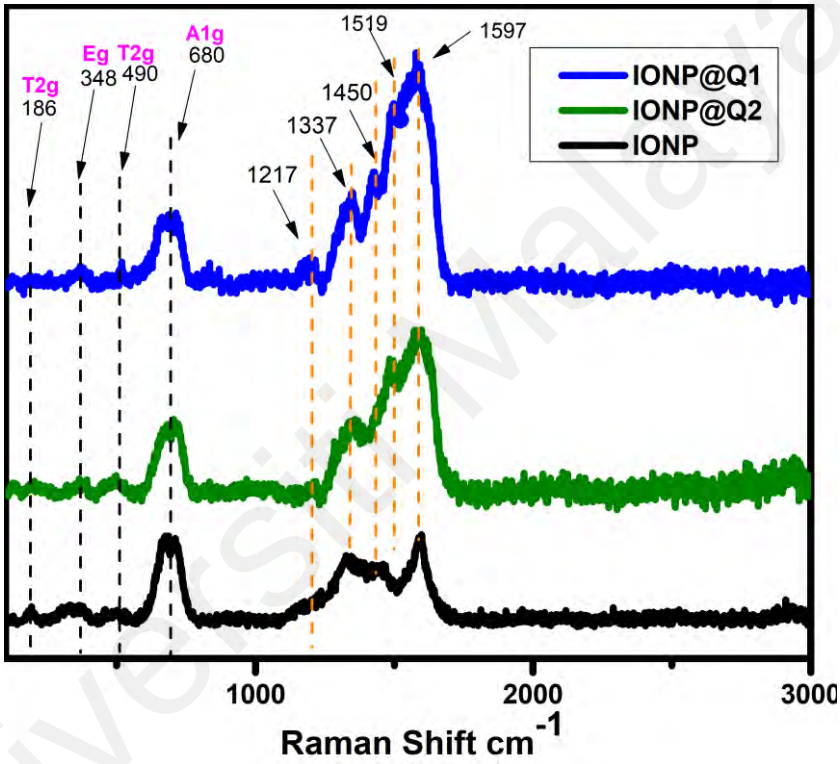

Figure 5.2. Raman Spectra of IONP@Q

5.2.3 X-ray Crystallographic Data (XRD) Analysis

The XRD curves for all the samples showed diffraction peaks at the 2θ value of 30, 35, 43, 57 and 63, which is around [220], [311], [400], [511] and [440] Bragg reflections, respectively (Figure 5.3). The result confirmed the presence of pure magnetite nanoparticle having the cubic inverse spinal structure (JCPDS No. 82-1533) (Dorniani et al., 2012). The absence of superlattice diffractions around 210, 213, and 300 exhibits the

absence of maghemite in all samples. Overall, it reflected that the functionalization could not change the phase of iron oxide.

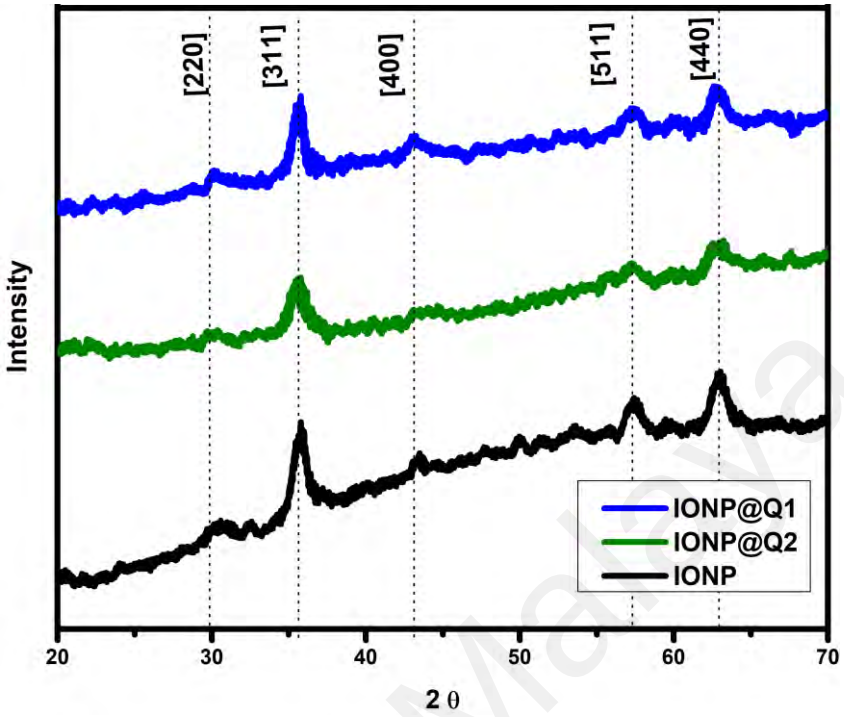

Figure 5.3. XRD Spectra of IONP@Q

5.2.4 Magnetic Properties

The saturated mass magnetization was determined by vibrating sample magnetometer. The magnetization values obtained were 64.19, 51.04 and 59.07 emu g^{-1} for IONP, IONP@Q1, and IONP@Q2, respectively. Figure 5.4 illustrates the hysteresis loops of the synthesized samples under the magnetic field at room temperature.

Table 5.1 summarizes the values for the saturation magnetizations for the synthesized samples. The results reveal that the synthesized nanoparticles exhibit super-paramagnetic behavior. The functionalized samples exhibited lower saturation magnetization values than the bulk magnetite (~92 emu g^{-1}) and unfunctionalized magnetite nanoparticles (Cornell & Schwertmann, 2006). Lower magnetization values for IONP@Q is because

of organic coating and impurities accumulated over the surface of the synthesized nano-composites (Dorniani et al., 2014; Dorniani et al., 2012; Ma et al., 2007).

Table 5.1 Magnetic properties of IONP@Q

Sample	Ms
IONP	64.19
IONP@Q1	51.04
IONP@Q2	59.07

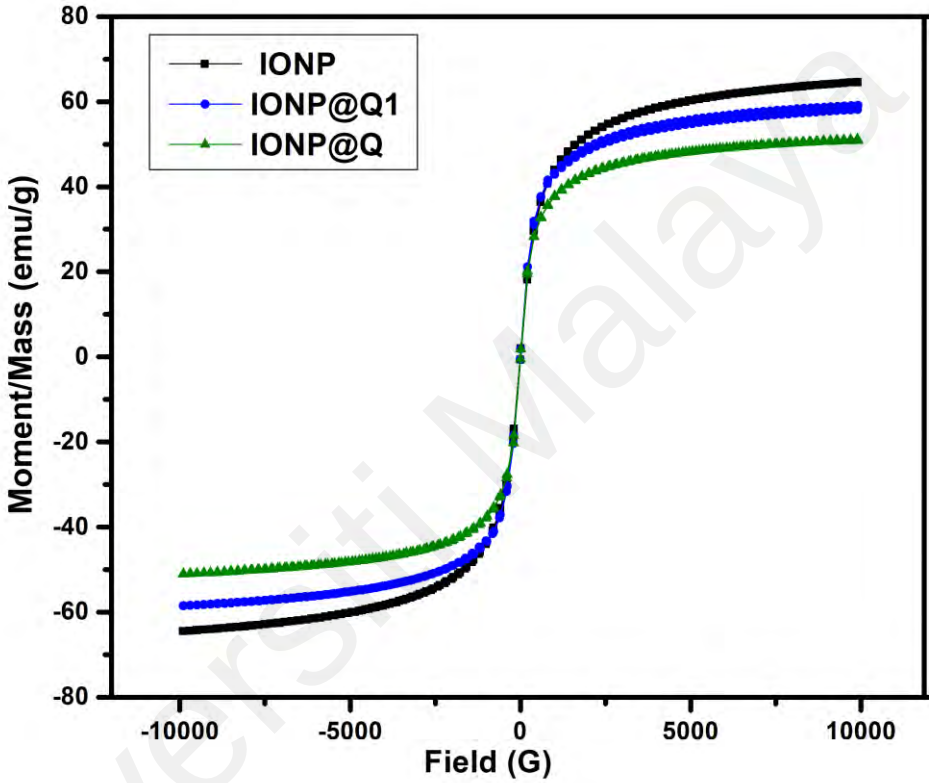

Figure 5.4. Magnetic Hysteresis Loops of IONP@Q

5.2.5 Morphology and Structure

High-Resolution Transmission Electron Microscopy (HRTEM) was carried out to observe the particle size and morphology of the synthesized IONP@Q samples and is illustrated in Figure 5.5. The average particle size observed was 10, 6 and 11 nm, for IONP, IONP@Q1, and IONP@Q2 correspondingly.

The particles were spherical in shape and they had uniform size distribution. The nanoparticles were aggregated to form a cluster. This occurred due to the magnetic characteristics of the synthesized particles. The crystal lattice fringe spacing 0.26 nm confirmed cubic magnetite nanoparticles (Iyengar et al., 2014).

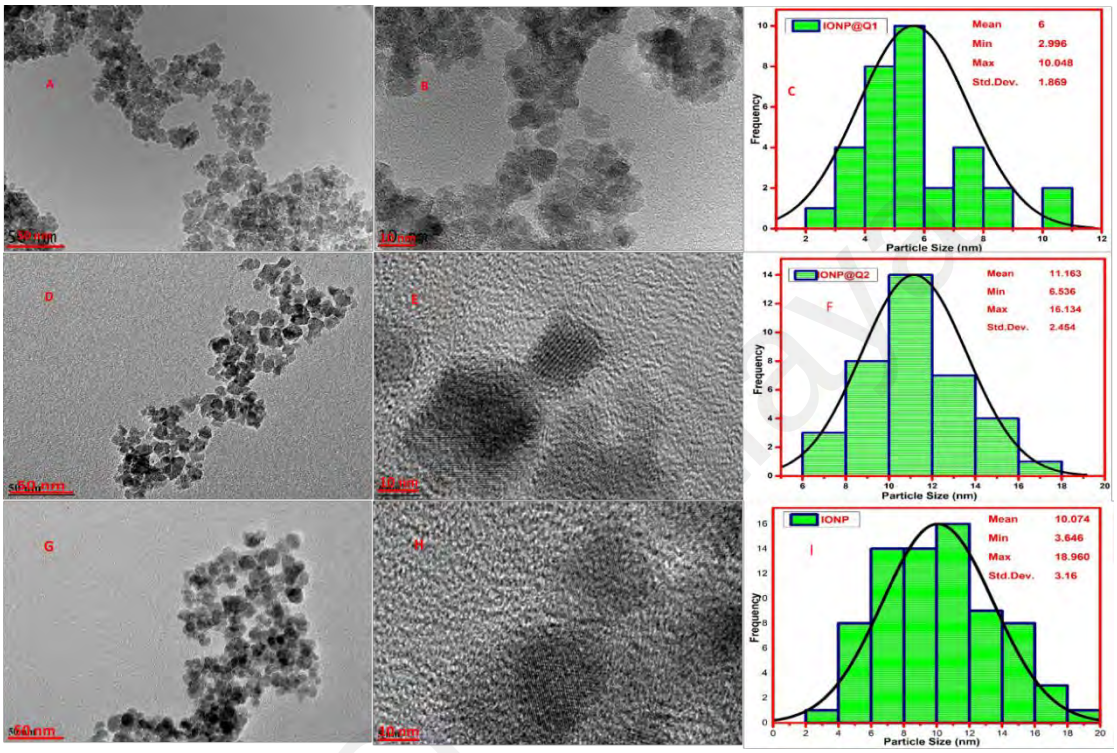

Figure 5.5. HRTEM images (A, B, D, E, G and H) and Particle Size Distribution (C, F and I) of IONP@Q

HRTEM images reflected that in-situ functionalized IONP@Q1 has a smaller particle size than the unfunctionalized IONP as well as post functionalized IONP@Q2. This reflects that the in-situ functionalization was efficient enough to control the size of the nanoparticles compared to other synthesis routes. This might be attributed to the formation of the metal-Q complex (Barreto et al., 2011) as shown in Figure 5.6.

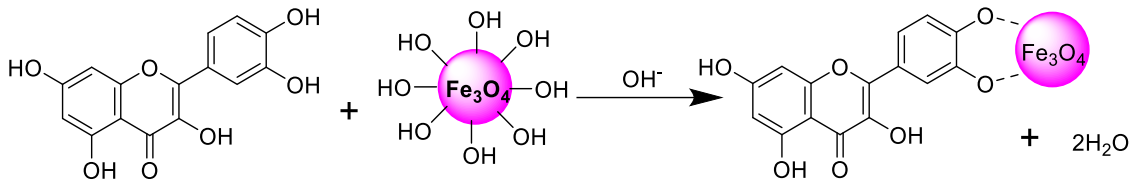

Figure 5.6 Proposed Scheme of the Magnetite–Quercetin Complex

The presence of hydroxyl groups, over the surface of IONPs allows the attachment of different functional groups. In aqueous medium, IONPs are hydroxyl functionalized which are amphoteric and may react with acids or bases (Laurent et al., 2008).

5.2.6 EDX Analysis

The existence of magnetite was confirmed by the presence of Fe and O content inside the sample. The organic phase is confirmed by the presence of C contents as shown in Table 2. The uniform distribution of the atoms was identified using the mapping images (Figure 20-22 A). After DPPH assay, N signals were also observed due to the attachment of DPPH which agrees with the FTIR. Figure 5.7, Figure 5.8 and Figure 5.9 show the EDX of IONP@Q1, IONP@Q2, and IONP respectively. Percentage of Nitrogen increased from 0 to 0.3 and 0 to 0.5 for IONP@Q1 and IONP@Q2 respectively, while carbon contents increased from 4.6 to 7.6, and 6.1 to 8.3 f for IONP@Q1 and IONP@Q2 respectively. However, nitrogen content was not varied for unfunctionalized IONP. This reflected that the free radicals failed to attach with the IONP surface.

Table 5.2 EDX Elemental Composition A) Before DPPH Assay B) After DPPH Assay

	A				B			
Sample	Fe	O	C	N	Fe	O	C	N
IONP	69.6	30.4	-	-	77.5	21.2	1.3	
IONP@Q1	69.7	25.7	4.6	-	63.2	28.9	7.6	0.3
IONP@Q2	69.4	24.5	6.1	-	65.2	26.1	8.3	0.5

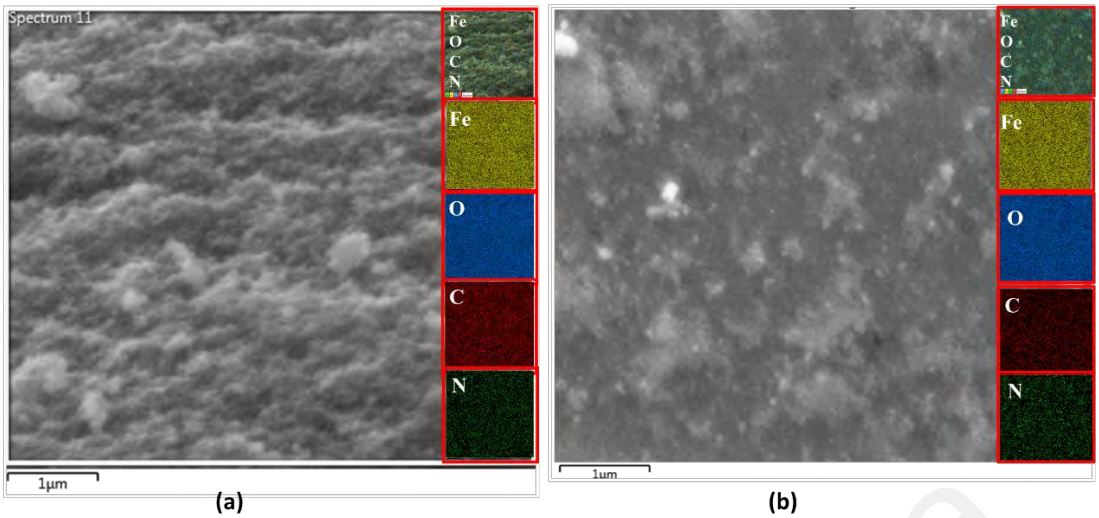

Figure 5.7. FESEM image (inset: EDX Elemental Map of Fe, O, C and N) of IONP@Q1 for the Following Elements: Fe, O, C and N A) Before DPPH Assay B) After DPPH Assay

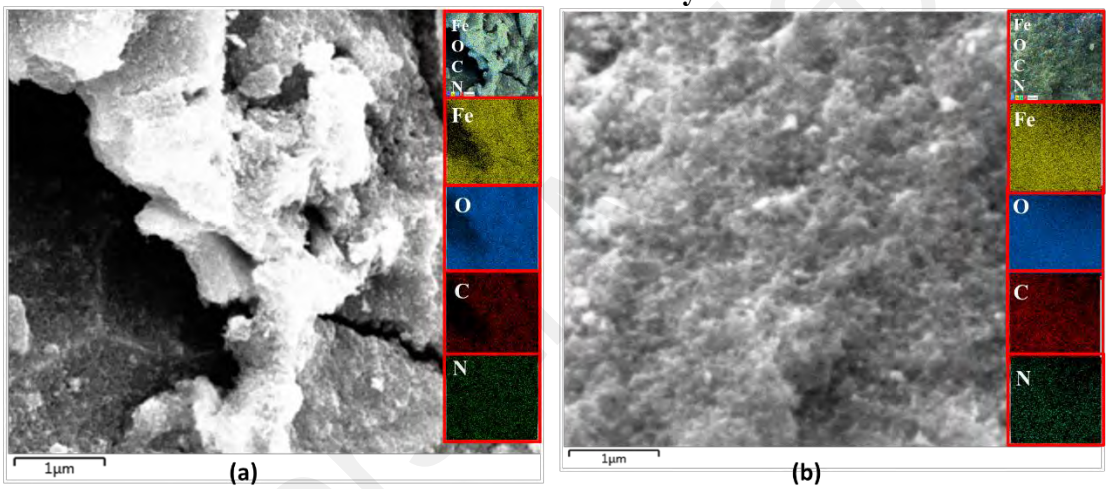

Figure 5.8. FESEM image (inset: EDX Elemental Map of Fe, O, C and N) of IONP@Q2 for the Fe, O, C and N A) Before DPPH Assay B) After DPPH Assay

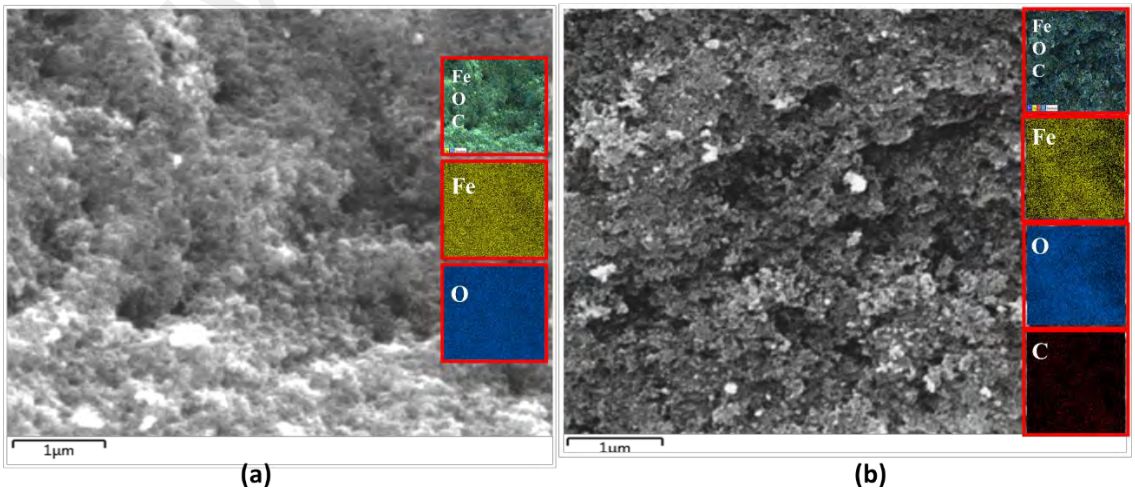

Figure 5.9. FESEM image (inset: EDX Elemental Map of Fe, O, C and N) of IONP for the Fe, O, C and N A) Before DPPH Assay B) After DPPH Assay

5.2.7 PASS- Predication

For designing novel free radical inhibitors for antioxidant drugs PASS prediction is useful (Kareem et al., 2015). PASS analysis can predict more than 4000 kinds of biological activity having a mean accuracy of about 95% (Kadir et al., 2014; A. V. Stepanchikova, A. A. Lagunin, D. A. Filimonov, & V. V. Poroikov, 2003). The results are depicted as the values obtained for appropriate Pa (probability "to be active") and Pi (probability "to be inactive") ratio. It is rational that the compounds having values Pa > Pi can exhibit those types of activities (PharmaExpert., 2015). Table 5.3 summarizes some portion of the predicted biological activity spectra (Lipid peroxidase inhibitor, antioxidant, a free radical scavenger, and anti-inflammatory) for the Q functionalized samples. Probable activities by PASS to be validated by experimental bioassay. Only predicted antioxidant and free radical scavenging activities of the PASS program were experimentally verified by DPPH assay. Pa>0.7 indicated that the corresponding compound was very likely to reveal activity in experiments, 0.5 <Pa<0.7 suggested that the compound was likely to reveal activity in experiments, while Pa<0.5 implied that the compound was unlikely to reveal activity in experiments. However, predictive antioxidant values and other biological activities for the Q with Pa>0.7, indicated that Q functionalized IONP surface could exhibit improved activity than the unfunctionalized iron oxide. This is due to its' biocompatibility which can aid in drug transportation system as well as bioimaging. Activities predicted by PASS were validated by experimental bioassay.

Table 5.3 Part of the Predicted Biological Activity Spectra of the Q on the Basis of PASS Prediction Software

Biological Activity	[a]Pa	[b]Pi
Antioxidant	0.878	0.003
Free Radical Scavenger	0.816	0.002
Lipid Peroxidase Inhibitor	0.813	0.003
Anti-inflammatory	0.704	0.015

[a] probability "to be active"; [b] probability "to be inactive"

1.1. Antioxidant Activity

The UV–Vis absorption curve obtained for the synthesized samples are illustrated in Figure 5.10. From the curve, it can be seen that the peak intensity of DPPH is continuously dropping. The decrease in absorbance around 517nm was used to calculate the free radical scavenging percentage. The inhibition of stable DPPH free radicals of the in-situ synthesized organic nano-compounds were found to be IONP@Q1 (IC50 3 ± 0.002 mg/ml; 58%), IONP@Q2 (0.7 ± 0.002 mg/ml; 75%) and at a 10^{-4} M. The values obtained are 1-3 times more than the unfunctionalized magnetite (IC50 4.7 ± 0.002 mg/ml; 50%) (Figure 5.11).

The sequence followed for DPPH scavenging properties can be shown as Q>IONP@Q2> IONP@Q1>IONP. The free radical scavenging phenomenon can be ascribed for the transfer of electrons from IONP@Q towards the free radicals located at the central nitrogen atom of the DPPH molecule. The scavenging properties of functionalized magnetite were increased as compared with that in the case of naked IONP. Quercetin itself was more potent scavenger than both, functionalized magnetite and naked IONP. The observed moderate antioxidant enhancement of functionalized magnetite could be attributed to the Q on nanoparticle surface.

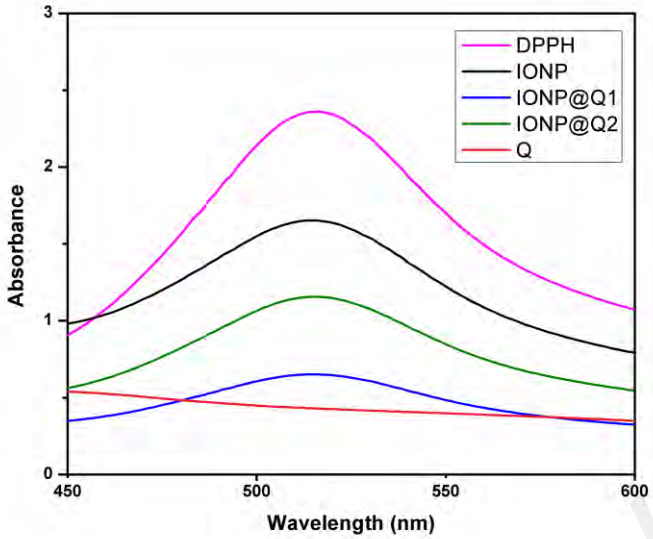

Figure 5.10 UV-Visible Spectra of IONP@Q

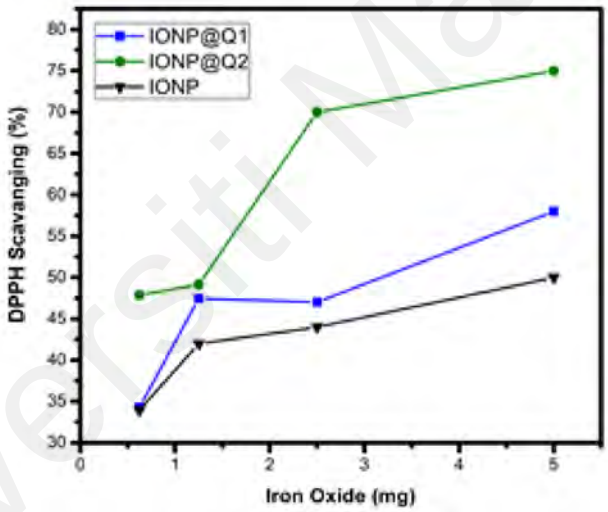

Figure 5.11. DPPH Scavenging Percentage by Nano Magnetite at Different Concentrations

5.2.8 Antimicrobial Activity

5.2.8.1 Antibacterial Activity

Agar well diffusion test was carried out and the results obtained are illustrated by Figure 5.12 A. The results are displayed in terms of percentage inhibition of diameter growth (PIDG) of bacterial strain using the concentration of IONP around 100 mg/ml. Both the synthesized sample functionalized using different routes exhibited antibacterial activity

for both Gram-positive and negative strains. Nevertheless, the highest PIDG values were obtained after using IONP@Q2. Minimum Inhibition Concentration (MIC) is given in Table 5.4. This showed its' efficient and prevailing bactericidal activity. Gram-positive bacteria have a thick peptidoglycan layer (10-30 nm), whereas Gram-negative bacteria have an additional outer layer with a thin peptidoglycan layer (10 nm). IONP@Q has shown different antibacterial activity for different bacterial strains. This was expected and can be explained depending on their cell wall composition for each type of strain. After adding the IONP@Q nanoparticles, bacterial growth inhibition will take place. This phenomenon takes place due to the internalization of functionalized IONPs inside the cell. This would destroy the cell wall by damaging the 1, 4 glycosidic bonds.

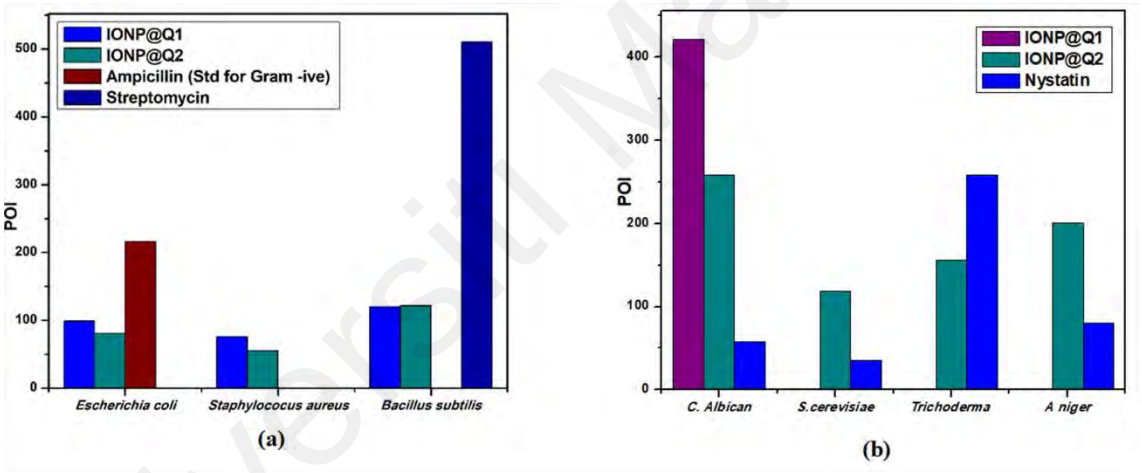

Figure 5.12. Percentage of Inhibition (POI) of (A) Bacterial Growth and (B) Fungal Growth, after Treatment with IONP@Q.

Table 5.4 MIC Values for Bacterial Strains

Bacterial species	Mean value true MIC (mg/mL)		
	IONP@Q1	**IONP@Q2**	**Q**
Staphylococcus aureus	25	10	5
Bacillus subtilis	25	10	5
Escherichia coli	10	10	5

Both ampicillin and streptomycin were used as standard for Gram-positive and Gram-negative bacteria respectively.

5.2.8.2 Antifungal Activity

Agar well diffusion test was carried out and the results obtained are illustrated by Figure 5.12 B. The antifungal activity of IONP@Q against *Aspergillus niger*, *Candida albicans*, *Trichoderma* sp. and *Saccharomyces cerevisiae* was analyzed. The potential antifungal activity of the synthesized compounds among all fungi strains used. IONP@Q2 compound had exhibited the highest percentage of inhibition (POI) for *Aspergillus niger*, *Candida albicans,* and *Saccharomyces cerevisiae*, while IONP@Q1 showed highest fungal activity against *Trichoderma sp*. MIC values reveal that antifungal activity of activity of IONP@Q2 was higher for some fungal strains compared to IONP@Q1 as shown in

Table **5.5**. The nanoparticles were attached with the respiratory system which leads to the antifungal activity of the synthesized sample. The attachment caused cell death (Rudramurthy et al., 2016). In general, smaller nanoparticles exhibit higher antimicrobial activity (Padmavathy & Vijayaraghavan, 2008). However, activities also depend on the formulation process and physical characteristics of nanoparticles (Slavin, Asnis, Häfeli, & Bach, 2017).

Table 5.5 MIC Value for Fungal Strains

Fungal species	Mean value true MIC (mg/mL)		
	IONP@Q1	**IONP@Q2**	**Q**
Aspergillus niger	25	25	5
Candida albicans	25	10	5
Trichoderma sp.	25	25	5
Saccharomyces cerevisiae	25	10	5

Nystatin was used as standard drug

5.3 Conclusions

In this research, IONP nanoparticles were successfully functionalized. Both in-situ and post-situ technique was used for functionalization. HRTEM analysis was carried out to determine the average particle size for both the sample functionalized in different techniques. For in-situ functionalized IONP, the particle size obtained was 6 nm whereas, after post-functionalization, the synthesized IONP@Q2 had the particle size 11 nm-slightly bigger than the in-situ one. The particle size obtained here followed the sequence of IONP@Q2 > IONP> IONP@Q1. Due to using the in-situ process, the particle size of IONP was controlled by Q. This is owing to the formation of a kind of IONP-Q complex. Predictive values for antioxidant activities and other biological activities for the Q with Pa>0.7 were presented. Owing to its' biocompatibility, it can be used as a promising candidate for drug delivery and bio-imaging agent. In this research, probable activities by PASS were validated by experimental bioassay. The scavenging activity of the sample using the DPPH was found to be in the order of IONP@Q2> IONP@Q1> IONP. Both the methods used here for functionalization of IONP has increased its' free radical scavenging capacity more than 1 to 3 fold compared to the unfunctionalized one. The

synergistic effect of the magnetite coated by Q had not only increased the free radical scavenging capacity but also controlled the particle size of IONP. The formation of IONP@Q-DPPH was confirmed by FTIR and EDX. Finally, IONP@Q showed potential antifungal and antibacterial effects on the strains under observation. The antimicrobial of IONP@Q2 was higher than IONP@Q1. This might be taken place through the destruction of the membrane. The findings here clearly reveal that the synthesized IONP@Q has combinatorial properties (magnetic, antioxidant and antimicrobial). Thus, the application of the synthesized sample can be promising for further clinical applications.

CHAPTER 6: DESIGN AND SYNTHESIS OF MULTIPOTENT ANTIOXIDANTS FOR FUNCTIONALIZATION OF IRON OXIDE NANOPARTICLES

6.1 Introduction

An antioxidant substance is a molecule or nanomaterial that can block or slow down the process of oxidation (Ingold & Pratt, 2014). Antioxidants have also been reported to be effective because of prophylatic and healing mediators for various diseases and/or toxic effects. Nanoparticles may act as nanocarriers and have a wide range of applications, such as drug delivery. Combining material science with nanotechnology and engineering leads to significant developments that decrease the production of free radicals (Eftekhari, Ahmadian, Panahi-Azar, et al., 2018). As a nanomaterial, nanoantioxidants can slow down the pace of auto-oxidation by trapping the chain-carrying radicals or limiting the number of events that initiate the process. Recently, a number of these nanoantioxidants have shown promising results in nanomedical research (Hasanzadeh et al., 2017; Hasanzadeh et al., 2018).

Organic species such as proteins and lipids undergo oxidative degradation due to free radicals chain mechanism. Alkyls radicles are converted to Peroxyl free radicals (RCOO') in the presence of oxygen. RCOO' further propagates the oxidative chain, and this phenomenon is said to be auto-oxidation. This happens under mild conditions due to the formation of hydroperoxides as a result of peroxidation (Ingold & Pratt, 2014). Moreover, hydroxyl and alkoxy free radicals are formed by homolytic cleavage of unstable hydroperoxides. These free radicals are exceedingly unstable and cause DNA damage by hitting the bases of DNA strands (Cadet & Wagner, 2014). Reactive carbonyl species

(such as 4-hydroxynonenal) are also formed by the cleavage of alkyl hydroperoxide, enhancing the oxidation process (Zhang & Forman, 2017). Oxidative stress is defined as an imbalance in the cell's ability to respond to ROS by eliciting an effective antioxidant response. Biomolecules such as proteins, enzymes, and DNA are damaged irreversibly by oxidative stress which causes genetic mutations and cell death.(Morry et al., 2017).

Natural antioxidants in our diet have a significant role in lowering ROS and minimising the risk of diseases linked to oxidative stress. Alpha-tocopherol, selenium and β-carotene supplements have been demonstrated to provide no cancer protection or even raise mortality risk in clinical trials (Morry et al., 2017). The reason behind such unexpected results is the no bioavailability of antioxidants to the target sites. In connection with this, nanoantioxidants present a golden opportunity because they can be tailored to have the best properties such as enhanced stability compared to small molecules, reduce the chances of rapid metabolic activity, and deliver them to the target sites (Morry et al., 2017). Several nanoantixodants such as gold nanoparticles (Bumbudsanpharoke et al., 2015), Trolox, and salvianic acid-functionalized gold nanoparticles (Libo Du et al., 2013; Medhe et al., 2014; Nie et al., 2007), functionalized AgNPs (Vilas et al., 2016). showed enhanced DPPH radical scavenging.

Biomedical applications of magnetite nanoparticles (Fe_3O_4) are extensively studied because of their magnetic nature, biodegradability, biocompatibility, and ease of functionalization (Popescu, Andronescu, & Vasile, 2019). The antioxidant properties of Fe_2O_3 nanoparticles have already been studied and showing that radical scavenging is due to electron transfer (Alves et al., 2016; Salvador et al., 2021; S. T. Shah et al., 2017). In another study, gallic acid and quercetin functionalized magnetite nanoparticles showed synergistic organic-inorganic hybrid antioxidant properties and potent antimicrobial

activity on various fungal and bacterial strains (S. Khan et al., 2020; S. T. Shah et al., 2017).

Numerous studies show that butylated hydroxytoluene (BHT) is one of the most commonly used synthetic antioxidants in food, oil, and cosmetics industries (Ariffin et al., 2014). An additional use for this synthetic antioxidant is in the field of medicine. However, certain characteristics of volatility and high-temperature instability and toxicities, as well as safety concerns, have severely hampered the effective therapeutic application (Elmadfa & Meyer, 2008). To this end, current research focuses on designing and synthesizing new BHT-derivatives to enhance antioxidant and therapeutic activities and reduce toxic side effects (Wageeh A Yehye et al., 2015). This study aimed to design and synthesize EG-ester of BHT-bearing antioxidant groups as an effective strategy to enhance the safety profile, solubility of BHT, and synthesis of new Multipotent Antioxidants (MPAO) functionalized Magnetic nanoantioxidant. Computational analyses were carried out prior to synthesizing MPAO to ensure that the molecules were built in accordance with the structure-activity-relationship (SAR) strategy. Rule of five, Polar surface area, and Lipinski parameters were used for predicting absorption, distribution, metabolism, excretion and toxicity **(**ADMET) properties (Daina, Michielin, & Zoete, 2017). PASS analysis was performed for MPAO to predict the potential biological activities of the molecule. MPAO were synthesized for functionalization of magnetite nanoparticles. Post functionalization technique was used to synthesize magnetic nanoantioxidants. Antioxidant assay and antimicrobial activities were carried out for IONP@AO.

6.2 Results and Discussion

6.2.1 FTIR Analysis

The FTIR spectra of IONP and IONP@AO are shown in Figure 6.1. Magnetite was observed in the nanoparticle samples by a strong absorption at 551, 555, and 562 cm^{-1} for IONP, IONP@AO1, and IONP@AO2, respectively. The peak observed at 3100-3200 cm^{-1} is due to stretching vibration of -OH. The peak at 1621 cm_{-1} has confirmed the existence of the carbonyl groups in both samples of IONP@AO (S. R. Kumar et al., 2014).

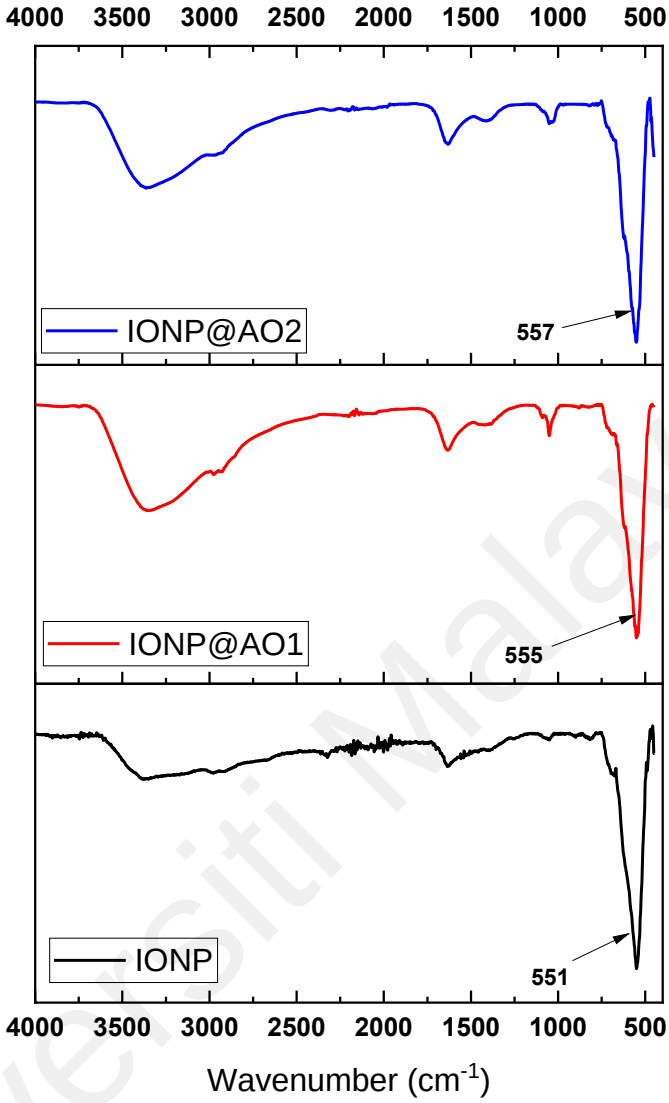

Figure 6.1 FTIR Spectra of Unfunctionalized IONP and Functionalized IONP@AO

6.2.2 Raman Analysis

Spectra obtained from Raman analysis are presented in Figure 6.2. The main band at 671 cm^{-1} (A1g) verified the presence of Magnetite (De Faria et al., 1997). IONP@AO has a main band centered at 675 cm^{-1} and peaks at ca. 478 cm^{-1} and 343 cm^{-1} are due to A1g, T2g, and Eg vibration band of Magnetite. Moreover, no peaks were observed for maghemite in Raman spectra of both functionalized and unfunctionalized IONP (Francisco et al., 2011; Shebanova & Lazor, 2003).

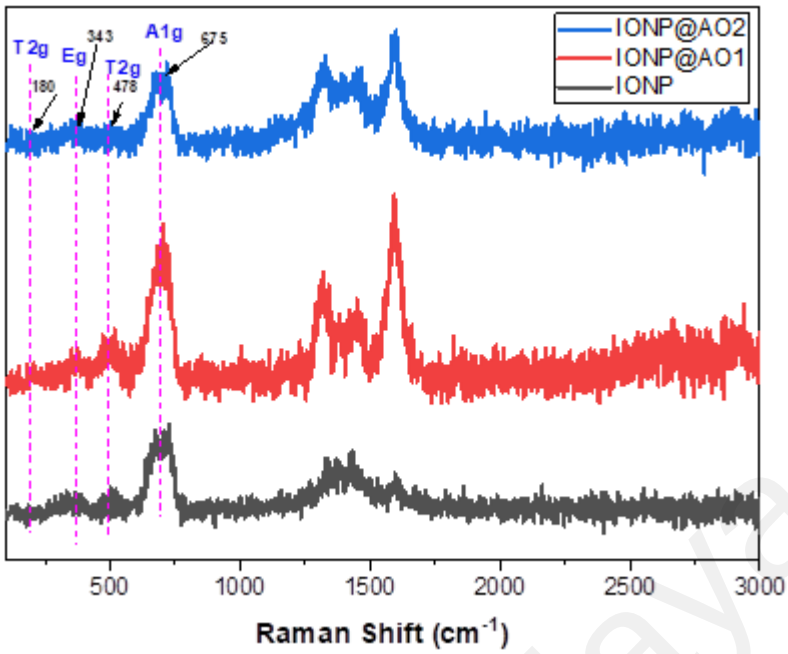

Figure 6.2. Raman Spectroscopy Analysis of Unfunctionalized IONP and Functionalized IONP@AO

6.2.3 XRD Analysis

Figure 6.3 shows the XRD spectra of the samples. All the samples demonstrated the diffraction peaks at the 2θ value of 30, 25, 43, 57 and 63, which correspond to [220], [311], [400], [422] and [440] Brag reflections, respectively. XRD pattern verified the magnetite nanoparticles with cubic inverse spinel structure (JCPDS No 96-101-1033). Moreover, the diffractions at 210, 213, and 300 were not observed, verifying that maghemite is absent in all samples. It can be seen that the functionalization of IONP did not change its phase.

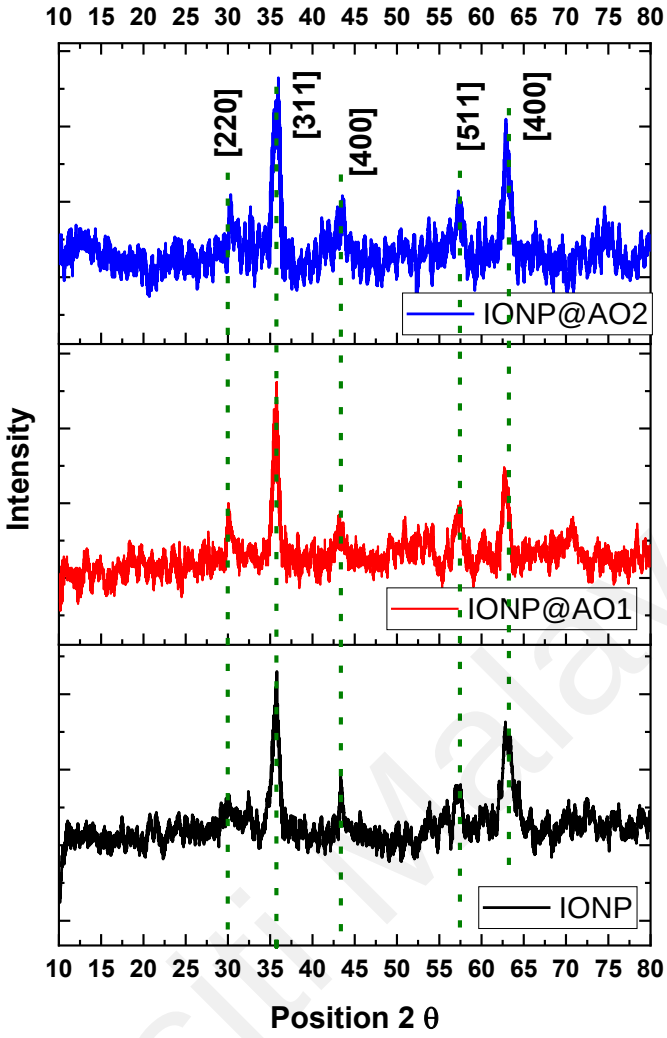

Figure 6.3 XRD Spectra Unfunctionalized IONP and Functionalized IONP@AO

6.2.4 Magnetic Properties

A Vibrating Sample Magnetometer (VSM) was used to determine saturated mass magnetization. The values of 64.19 and 45 emu g^{-1} were given for bare Iron oxide nanoparticles and functionalized IONP@AO, respectively (Table 6.1). The hysteresis loops are shown in Figure 6.4 as functions of the magnetic field at room temperature. All samples showed superparamagnetic behavior, and their saturation magnetization was lower than Magnetite in bulk (92 emu g^{-1} (Cornell & Schwertmann, 2006). Functionalized IONP@AO1 and IONP@AO2 saturation magnetization were reduced

compared to unfunctionalized IONP, probably because of organic species on its surface (Dorniani et al., 2014; Dorniani et al., 2012; Ma et al., 2007).

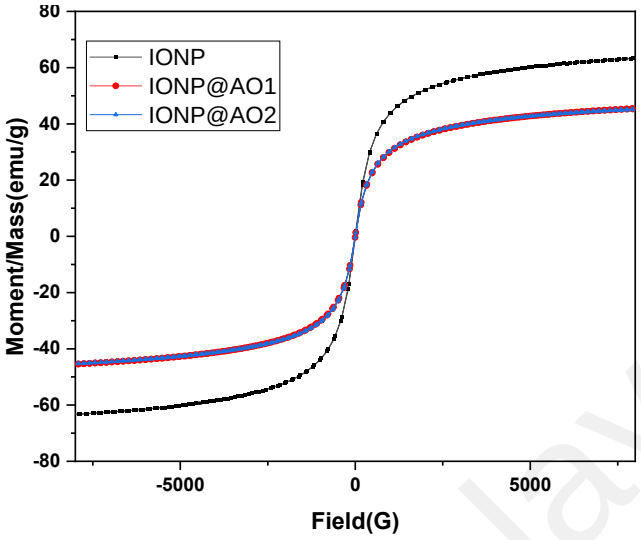

Figure 6.4 Room temperature Hysteresis Loops for Unfunctionalized IONP and Functionalized IONP@AO

Table 6.1 Magnetic Properties of Unfunctionalized IONP and Functionalized IONP@AO

Sample	Ms
IONP	64.19
IONP@AO1	45.43
IONP@AO2	45.25

6.2.5 Morphology and Structure

Morphology of the functionalized and unfunctionlazed IONP was studied by High-Resolution Transmission electron Microscopy (HRTEM). Figure 6.5 shows the High resolution electron images and size distribution of the nanoparticles. The analysis of the TEM images revealed a particle size on average was 10.07 and 10.08 nm and 11 nm for IONP, IONP@AO1, and IONP@AO2, respectively. The results shows that particles are distributed uniformly and have a spherical shape. The agglomeration of nanoparticles is because of the superparamagnetic behavior of nanoparticles. The crystal lattice fringe spacing was 0.26nm, which corresponds to the (220) lattice plane of IONP (Iyengar et al., 2014).

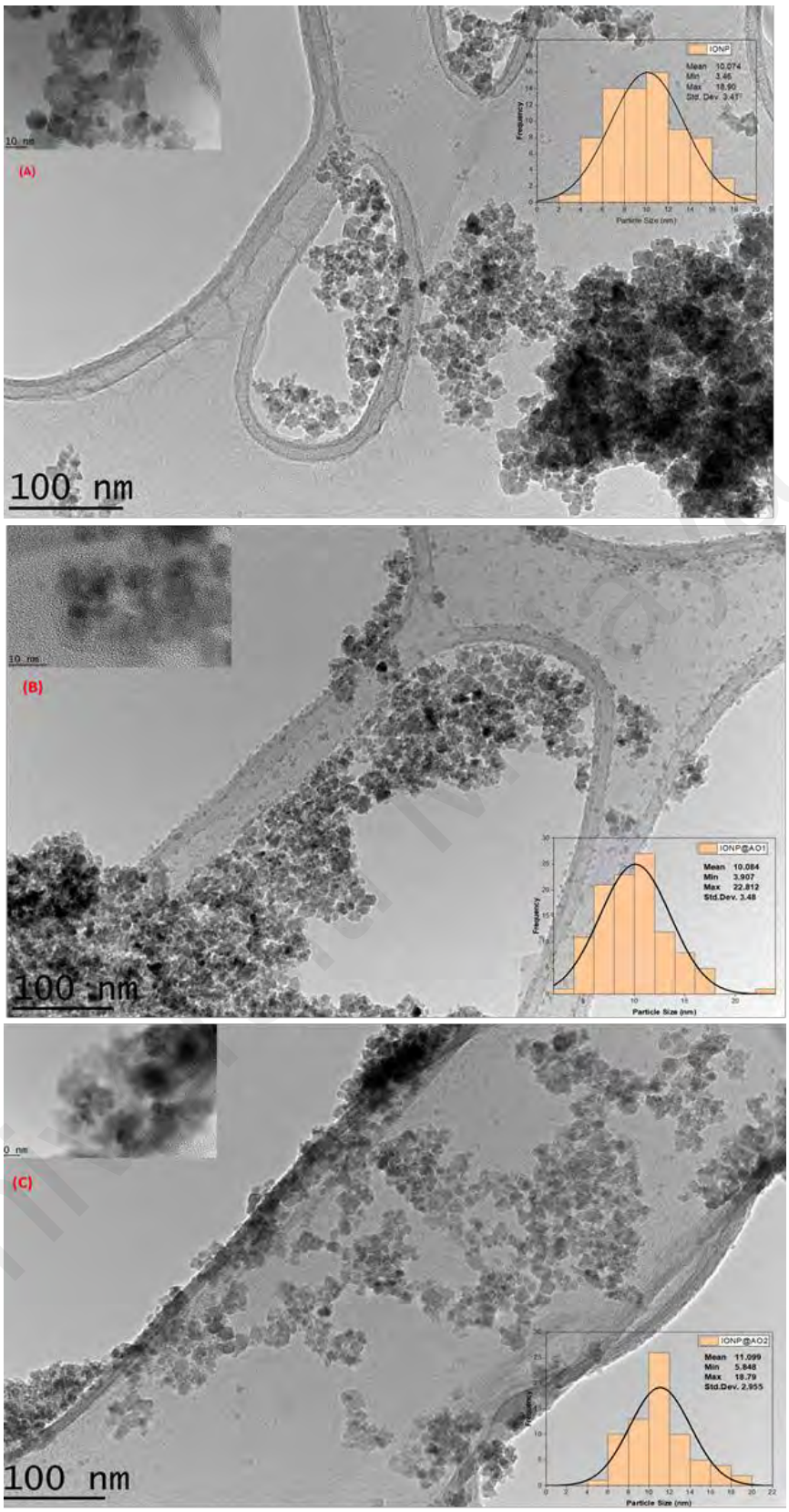

Figure 6.5 HRTEM Images (A) Unfuntionalized IONP (B) Functionalized IONP@AO1 (C) Functionalized IONP@AO2 inset showing Particle Size Distribution

6.2.6 EDX Analysis

Table 6.2 represents the elemental composition of the samples. Magnetite nanoparticles showed Fe and O signals in all samples, whereas the C and S signals are due to organic moieties present in IONP@AO1 and IONP@AO2. Furthermore, EDX mapping confirmed the uniform distribution of the elements present in the samples. The mapping of C and S is uniform, as shown in Figure 6.6, which confirmed that nanoparticles are functionalized well.

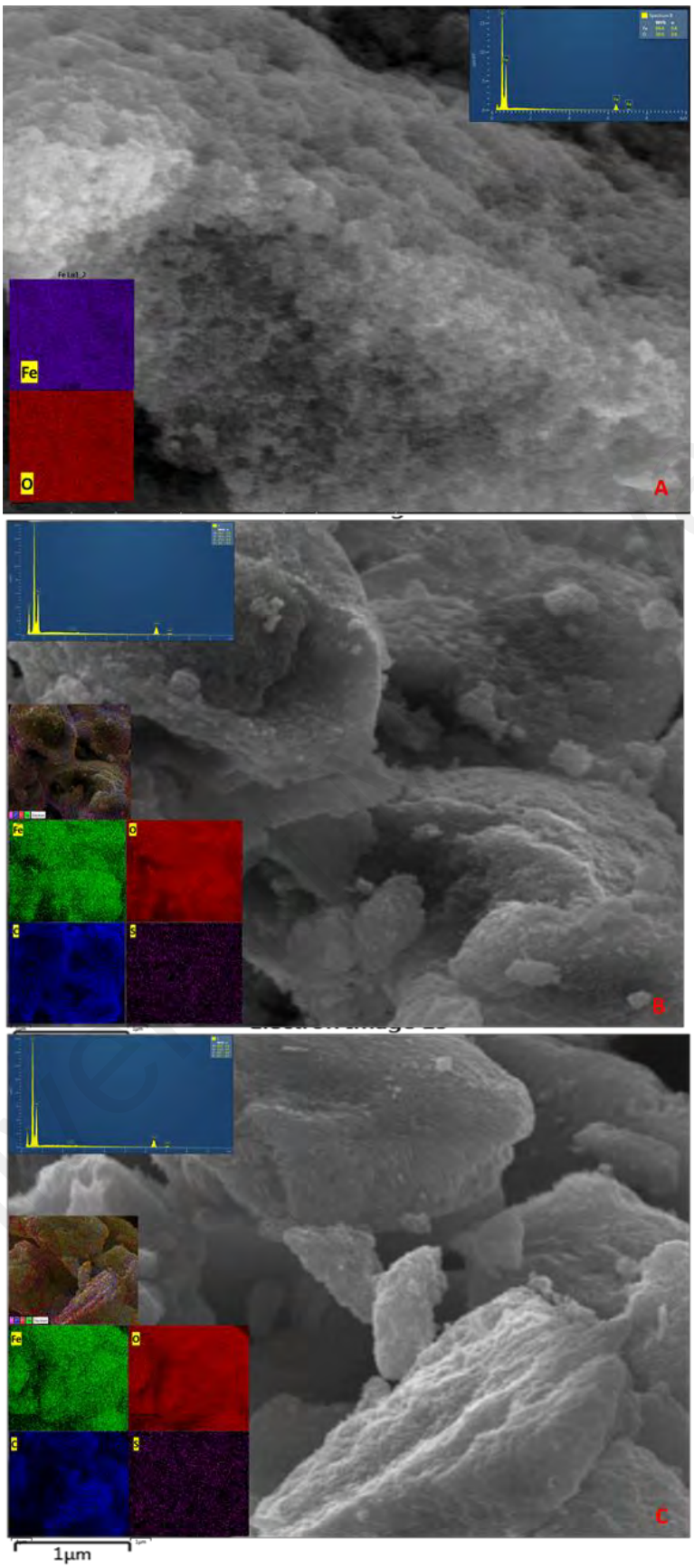

Figure 6.6 EDX of (A) IONP (B) IONP@AO1 (C) IONP@AO2

Table 6.2 Elemental Composition Analysis Employing SEM–EDX a Energy-Dispersive X-ray Spectrum

Sample	Fe	O	C	S
IONP	69.4	30.6	-	-
IONP@AO1	61.7	25.1	13.4	0.1
IONP@AO2	65.9	25.4	8.3	0.1

6.2.7 Computational Analysis

6.2.7.1 ADMET Studies

The physicochemical characteristics of synthesized MPAO was analyzed and calculated based on Lipinski rule of five (Mol. Weight ≤500 Da, Log P≤ 5, H-bond donor ≤5 and H bond accepter ≤10). Table 6.3 shows properties predicted by ADMET. Figure 6.8 (A-D) shows Molecular Lipophilicity Potential (MLP) to visualize hydrophobicity (blue and violet colors) and hydrophilicity (red and orange) on the molecular surface. miLogP method is used for MLP calculation from atomic hydrophobicity contributions; this method is the same as calculating the octanol-water partition coefficient (logP). MLP is valuable for rationalizing a variety of molecular Adsorption Distribution Metabolism and Excretion (ADME) properties (such as a membrane penetration or plasma-protein binding). 3D distribution of hydrophobicity on the molecule's surface is helpful to explain the difference in observed ADME properties of molecules having the same logP values (Zoete, Daina, Bovigny, & Michielin, 2016). The 3D parameter has more information than logP expressed by just a single value. Figure 6.7 shows boiled egg predictive model of lipophilicity (WLOGP) and polarity (tPSA) computation. The white region of the plot shows a higher probability of absorption in the gastrointestinal tract, while the yellow

region (yolk) suggests a higher probability of permeation in the brain (Daina & Zoete, 2016; Tortosa et al., 2020).

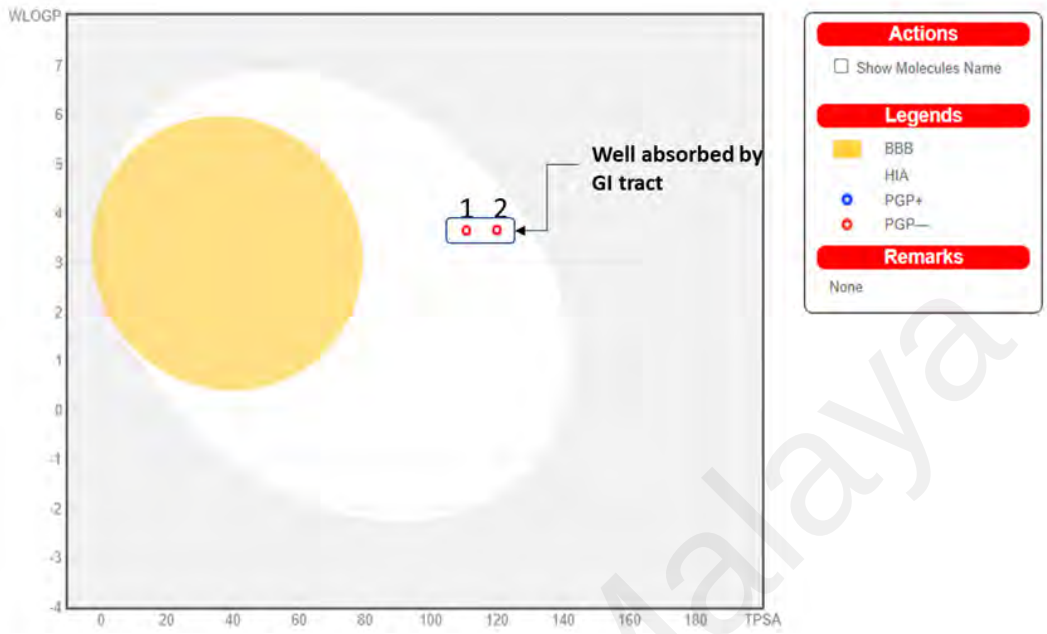

Figure 6.7 Boiled Egg Predictive Model of MPAO

Table 6.3 Predicted Absorption, Distribution, Metabolism, Excretion, and Toxicity (ADMET) Properties from Computational Analysis

Physicochemical Properties		
Formula	$C_{23}H_{38}O_6S$	$C_{25}H_{42}O_7S$
MW	442.61	486.66
#Heavy atoms	30	33
#Aromatic heavy atoms	6	6
Fraction Csp3	0.7	0.72
#Rotatable bonds	15	18
#H-bond acceptors	6	7
#H-bond donors	2	2
MR	122.63	133.33
TPSA	110.52	119.75
Lipophilicity		
iLOGP	4.57	4.78
XLOGP3	4.3	4.15
WLOGP	3.64	3.65
MLOGP	2.39	2.01
Silicos-IT Log P	5.47	5.89
Consensus Log P	4.07	4.1
Water Solubility		

ESOL Log S	-4.45	-4.42
ESOL Solubility (mg/ml)	1.57E-02	1.86E-02
ESOL Solubility (mol/l)	3.54E-05	3.82E-05
ESOL Class	Moderately soluble	Moderately soluble
Ali Log S	-6.33	-6.37
Ali Solubility (mg/ml)	2.05E-04	2.06E-04
Ali Solubility (mol/l)	4.63E-07	4.24E-07
Ali Class	Poorly soluble	Poorly soluble
Silicos-IT LogSw	-6.07	-6.57
Silicos-IT Solubility (mg/ml)	3.77E-04	1.30E-04
Silicos-IT Solubility (mol/l)	8.51E-07	2.67E-07
Silicos-IT class	Poorly soluble	Poorly soluble
Pharmacokinetics		
GI absorption	High	High
BBB permeant	No	No
Pgp substrate	No	No
CYP1A2 inhibitor	No	No
CYP2C19 inhibitor	No	No
CYP2C9 inhibitor	No	No
CYP2D6 inhibitor	Yes	No
CYP3A4 inhibitor	Yes	Yes
log Kp (cm/s)	-5.95	-6.32
Druglikeness		
Lipinski #violations	0	0
Ghose #violations	0	3
Veber #violations	1	1
Egan #violations	0	0
Muegge #violations	0	1
Bioavailability Score	0.55	0.55
Medicinal Chemistry		
PAINS #alerts	0	0
Brenk #alerts	0	0
Leadlikeness #violations	3	3
Synthetic Accessibility	4.04	4.32

6.2.7.2 PASS Analysis

PASS predictions forecasted the bioactivities of synthesized compounds. The multi-level neighbour of atoms (MNA) descriptors (2D molecular fragment) is used in PASS studies to describe biological activity is a molecular structure-function. The predictive score for activities is given as probability ratios between 'Probability to be active (Pa)' and

'probability of being non-active (Pi)'. Higher values of Pa represent the higher activity of organic molecules. Table 6.4 shows the selected bioactivities with higher Pa values when Pa>Pi. Figure 6.8 A-D shows the polar surface area and Molecular Lipophilicity Potential (MLP) of MPAO.

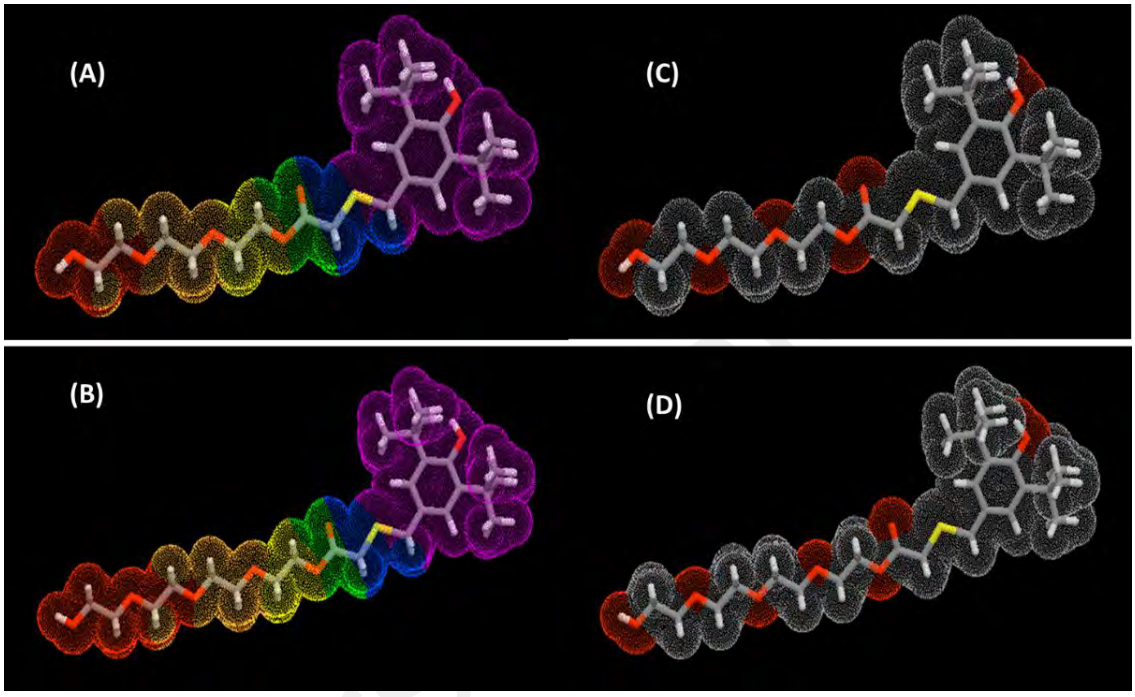

Figure 6.8(A)& (B) Molecular Lipophilicity Potential (MLP) (C)&(D) Polar Surface Area

Table 6.4 Part of the Predicted Biological Activity Spectra of the MPAO Based on PASS Prediction Software

MPAO		
[a]Pa	**[b]Pi**	**Biological Activity**
0.410	0.017	Free radical scavenger
0.420	0.030	Lipid peroxidase inhibitor
0.301	0.023	Antioxidant
0.308	0.078	Antifungal
0.262	0.077	Antibacterial

[a]Probability "to be active".
[b]Probability "to be inactive".

Antioxidant values and other predicted bioactivities of the MPAO having Pa > 0.7 suggest that nanomaterial functionalized with MPAO could display enhanced activities compared to nanoparticles without functionalization. This is owing to its biocompatibility, which can assist in the drug transportation system and bioimaging. Biological testing verified the predicted results.

6.2.8 Antioxidant Activity

Figure 6.9 shows UV-Visible spectra of the samples. At 517 nm, there is a reduction in peak intensity. The reduction in pak height was used to calculate the free radical scavenging percentage. The IC50 value (Table 6.5) and percentage inhibition of stable free radical DPPH for the synthesized nanoantioxidants were found to be 1.5 ± 0.002 mg/ml; 79% for IONP@AO1 and 2.4 ± 0.002 mg/ml; 58% for IONP@AO2 at a 10^{-4} M, which is two to four times more in comparison with bare iron oxide nanoparticles (IC50 4.7 ± 0.002 mg/ml; 50%), which is used as a reference in this experiment. In comparison to IONP, IONP@AO exhibited a greater capacity for free radical scavenging. The

electron transfer reaction between IONP@AO and DPPH is most likely responsible for the increased radical scavenging. Nanoparticles and MPAO promote good radical scavenging.

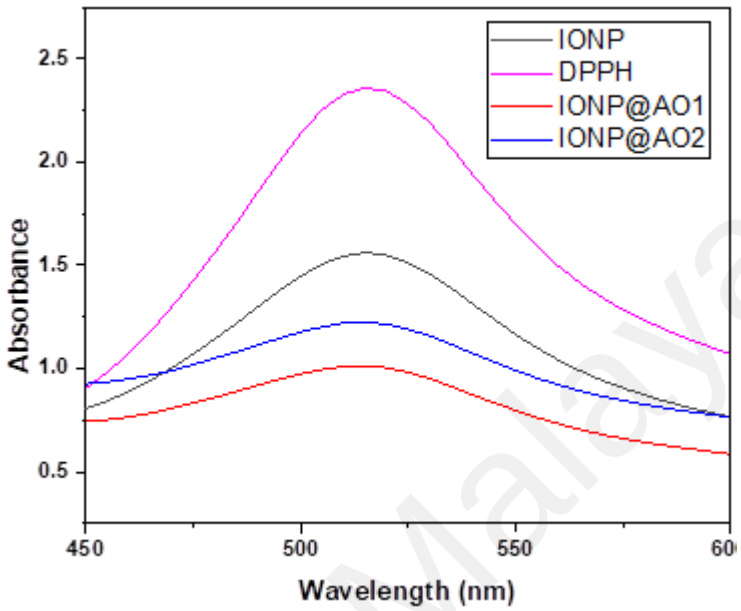

Figure 6.9 UV-Visible Spectra (a), DPPH Scavenging Percentage by IONP@AO at Different Concentrations

Table 6.5 IC50 of IONP@AO

IC50 [a] Values (mg) ± S.E.M [b] and Max. inhibition %			
Sample		**IC50 mg/ml**	**% Inhibition**
IONP	5 mg	4.7 ± 0.002	50
IONP@AO1	5 mg	1.5 ± 0.002	79
IONP@AO2	5 mg	2.4 ± 0.002	58

[a]IC50, 50% effective concentration.
[b]S.E.M, standard error of the mean.

6.2.9 Antimicrobial Activity

6.2.9.1 Antibacterial Activity

The results of the agar well diffusion technique are summarized in Figure 6.10 A. The percentage inhibition of bacteria's diameter growth (PIGD) is plotted against the 100 mg/ml experimental sample concentration. Antibacterial activity against Gram-negative and Gram-positive species of bacteria was observed for functionalized IONP@AO. For the most effective samples, the minimal inhibitory concentration was estimated. IONP@AO exhibited distinct bactericidal effects against Gram-positive and Gram-negative bacteria. Different varieties of bacteria had distinct types of cell walls leading to this finding. Gram-positive bacteria have a relatively substantial, thicker peptidoglycan layer (10–30 nm) on their surface, while Gram-negative bacteria have an additional outer layer with a thin layer of peptidoglycan (10 nm). IONP@AO has been shown to have varying degrees of antibacterial activity against a range of bacterial species. Internalization of functionalized IONPs within the cells happens when IONP@AO is introduced to bacterial strains, resulting in inhibition. Because the 1,4 glycosidic linkages are broken, the cell wall is eventually destroyed.

6.2.9.2 Antifungal Activity

The results obtained for an agar-well diffusion method are illustrated in Figure 6.10 B. Antifungal activity was observed for *Aspergillus Niger, Trichoderma spp., Candida albicans*, and *Saccharomyces cerevisiae*. For *Aspergillus Niger, Saccharomyces cerevisiae*, and *Candida albicans*, IONP@AO has shown enhanced antifungal activity. It has exhibited reduced antifungal activity for *Trichoderma sp*. Functionalized nanoparticles prompted cellular damage and death of the treated cells eventually. In

general, ultra-small nanoparticles have fungicidal activities. Nevertheless, it is determined by the synthesis protocol and physicochemical attributes of the nanoparticles.

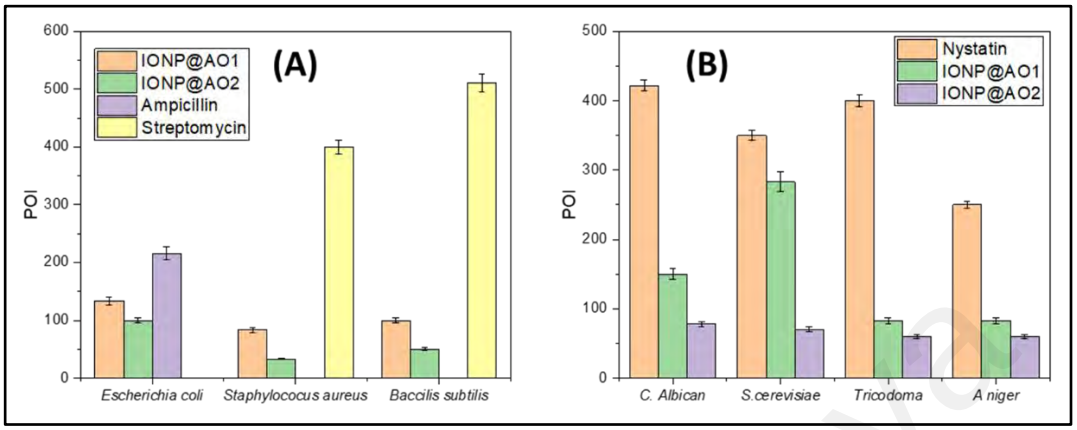

Figure 6.10. Percentage of Inhibition (POI) of (A) Bacterial Growth and (B) Fungal Growth, after treatment with IONP@AO

6.3 Conclusions

IONP functionalized with MPAO has been successfully synthesized by post-functionalization procedures. The possible bioactivities and safety profile of MPAO molecule were studied and predicted before the synthesis procedure by PASS analysis and ADMET studies using the structure-based virtual screening technique. The average particle size was 10 nm and 11nm for functionalized IONP@AO1 and IONP@AO2, respectively. The synthesized nanoparticles were analyzed using XRD, FTIR, VSM, EDX, HRTEM, and Raman analysis. It was observed that Magnetite retained its properties after functionalization with MPAO. All samples showed superparamagnetic behavior confirmed by VSM. IONP@AO1 showed better radical scavenging and antimicrobial activities compared to IONP@AO2 and IONP. MPAO functionalized IONP showed promising free radical scavenging properties and antimicrobial properties.

CHAPTER 7: SURFACE FUNCTIONALIZATION OF MAGNETITE NANOPARTICLES WITH MULTIPOTENT ANTIOXIDANT AS POTENTIAL MAGNETIC NANOANTIOXIDANTS AND ANTIMICROBIAL AGENTS

Antioxidants, recognized as prophylactic and therapeutic molecules, have various applications in the field of pharmaceuticals, cosmetics and nutraceuticals for many health benefits associated with their usage (Sandhir et al., 2015). Further study is being done to better understand antioxidants' involvement in the redox biological pathway, and to strengthen their ability to protect cells from reactive oxygen species (ROS). The phrase oxidative stress refers to an imbalance between the production of ROS and the body's response to these ROS. Internally generated ROS damage proteins, DNA, and lipids permanently to cause genetic mutations and ultimately lead to cell death (Nita & Grzybowski, 2016). Parkinson's disease, malignancies, Alzheimer's disease, and diabetes are all linked to the overproduction of reactive oxygen species (Liguori et al., 2018; Masoudkabir et al., 2017). Redox balance between pro- and antioxidants is critical in the treatment and prevention of many diseases. The use of antioxidants is generally restricted by their sensitivity to light, oxygen, and pH, as well as their poor solubility in physiological fluid, low bioavailability, and ineffective transport to undesirable cellular compartments, even if their potential is tremendous (Milinčić et al., 2019; Souto et al., 2013; Valgimigli et al., 2018). To promote healthy aging and prevent oxidative stress, researchers are always searching for new antioxidant species.

Nanoparticles can act as smart nanocarriers and have various applications such drug delivery. Combinatorial effects of material science with nanotechnology and engineering lead to important developments that decrease free radicals' production (Eftekhari, Ahmadian, Panahi-Azar, et al., 2018). 'Nanoantioxidants' are smart

nanocarriers with antioxidant capabilities that have been developed in recent years through nanotechnology application (Khalil et al., 2020). Using nanoantioxidant systems could overcome many of the limitations of standard antioxidant molecules and increase their efficiency, thanks to their prolonged stability, improved bioavailability, the capacity to evade quick metabolic clearance, and the potential to give a regulated and targeted delivery (Deligiannakis et al., 2012).

Smart nanocarriers surface can be functionalized with antioxidant molecules to transform nanoparticles into nanoantioxidants. In recent years, surface functionalization of nanoparticles with antioxidant has been used which improve their biostability, biocompatibility and ability to boost immune system (Marrazzo & O'Leary, 2020). Specifically, the simultaneous loading and functionalization of nanocarriers with antioxidants provides the advantage of delivering high antioxidant amounts and the possibility for the co-delivery of other drugs and, thus, for the use of these devices to exploit any synergic effects (Marina Massaro et al., 2016). Surface functionalization of nanoparticles with natural antioxidants also impart specific biological activity, which mainly depend upon the material used for functionalization such anticancer, antimicrobial, anti-Alzheimer's and antidiabetic. Rutin and caffeic acid functionalized silica nanoparticles were synthesized by Elle et al. which showed promising results minimizing ROS production (Ebabe Elle, Rahmani, Lauret, Morena, Bidel, Boulahtouf, Balaguer, Cristol, Durand, & Charnay, 2016). DPPH assay and radical scavening assay of Gold nanoparticle (AuNP) immobalized on Kraft paper and cellulose fibre was performed in both dark and light conditions. (Bumbudsanpharoke et al., 2015). Polyethylene glycol ($C_{2n}H_{4n+2}O_{n+1}$), PEG coated gold (AuNPs) was functionalized using the antioxidant of salvianic ($C_9H_{10}O_5$) acid (Au@PEG3SA). The antioxidant properties of the functionalized Au@PEG3SA was observed. The free radical -

scavenging rate of Au@PEG3SA was 9 times higher than that of the plain salvianic acid A monomers (Libo Du et al., 2013). The new potent nano-antioxidant of sulfur-containing butylated hydroxytoluene ligands (S-BHTLs)-conjugated with gold nanoparticles, Au-S-BHTLs, was synthesized by a conjugation of sulfur-containing ligands derived from BHT on the surface of gold nanoparticles (AuNPs). The in-house developing eight sulfur-containing BHT-ligands (S-BHTLs) were used for further study on functionalization with AuNPs and their biological activities (Ahmad et al., 2021). The antioxidant properties of iron oxide nanoparticles has already been studied and showing that radical scavening is due to electron transfer (Alves et al., 2016; Salvador et al., 2021). In another study, gallic acid and quercetin functionalized magnetite nanoparticles showed synergistic organic–inorganic hybrid antioxidant properties and potent antimicrobial activity on various fungal and bacterial strains (S. T. Shah, Yehye, Chowdhury, & Simarani, 2019; S. T. Shah et al., 2017).

Among the most commonly used synthetic antioxidants is butylated hydroxytoluene (BHT), with many reports confirming the potent antioxidant activity in various industrial applications such as food, oil, and cosmetics industries (Ariffin et al., 2014). In addition, this synthetic phenolic antioxidant has also been applied in therapeutic fields, however, certain features of volatility and high-temperature instability, as well as toxicities and safety concerns have greatly limited the effective therapeutic application (Elmadfa & Meyer, 2008). To this end, current research focuses on designing and synthesizing new BHT-derivatives to enhance antioxidant and therapeutic activities and reduce toxic side effects [5]. This study aimed to design and synthesize EG-ester of BHT bearing antioxidant groups as an effective strategy to enhance the safety profile, solubility of BHT, and synthesis of new multipotent antioxidant (MPAO) functionalized Magnetic nanoantioxidant. Prior to the synthesis of MPAO, computational studies were carried out

to verify whether the designed molecules is based on structure activity relation (SAR) strategy. Rule of five, Polar surface area and Lipinski parameters were used for predicting ADMET properties. PASS analysis was performed for MPAO to predict the potential biological activities of the molecule. Post functionalization technique was used to synthesize magnetic nanoantioxidants. Antioxidant assay and antimicrobial activities were carried out for IONP@AO.

7.1 Results and Discussion

7.1.1 FTIR Analysis

The FTIR spectra of Iron oxide nanoparticles (IONP) and antioxidant functionalized iron oxide nanoparticles IONP@AO are shown in Figure 7.1. Magnetite was observed in the nanoparticle samples by a strong absorption at 556 and 562 cm^{-1} for IONP and IONP@AO, respectively, which corresponds to Fe-O stretching vibrations (Sosa-Acosta et al., 2018). All the peaks represent the hydroxyl, carboxylic and aromatic groups present in organic molecule. The wide peak at 3100-3200 cm^{-1} represents the-OH stretching vibration. The peak at 1621 cm^{-1} confirms the existence of the carbonyl groups in IONP@AO (S. R. Kumar et al., 2014).

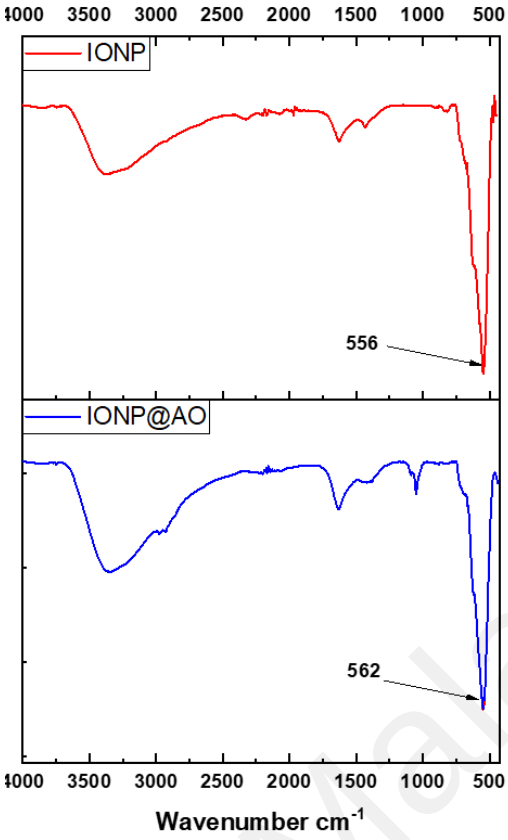

Figure 7.1. Surface Functional Groups Identification Using Fourier-Transform Infrared Spectra of IONP@AO

7.1.2 Raman Spectra

Figure 7.2 shows Raman spectra of the functionalized IONP and unfunctionalized IONP. The main band confirmed the presence of magnetite at 678 cm^{-1} (A1g) [11]. IONP@AO have a main band centered at 678 cm^{-1} and peaks at ca. 464 cm^{-1} and 344 cm^{-1} are due to A1g, T2g and Eg vibrations of magnetite. Raman spectra confirmed that the samples did not contain maghemite (Francisco et al., 2011; Shebanova & Lazor, 2003).

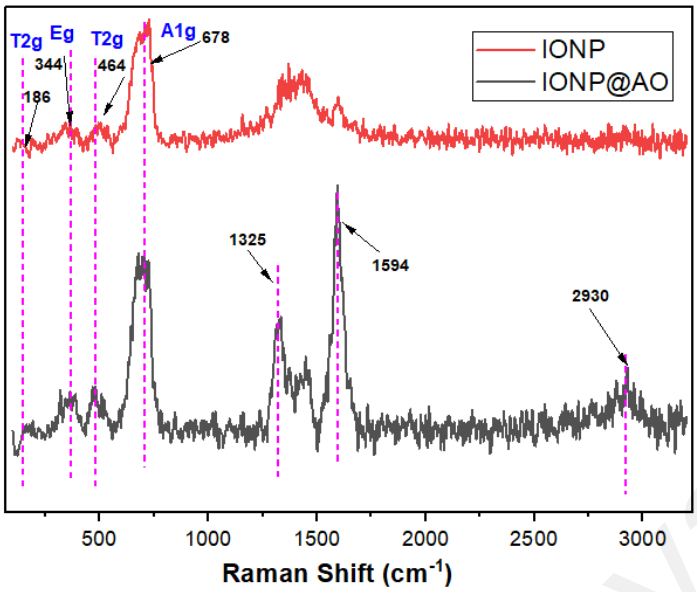

Figure 7.2. Raman Spectra of IONP@AO

7.1.3 XRD Analysis

XRD spectra for IONP and IONP@AO is shown in Figure 7.3. Diffraction peaks were observed in all samples at 2θ values of 30, 25, 43, 57, and 63, which correspond to Bragg reflections in [220], [311,] [400], [422] and [440] planes, respectively. Magnetite nanoparticles synthesized here have a cubic inverse spinal framework based on the XRD pattern (JCPDS No. 82-1533). The superlattice diffraction at 210, 213 and 300 were not present, confirming the absence of maghemite in the sample. Furthermore, no phase change was observed, which confirmed that functionalization with organic moieties did not affect the phase of magnetite.

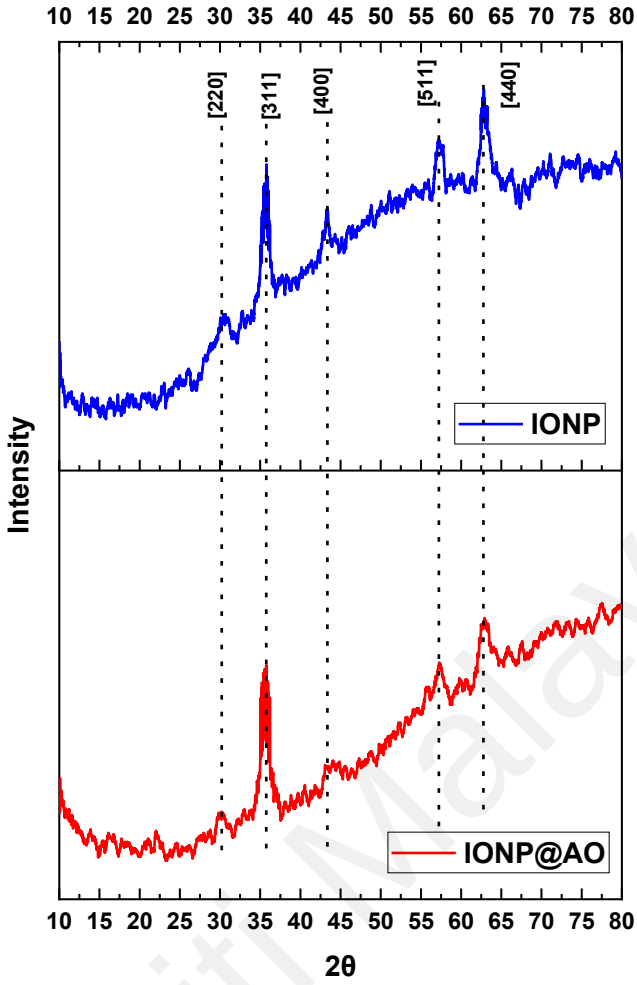

Figure 7.3. X-Ray Diffraction Spectra of IONP@AO

7.1.4 Magnetic Properties

A Vibrating Sample Magnetometer (VSM) was used to determine saturated mass magnetization. The values of 64.19 and 45 emu g^{-1} were given for bare Iron oxide nanoparticles and functionalized IONP@AO, respectively. Figure 7.4 shows the hysteresis loops as a function of the magnetic field at room temperature. All samples showed superparamagnetic behaviour, and their saturation magnetization was lower as compared to bulk Magnetite (92 emu g^{-1} (Cornell & Schwertmann, 2006). The decrease in saturation magnetization of IONP@AO over the surface of the produced nanoparticles

is most likely due to organic molecules and impurities (Dorniani et al., 2014; Dorniani et al., 2012; Ma et al., 2007).

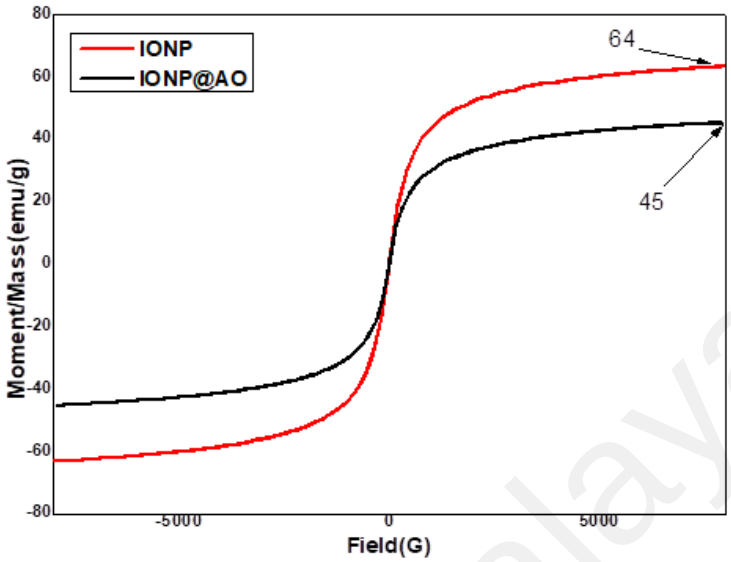

Figure 7.4. VSM of IONP@AO

7.1.5 Morphological and Structural Studies

High-Resolution Transmission Electron Microscopy (HRTEM) was used to analyze morphology of IONP@AO. HRTEM Image and size distribution for IONP and IONP@AO is shown in Figure 7.5. The TEM images revealed that the mean particle size was 10.07 and 10 nm for IONP and IONP@AO, respectively. The particles are spherical in shape and have a homogeneous size distribution. The magnetic behaviour of the samples causes the aggregation of iron oxide nanoparticles. The lattice fringe spacing of 0.26 corresponds to (220) lattice pane of magnetite nanoparticles (Iyengar et al., 2014).

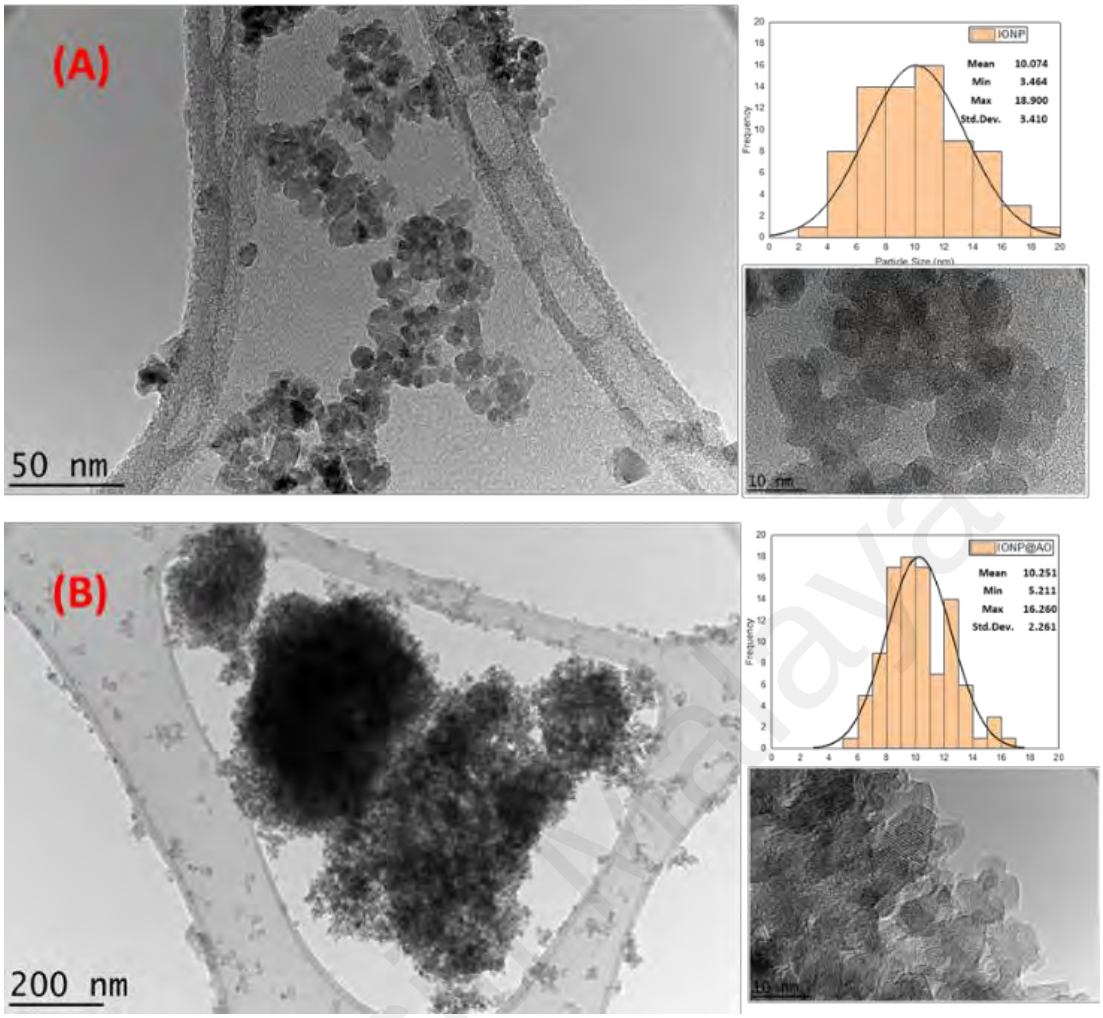

Figure 7.5. HRTEM of IONP@AO

.

7.1.6 EDX Analysis

An energy-dispersive X-ray spectroscopy (EDX) analysis was used to determine the elements in IONP and IONP@AO, respectively. Table 7.1 shows the elemental analysis of the synthesized IONP@AO. Figure 7.6 shows the EDX and elemental map of Fe, O, C and S for functionalized and unfunctionalized IONP. The EDX spectrum of the IONP@AO consisted of different peaks for Fe, O, C, and S confirming the successful formation of IONP@AO. The Fe and O signals are due to iron oxide, while is carbon signals are due to organic matrix. Furthermore, the IONP@AO elemental mapping revealed that MPAO was spread uniformly throughout the microstructure of the IONP.

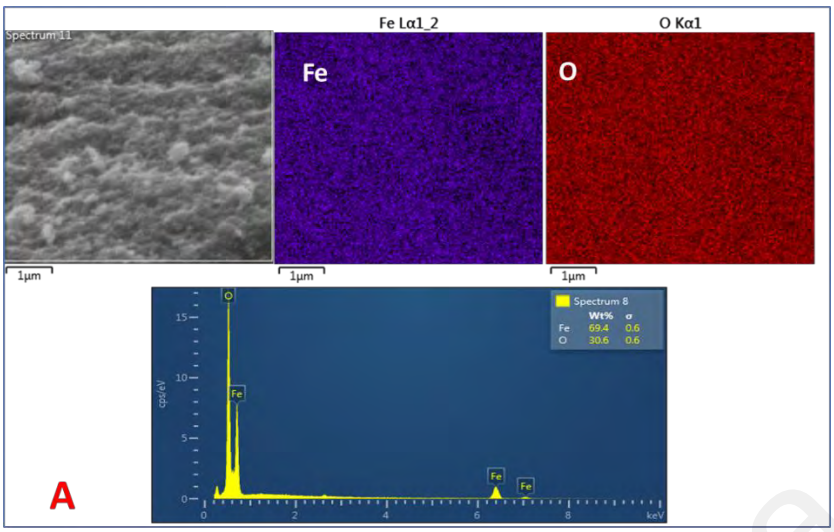

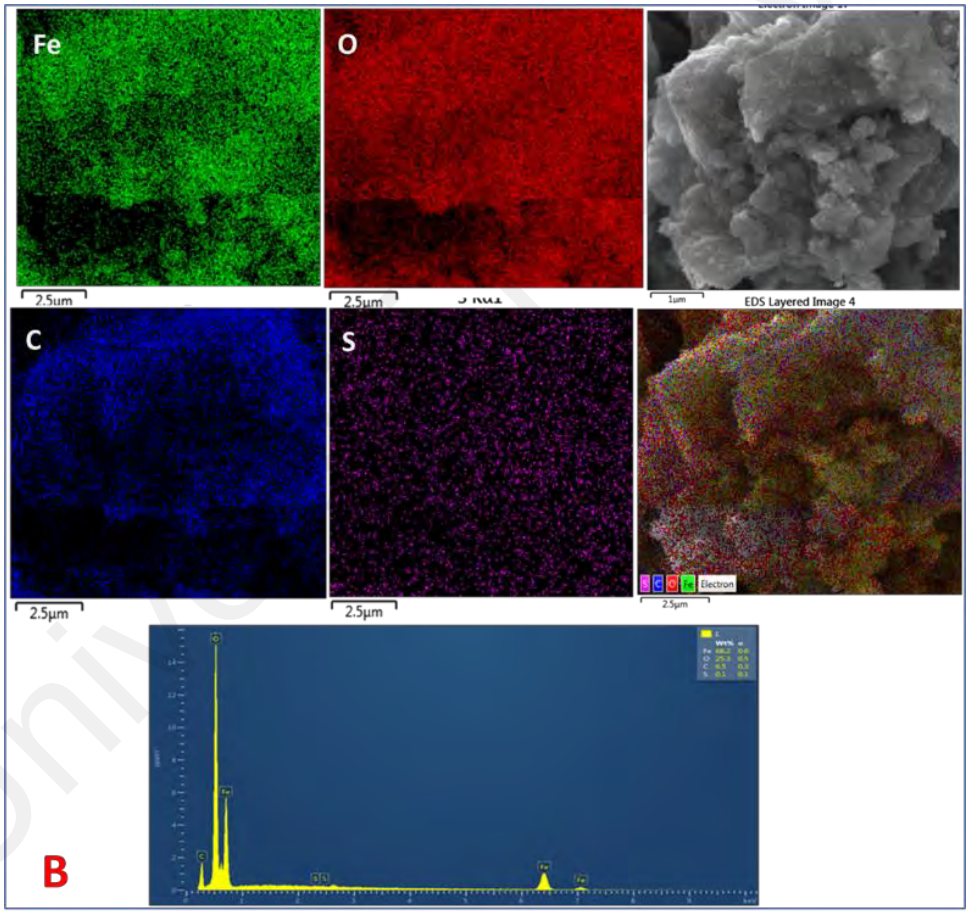

Figure 7.6. FESEM image, EDX and elemental map of Fe, O, C and S) of IONP@AO

Table 7.1. EDX Elemental Analysis of IONP@AO

Sample	Fe	O	C	S
IONP	69.4	30.6	-	-
IONP@AO	68.2	25.3	6.5	0.1

7.1.7 Computational Analysis

7.1.7.1 ADMET Studies

The physicochemical characteristics of synthesized MPAO was analyzed and calculated based on Lipinski rule of five (Mol. Weight ≤500 Da, Log P≤ 5, H-bond donor ≤5 and H bond accepter ≤10). Table 2 shows properties predicted by ADMET. Figure 7.7 A shows molecular lipophilicity potential (MLP) to visualize hydrophobicity (violet and blue colors) and hydrophilicity (orange and red) on the molecular surface. miLogP method is used for MLP calculation from atomic hydrophobicity contributions; this method is the same as calculating the octanol-water partition coefficient (logP). MLP is a valuable property to rationalize various molecular ADME characteristics (like membrane penetration or plasma-protein binding). 3D distribution of hydrophobicity on the molecule's surface is helpful to explain the difference in observed ADME properties of molecules having the same logP values (Zoete et al., 2016). The 3D parameter have more information than logP expressed by just a single value. Figure 7.7 C shows boiled egg predictive model of lipophilicity (WLOGP) and polarity (tPSA) computation. The white region of the plot shows higher probability of absorption in the gastrointestinal tract, while the yellow region (yolk) suggest a higher probability of permeation in the brain (Daina & Zoete, 2016).

Table 7.2 Predicted ADMET Properties from Computational Analysis

Physicochemical Properties	
#Rotatable bonds	13
#H-bond acceptors	5
#H-bond donors	1
MR	116.67
TPSA	90.29
Lipophilicity	
iLOGP	4.58
XLOGP3	4.98
WLOGP	4.27
MLOGP	2.99
Silicos-IT Log P	5.62
Consensus Log P	4.49
Water Solubility	
ESOL Log S	-4.84
ESOL Solubility (mg/ml)	6.02E-03
ESOL Solubility (mol/l)	1.46E-05
ESOL Class	Moderately soluble
Pharmacokinetics	
GI absorption	High
BBB permeant	No
Pgp substrate	No
CYP1A2 inhibitor	No
CYP2C19 inhibitor	No
CYP2C9 inhibitor	No
CYP2D6 inhibitor	Yes
CYP3A4 inhibitor	Yes
log Kp (cm/s)	-5.28
Druglikeness	
Lipinski #violations	0
Ghose #violations	0
Veber #violations	1
Egan #violations	0
Muegge #violations	0
Bioavailability Score	0.55
Medicinal Chemistry	
PAINS #alerts	0
Brenk #alerts	0
Leadlikeness #violations	3
Synthetic Accessibility	3.89

7.1.7.2 PASS Analysis

PASS predictions predicted the bioactivities of synthesized compounds. The multi-level neighbour of atoms (MNA) descriptors (2D molecular fragment) is used in PASS studies which describe that biological activity is a function of molecular structure. The predictive score for activities is given as probability ratios between 'Probability to be active (Pa)' and 'probability of being non-active (Pi)'. Higher values of Pa represent the higher activity of organic molecules.

Table **7.3** show the selected bioactivities with higher Pa values when Pa>Pi. Figure 7.8 A and B shows polar surface area and Molecular Lipophilicity Potential (MLP) of MPAO respectively.

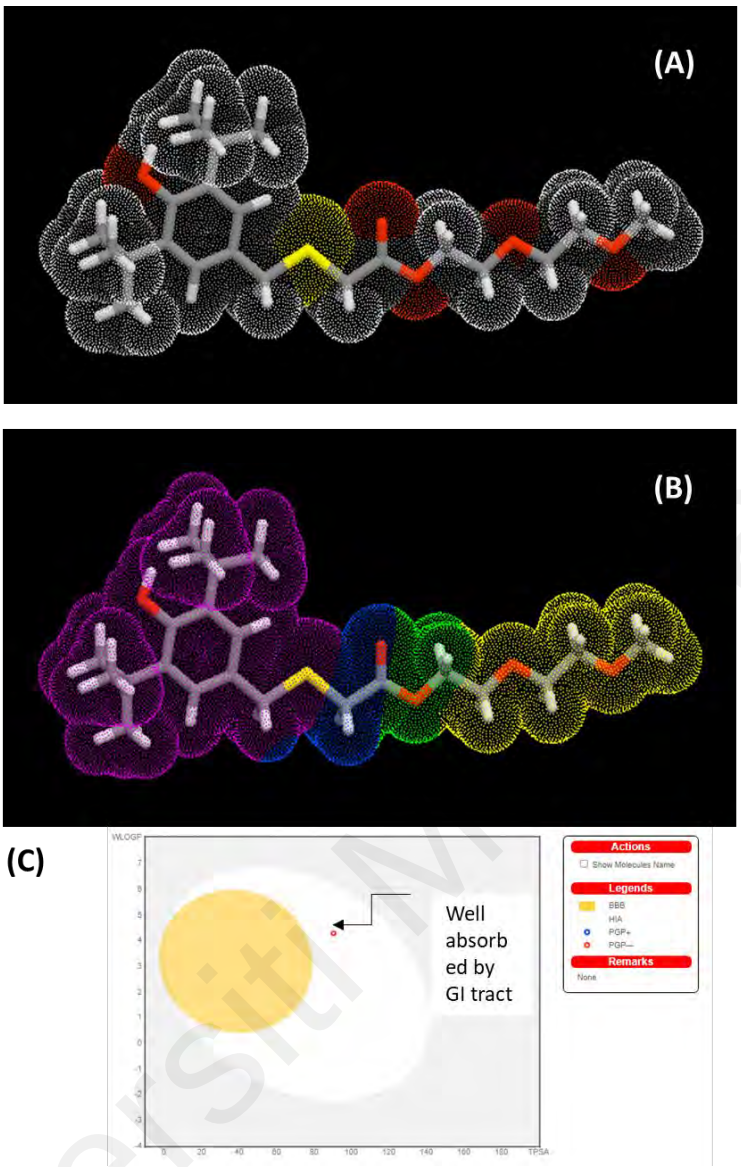

Figure 7.7. (A) Polar Surface Area (B) Molecular Lipophilicity Potential (MLP) and (C) Boiled Egg Predictive Model of MPAO

Table 7.3. Part of the Predicted Biological Activity Spectra of the MPAO Based on PASS Prediction Software

[a]Pa	[b]Pi	Biological Activity
0.456	0.013	Free radical scavenger
0.351	0.049	Lipid peroxidase inhibitor
0.285	0.026	Antioxidant
0.268	0.097	Antifungal
0.224	0.098	Antibacterial

[a]Probability "to be active."
[b]Probability "to be inactive."

Antioxidant values and other predicted bioactivities of the MPAO having Pa > 0.7 suggest that nanomaterial functionalized with MPAO could display enhanced activities compared to nanoparticles without functionalization. This is owing to its biocompatibility, which can assist in the drug transportation system and bioimaging. Biological testing verified the predicted results.

7.1.8 Antioxidant Activity

Figure 7.8 A shows UV-Visible spectra of the samples. The intensity of DPPH peak at 517nm is decreasing. The IC50 value and the reduction in peak intensity were used to determine the free radical scavenging properties (

Table 7.4). The per cent inhibition of stable free radical DPPH for synthesized nanoantioxidant was determined to be IONP@AO (1 ± 0.002 mg/ml; 83 per cent) and at a 10-4 M, which is 4 times higher than unfunctionalized IONP (IC50 4.7 ± 0.002 mg/ml; 50 per cent). In comparison to IONP, IONP@AO demonstrated greater free radical scavenging properties. Antioxidant activity depends on the presence of amount of total antioxidant compounds (Gangwar et al., 2014). The nanoantioxidant scavenges free radicals by transferring electrons from functionalized IONP@AO to the center nitrogen atoms of the DPPH. The synergistic effect of IONP and MPAO results in an increase in the free radical scavenging activity of IONP@AO.

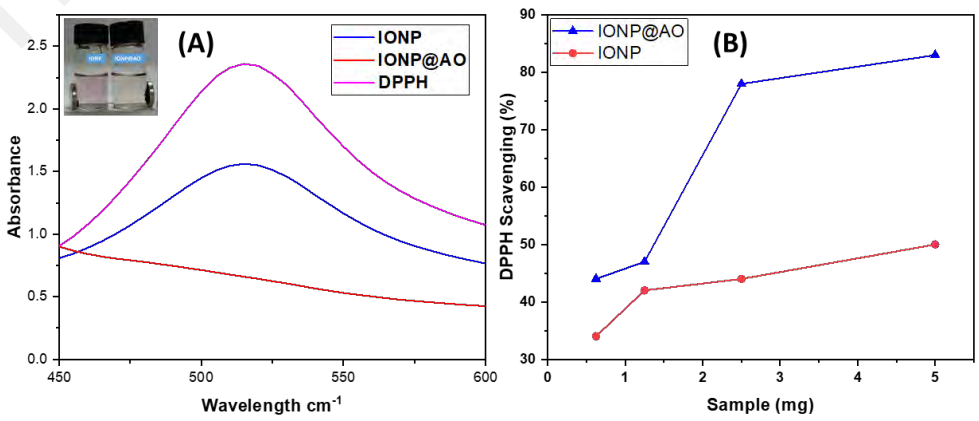

Figure 7.8. (A) UV-Visible Spectrum (B), DPPH Scavenging percentage by IONP@AO at Different Concentrations

Table 7.4. IC50 of IONP@AO

IC50[a] Values (mg) ± S.E.M[b] and Max. inhibition %			
Sample		IC50 mg/ml	% Inhibition
IONP	5 mg	4.7 ± 0.002	50
IONP@AO	5 mg	1 ± 0.002	83

[a]IC50, 50% effective concentration.
[b]S.E.M, standard error of the mean.

7.1.9 Antimicrobial Activity

7.1.9.1 Antibacterial Activity

The results of the agar well diffusion technique are summarized in Figure 7.9 A. The percentage inhibition of diameter growth (PIGD) of bacteria is plotted against the experimental sample concentration of 100 mg/ml. Antibacterial activity against Gram-negative and Gram-positive species of bacteria was observed for functionalized IONP@AO. For the most effective samples, the minimal inhibitory concentration was estimated. IONP@AO exhibited distinct bactericidal activity against Gram-positive and Gram-negative bacteria. Different varieties of bacteria had distinct types of cell walls leading to this finding. Gram-positive bacteria have a relatively substantial, thicker peptidoglycan layer (10–30 nm) on their surface, while Gram-negative bacteria have an additional outer layer with a thin layer of peptidoglycan (10 nm). IONP@AO has been shown to have varying degrees of antibacterial activity against a range of bacterial species. When IONP@AO is added to bacterial strains, inhibition occurs due to the internalization of functionalized IONPs within the cells. This ultimately results in the cell wall being destroyed by breaking the 1,4 glycosidic linkages.

7.1.9.2 Antifungal Activity

The results obtained for an agar-well diffusion method are illustrated in Figure 7.9 B. Antifungal activity was observed for *Aspergillus Niger, Trichoderma spp., Candida albicans*, and *Saccharomyces cerevisiae*. For *Aspergillus Niger, Saccharomyces cerevisiae*, and *Candida albicans*, IONP@AO has shown enhanced antifungal activity. It has exhibited reduced antifungal activity for *Trichoderma sp*. Functionalized nanoparticles prompted cellular damage and death of the treated cells eventually. In general, ultra-small nanoparticles have fungicidal activities. Nevertheless, it is determined by the synthesis protocol and physicochemical attributes of the nanoparticles.

In addition, the nanoparticle's high surface-to-volume ratio clings well to fungal cell surfaces. A smaller size also means that it can harm the cell wall directly because of its cellular penetrating nature. The direct contact between the nanoparticles and cell surface alters membrane permeability and results in the suppression of cell proliferation and eventually cell death of fungal cells (Xie, He, Irwin, Jin, & Shi, 2011).

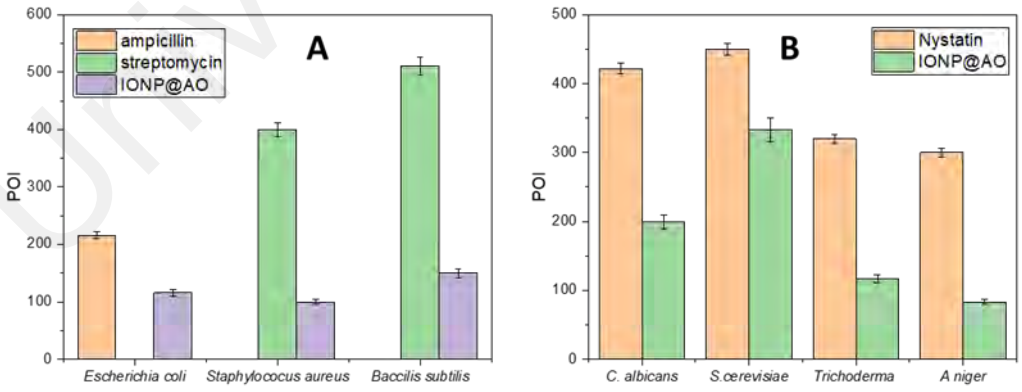

Figure 7.9. Percentage of Inhibition (POI) of (A) Bacterial Growth and (B) Fungal Growth, After Treatment with IONP@AO

7.2 Conclusions

MPAO functionalized IONP has been successfully synthesized using a post-functionalization procedure. For post-functionalized IONP@AO, the average particles size was 10 nm. The IONP@AO was studied using XRD, FTIR, VSM, EDX, HRTEM, and Raman analysis, which demonstrated that it had properties similar to magnetite. VSM confirmed the superparamagnetic nature of produced nanoparticles. In order to uncover and anticipate the molecule's potential bioactivities and safety profile, the structure-based virtual screening of MPAO was carried out via PASS analysis and ADMET studies. IONP@AO showed better radical scavenging and antimicrobial activities. MPAO functionalized IONP showed promising free radical scavenging.

CHAPTER 8: CONCLUSIONS

Nanoparticles of Fe_3O_4 were synthesized using a co-precipitation approach of Fe^{2+} and Fe^{3+} ions in a basified aqueous solution followed by a surface functionalization. Surface functionalization techniques were used to coat the nanoparticles with natural antioxidants and generate a variety of antioxidants (in-situ and post-synthesis approaches). Multipotent antioxidants (MPAO) were synthesized and characterized by NMR.The functionalized nanoparticles (IONP@AO) were characterised by FTIR, XRD, Raman, HRTEM, FESEM, VSM, and EDX. As IONP@GA is synthesised in-situ, it has an average particle size of 6-8 nanometers (nm), which is incredibly small compared to the typical particle sizes of IONP and post-functionalized magnetite. In addition, all nanoparticles had a high saturation magnetization of roughly 45-59 emu/g. Prediction Activity Spectra of Substances (PASS) software and Adsorption, Distribution, Metabolism, and Toxicity (ADMET) was used to predict the biological activities and safety profile of antioxidants prior to beginning experimental lab work, and it was discovered that experimental antioxidant activity using the 2,2-diphenyl-1-picrylhydrazyl (DPPH) assay is in good agreement with simulated results. In addition, when compared to unfunctionalized IONP, the half maximum inhibitory concentration (IC50) values of the DPPH antioxidant experiment were 2–4 times lower. Additionally, functionalized IONPs demonstrated exceptional antibacterial activity during testing on several bacterial and fungal strains. Because of their high hydrophilicity/lipophilicity, the newly discovered nanoantioxidants have the potential to interact with biological entities such as enzymes, proteins, amino acids, and DNA. The results reveal that the synthesized nanoparticles can be successfully used for the development of biomedicines which can be subsequently applied as antioxidant, anti-inflammatory, antibacterial and anticancer agent.

8.1 Recommendation for Future Research

The use of natural and synthetic antioxidants for the treatment of oxidative stress-induced disorders is now obsolete. Recently, nanoantioxidants have demonstrated the capacity to minimize oxidative stress with better sensitivity, cellular antioxidant activity, least cytotoxic effects, and tailored delivery in inorganic nanoparticles developed over the previous few decades. Antioxidants can be covalently attached or encapsulated with nanospheres of many types, such as inorganic nanoparticles, metal nanoparticles, and many more combinations, for various uses. However, a thorough understanding of the nanoantioxidant composites' origin, physicochemical properties, and mechanism of action is required to acquire the best catalytic and biological activity. In addition, comprehensive toxicity testing for nonbiodegradable and insoluble nanoparticles is required before any further biomedical application can be carried out. In addition, it is necessary to identify and assess the benefits and negative effects of the synthesised nanoantioxidants before they can be properly utilised in vivo, particularly for long-term treatment.

8.2 Limitation of this Study

There is a need for new nanoantioxidants, as well as new methods for measuring their antioxidant activity that are more precise and dependable. Because of this, nanoantioxidant treatments in the future will be shaped by advances in molecular knowledge, as well as the development of new nanostructures.

REFERENCES

Abdel-Aziz, M. S., Shaheen, M. S., El-Nekeety, A. A., & Abdel-Wahhab, M. A. (2014). Antioxidant and Antibacterial Activity of Silver Nanoparticles Biosynthesized Using Chenopodium Murale Leaf Extract. *Journal of Saudi Chemical Society, 18*(4), 356-363.

Abdoli, M., Arkan, E., Shekarbeygi, Z., & Khaledian, S. (2021). Green Synthesis of Gold Nanoparticles Using Centaurea Behen Leaf Aqueous Extract and Investigating Their Antioxidant and Cytotoxic Effects on Acute Leukemia Cancer Cell Line (Thp-1). *Inorganic Chemistry Communications, 129*, 108649.

Abdullah, J. A. A., Salah Eddine, L., Abderrhmane, B., Alonso-González, M., Guerrero, A., & Romero, A. (2020). Green Synthesis and Characterization of Iron Oxide Nanoparticles by Pheonix Dactylifera Leaf Extract and Evaluation of Their Antioxidant Activity. *Sustainable Chemistry and Pharmacy, 17*, 100280.

Adefegha, S. A., Oboh, G., Ejakpovi, I. I., & Oyeleye, S. I. (2015). Antioxidant and Antidiabetic Effects of Gallic and Protocatechuic Acids: A Structure-Function Perspective. *Comparative Clinical Pathology, 24*(6), 1579-1585.

Adewale, O. B., Egbeyemi, K. A., Onwuelu, J. O., Potts-Johnson, S. S., Anadozie, S. O., Fadaka, A. O., . . . Onasanya, A. (2020). Biological Synthesis of Gold and Silver Nanoparticles Using Leaf Extracts of Crassocephalum Rubens and Their Comparative in Vitro Antioxidant Activities. *Heliyon, 6*(11), e05501.

Aghamirzaei, M., Khiabani, M. S., Hamishehkar, H., Mokarram, R. R., & Amjadi, M. (2021). Antioxidant, Antimicrobial and Cytotoxic Activities of Biosynthesized Gold Nanoparticles (Aunps) from Chinese Lettuce (Cl) Leave Extract (Brassica Rapa Var. Pekinensis). *Materials Today Communications, 29*, 102831.

Ahamed, M., Akhtar, M. J., Khan, M. M., Alhadlaq, H. A., & Alshamsan, A. (2016). Cobalt Iron Oxide Nanoparticles Induce Cytotoxicity and Regulate the Apoptotic Genes through Ros in Human Liver Cells (Hepg2). *Colloids and surfaces B: biointerfaces, 148*, 665-673.

Ahmad, M. H., Yehye, W. A., Rahman, N. A., Al-Ani, L. A., Johan, M. R., Lu, J., & Hashim, N. M. (2021). Antioxidant and Cytotoxicity Activities of Butylated Hydroxytoluene Ligands Capped Gold Nanoparticles. *CHIANG MAI JOURNAL OF SCIENCE, 48*(2), 405-419.

Akiyama, H., Fujii, K., Yamasaki, O., Oono, T., & Iwatsuki, K. (2001). Antibacterial Action of Several Tannins against Staphylococcus Aureus. *Journal of antimicrobial chemotherapy, 48*(4), 487-491.

Alves, A. d. C. S., Mainardes, R. M., & Khalil, N. M. (2016). Nanoencapsulation of Gallic Acid and Evaluation of Its Cytotoxicity and Antioxidant Activity. *Materials Science and Engineering: C, 60*, 126-134.

Amorati, R., & Valgimigli, L. (2015). Advantages and Limitations of Common Testing Methods for Antioxidants. *Free Radical Research, 49*(5), 633-649.

Anagnostopoulou, M. A., Kefalas, P., Papageorgiou, V. P., Assimopoulou, A. N., & Boskou, D. (2006). Radical Scavenging Activity of Various Extracts and Fractions of Sweet Orange Peel (Citrus Sinensis). *Food Chemistry, 94*(1), 19-25.

Anzali, S., Barnickel, G., Cezanne, B., Krug, M., Filimonov, D., & Poroikov, V. (2001). Discriminating between Drugs and Nondrugs by Prediction of Activity Spectra for Substances (Pass). *Journal of Medicinal Chemistry, 44*(15), 2432-2437.

Ariffin, A., Rahman, N. A., Yehye, W. A., Alhadi, A. A., & Kadir, F. A. (2014). Pass-Assisted Design, Synthesis and Antioxidant Evaluation of New Butylated Hydroxytoluene Derivatives. *European Journal of Medicinal Chemistry, 87*, 564-577.

Armstrong, D., Bharali, D. J., Armstrong, D., & Bharali, D. (2013). Oxidative Stress and Nanotechnology. *Methods and Protocols, 1028*.

Arriagada, F., Correa, O., Günther, G., Nonell, S., Mura, F., Olea-Azar, C., & Morales, J. (2016). Morin Flavonoid Adsorbed on Mesoporous Silica, a Novel Antioxidant Nanomaterial. *PLoS One, 11*(11), e0164507.

Aygün, A., Özdemir, S., Gülcan, M., Cellat, K., & Şen, F. (2020). Synthesis and Characterization of Reishi Mushroom-Mediated Green Synthesis of Silver Nanoparticles for the Biochemical Applications. *Journal of Pharmaceutical and Biomedical Analysis, 178*, 112970.

Aziz, N., Farag, S., Mousa, L., & Abo-Zaid, M. J. M. (1998). Comparative Antibacterial and Antifungal Effects of Some Phenolic Compounds. *93*(374), 43-54.

Babay, S., Mhiri, T., & Toumi, M. (2015). Synthesis, Structural and Spectroscopic Characterizations of Maghemite Γ-Fe2o3 Prepared by One-Step Coprecipitation Route. *Journal of Molecular Structure, 1085*, 286-293.

Badmus, J. A., Oyemomi, S. A., Adedosu, O. T., Yekeen, T. A., Azeez, M. A., Adebayo, E. A., . . . Marnewick, J. L. (2020). Photo-Assisted Bio-Fabrication of Silver Nanoparticles Using Annona Muricata Leaf Extract: Exploring the Antioxidant, Anti-Diabetic, Antimicrobial, and Cytotoxic Activities. *Heliyon, 6*(11), e05413.

Balaji, S., Mandal, B. K., Ranjan, S., Dasgupta, N., & Chidambaram, R. (2017). Nano-Zirconia–Evaluation of Its Antioxidant and Anticancer Activity. *Journal of Photochemistry and Photobiology B: Biology, 170*, 125-133.

Barajas-Carmona, J. G., Francisco-Aldana, L., & Morales-Narv ez, E. (2017). Wearable Nanoplasmonic Patch Detecting Sun/Uv Exposure. *Analytical Chemistry, 89*(24), 13589-13595.

Barana, D., Orlandi, M., Zoia, L., Castellani, L., Hanel, T., Bolck, C., & Gosselink, R. (2018). Acs Sustainable Chem. *Eng, 6*, 11843-11852.

Baranwal, A., Mahato, K., Srivastava, A., Maurya, P. K., & Chandra, P. (2016). Phytofabricated Metallic Nanoparticles and Their Clinical Applications. *Rsc Advances, 6*(107), 105996-106010.

BarathManiKanth, S., Kalishwaralal, K., Sriram, M., Pandian, S. R. K., Youn, H.-s., Eom, S., & Gurunathan, S. (2010). Anti-Oxidant Effect of Gold Nanoparticles Restrains Hyperglycemic Conditions in Diabetic Mice. *J. Nanobiotechnology, 8*, 16-16.

Barreto, A. C. H., Santiago, V. R., Mazzetto, S. E., Denardin, J. C., Lavin, R., Mele, G., . . . Fechine, P. B. A. (2011). Magnetic Nanoparticles for a New Drug Delivery System to Control Quercetin Releasing for Cancer Chemotherapy. *Journal of Nanoparticle Research, 13*(12), 6545-6553.

Baygar, T., & Ugur, A. (2017). Biosynthesis of Silver Nanoparticles by Streptomyces Griseorubens Isolated from Soil and Their Antioxidant Activity. *IET Nanobiotechnology, 11*(3), 286-291.

Bhattacharya, K., Gogoi, B., Buragohain, A. K., & Deb, P. (2014). Fe2o3/C Nanocomposites Having Distinctive Antioxidant Activity and Hemolysis Prevention Efficiency. *Materials Science and Engineering C, 42*, 595-600.

Blanco-Andujar, C., Ortega, D., Southern, P., Pankhurst, Q. A., & Thanh, N. T. (2015). High Performance Multi-Core Iron Oxide Nanoparticles for Magnetic Hyperthermia: Microwave Synthesis, and the Role of Core-to-Core Interactions. *Nanoscale, 7*(5), 1768-1775.

Boyer, C., Whittaker, M. R., Bulmus, V., Liu, J., & Davis, T. P. (2010). The Design and Utility of Polymer-Stabilized Iron-Oxide Nanoparticles for Nanomedicine Applications. *NPG Asia Materials, 2*(1), 23-30.

Brand, M. D., Affourtit, C., Esteves, T. C., Green, K., Lambert, A. J., Miwa, S., . . . Parker, N. (2004). Mitochondrial Superoxide: Production, Biological Effects, and Activation of Uncoupling Proteins. *Free Radical Biology and Medicine, 37*(6), 755-767.

Bukhari, S. B., Memon, S., Mahroof-Tahir, M., & Bhanger, M. I. (2009). Synthesis, Characterization and Antioxidant Activity Copper–Quercetin Complex. *Spectrochimica Acta Part A: Molecular and Biomolecular Spectroscopy, 71*(5), 1901-1906.

Bumbudsanpharoke, N., Choi, J., Park, I., & Ko, S. (2015). Facile Biosynthesis and Antioxidant Property of Nanogold-Cellulose Fiber Composite. *Journal of Nanomaterials, 16*(1), 195.

Cadet, J., & Wagner, J. R. (2014). Oxidatively Generated Base Damage to Cellular DNA by Hydroxyl Radical and One-Electron Oxidants: Similarities and Differences. *Archives of Biochemistry and Biophysics, 557*, 47-54.

Cafun, J., Kvashnina, K., Casals, E., Puntes, V., & Glatzel, P. (2013). Absence of Ce 3+ Sites in Chemically Active Colloidal Ceria Nanoparticles. Acs Nano 7, 10726–10732. In.

Caputo, F., De Nicola, M., Sienkiewicz, A., Giovanetti, A., Bejarano, I., Licoccia, S., . . . Ghibelli, L. (2015). Cerium Oxide Nanoparticles, Combining Antioxidant and Uv Shielding Properties, Prevent Uv-Induced Cell Damage and Mutagenesis. *Nanoscale, 7*(38), 15643-15656.

Casas-Grajales, S., & Muriel, P. (2015). Antioxidants in Liver Health. *World Journal of Gastrointestinal Pharmacology and Therapeutics, 6*(3), 59-72.

Cedrowski, J., Litwinienko, G., Baschieri, A., & Amorati, R. (2016). Hydroperoxyl Radicals (Hoo.): Vitamin E Regeneration and H-Bond Effects on the Hydrogen Atom Transfer. *Chemistry–A European Journal, 22*(46), 16441-16445.

Celardo, I., Pedersen, J. Z., Traversa, E., & Ghibelli, L. (2011). Pharmacological Potential of Cerium Oxide Nanoparticles. *Nanoscale, 3*(4), 1411-1420.

Chakraborty, B., Kumar, R. S., Almansour, A. I., Kotresha, D., Rudrappa, M., Pallavi, S. S., . . . Nayaka, S. (2021). Evaluation of Antioxidant, Antimicrobial and Antiproliferative Activity of Silver Nanoparticles Derived from Galphimia Glauca Leaf Extract. *Journal of King Saud University - Science, 33*(8), 101660.

Chang, C. H., Lee, K.-Y., & Shim, Y. H. (2017). Normal Aging: Definition and Physiologic Changes. *jkma, 60*(5), 358-363.

Chang, K.-H., & Chen, C.-M. (2020). The Role of Oxidative Stress in Parkinson's Disease. *Antioxidants, 9*(7), 597.

Chang, Y., Zheng, C., Chinnathambi, A., Alahmadi, T. A., & Alharbi, S. A. (2021). Cytotoxicity, Anti-Acute Leukemia, and Antioxidant Properties of Gold Nanoparticles Green-Synthesized Using Cannabis Sativa L Leaf Aqueous Extract. *Arabian Journal of Chemistry, 14*(4), 103060.

Chatterjee, D. K., Gnanasammandhan, M. K., & Zhang, Y. (2010). Small Upconverting Fluorescent Nanoparticles for Biomedical Applications. *Small, 6*(24), 2781-2795.

Chavan, R. R., Bhinge, S. D., Bhutkar, M. A., Randive, D. S., Wadkar, G. H., Todkar, S. S., & Urade, M. N. (2020). Characterization, Antioxidant, Antimicrobial and Cytotoxic Activities of Green Synthesized Silver and Iron Nanoparticles Using Alcoholic Blumea Eriantha Dc Plant Extract. *Materials Today Communications, 24*, 101320.

Chen, J., Li, Y., Fang, G., Cao, Z., Shang, Y., Alfarraj, S., . . . Duan, X. (2021). Green Synthesis, Characterization, Cytotoxicity, Antioxidant, and Anti-Human Ovarian Cancer Activities of Curcumae Kwangsiensis Leaf Aqueous Extract Green-Synthesized Gold Nanoparticles. *Arabian Journal of Chemistry, 14*(3), 103000.

Chen, Z., Yin, J.-J., Zhou, Y.-T., Zhang, Y., Song, L., Song, M., . . . Gu, N. (2012). Dual Enzyme-Like Activities of Iron Oxide Nanoparticles and Their Implication for Diminishing Cytotoxicity. *ACS Nano, 6*(5), 4001-4012.

Chorny, M., Hood, E., Levy, R. J., & Muzykantov, V. R. (2010). Endothelial Delivery of Antioxidant Enzymes Loaded into Non-Polymeric Magnetic Nanoparticles. *Journal of Controlled Release, 146*(1), 144-151.

Cîrcu, M., Nan, A., Borodi, G., Liebscher, J., & Turcu, R. (2016). Refinement of Magnetite Nanoparticles by Coating with Organic Stabilizers. *Nanomaterials, 6*(12), 228.

Cornell, R. M., & Schwertmann, U. (2006). *The Iron Oxides: Structure, Properties, Reactions, Occurrences and Uses*: John Wiley & Sons.

Corr, S. A., Rakovich, Y. P., & Gun'ko, Y. K. (2008). Multifunctional Magnetic-Fluorescent Nanocomposites for Biomedical Applications. *Nanoscale Research Letters, 3*(3), 87.

Czochara, R., Kusio, J., & Litwinienko, G. (2017). Fullerene C 60 Conjugated with Phenols as New Hybrid Antioxidants to Improve the Oxidative Stability of Polymers at Elevated Temperatures. *Rsc Advances, 7*(70), 44021-44025.

Dabhade, P., & Kotwal, S. (2013). Tackling the Aging Process with Bio-Molecules: A Possible Role for Caloric Restriction, Food-Derived Nutrients, Vitamins, Amino Acids, Peptides, and Minerals. *Journal of Nutrition in Gerontology and Geriatrics, 32*(1), 24-40.

Daina, A., Michielin, O., & Zoete, V. (2017). Swissadme: A Free Web Tool to Evaluate Pharmacokinetics, Drug-Likeness and Medicinal Chemistry Friendliness of Small Molecules. *Scientific Reports, 7*(1), 42717.

Daina, A., & Zoete, V. (2016). A Boiled-Egg to Predict Gastrointestinal Absorption and Brain Penetration of Small Molecules. *ChemMedChem, 11*(11), 1117-1121.

Das, D., Ghosh, R., & Mandal, P. (2019). Biogenic Synthesis of Silver Nanoparticles Using S1 Genotype of Morus Alba Leaf Extract: Characterization, Antimicrobial and Antioxidant Potential Assessment. *SN Applied Sciences, 1*(5), 498.

Das, S., Dowding, J. M., Klump, K. E., McGinnis, J. F., Self, W., & Seal, S. (2013). Cerium Oxide Nanoparticles: Applications and Prospects in Nanomedicine. *Nanomedicine, 8*(9), 1483-1508.

Dasari, S., Suresh, K. A., Rajesh, M., Siva Reddy, C. S., Hemalatha, C. S., Wudayagiri, R., & Valluru, L. (2013). Biosynthesis, Characterization, Antibacterial and Antioxidant Activity of Silver Nanoparticles Produced by Lichens. *Journal of Bionanoscience, 7*(3), 237-244.

De Faria, D., Venâncio Silva, S., & De Oliveira, M. (1997). Raman Microspectroscopy of Some Iron Oxides and Oxyhydroxides. *Journal of Raman Spectroscopy, 28*(11), 873-878.

Deligiannakis, Y., Sotiriou, G. A., & Pratsinis, S. E. (2012). Antioxidant and Antiradical Sio2 Nanoparticles Covalently Functionalized with Gallic Acid. *Acs Applied Materials & Interfaces, 4*(12), 6609-6617.

Dong, J., Song, L., Yin, J.-J., He, W., Wu, Y., Gu, N., & Zhang, Y. (2014). Co3o4 Nanoparticles with Multi-Enzyme Activities and Their Application in Immunohistochemical Assay. *Acs Applied Materials & Interfaces, 6*(3), 1959-1970.

Dorniani, D., Bin, H. M. Z., Kura, A. U., Fakurazi, S., Hussein-Al-Ali, S. H., Shaari, A. H., & Ahmad, Z. (2014). In Vitro Sustained Release Study of Gallic Acid Coated with Magnetite-Peg and Magnetite-Pva for Drug Delivery System. *Scientific World J.*, 1-11.

Dorniani, D., Hussein, M. Z. B., Kura, A. U., Fakurazi, S., Shaari, A. H., & Ahmad, Z. (2012). Preparation of Fe3o4 Magnetic Nanoparticles Coated with Gallic Acid for Drug Delivery. *Int. J. Nanomedicine, 7*, 5745-5756.

Du, L., Li, J., Chen, C., & Liu, Y. (2014). Nanocarrier: A Potential Tool for Future Antioxidant Therapy. *Free Radical Research, 48*(9), 1061-1069.

Du, L., Suo, S., Wang, G., Jia, H., Liu, K. J., Zhao, B., & Liu, Y. (2013). Mechanism and Cellular Kinetic Studies of the Enhancement of Antioxidant Activity by Using Surface-Functionalized Gold Nanoparticles. *Chemistry–A European Journal, 19*(4), 1281-1287.

Ebabe Elle, R., Rahmani, S., Lauret, C., Morena, M., Bidel, L. P. R., Boulahtouf, A., . . . Charnay, C. (2016). Functionalized Mesoporous Silica Nanoparticle with Antioxidants as a New Carrier That Generates Lower Oxidative Stress Impact on Cells. *Molecular pharmaceutics, 13*(8), 2647-2660.

Ebabe Elle, R., Rahmani, S., Lauret, C., Morena, M., Bidel, L. P. R., Boulahtouf, A., . . . Badia, E. (2016). Functionalized Mesoporous Silica Nanoparticle with Antioxidants as a New Carrier That Generates Lower Oxidative Stress Impact on Cells. *Molecular pharmaceutics, 13*(8), 2647-2660.

Ebrahimi, N., Rasoul-Amini, S., Niazi, A., Erfani, N., Moghadam, A., Ebrahiminezhad, A., & Ghasemi, Y. (2016). Cytotoxic and Apoptotic Effects of Three Types of Silver-Iron Oxide Binary Hybrid Nanoparticles. *Current pharmaceutical biotechnology, 17*(12), 1049-1057.

Ebrahiminezhad, A., Zare-Hoseinabadi, A., Sarmah, A. K., Taghizadeh, S., Ghasemi, Y., & Berenjian, A. (2018). Plant-Mediated Synthesis and Applications of Iron Nanoparticles. *Molecular Biotechnology, 60*(2), 154-168.

Eftekhari, A., Ahmadian, E., Azami, A., Johari-Ahar, M., & Eghbal, M. A. (2018). Protective Effects of Coenzyme Q10 Nanoparticles on Dichlorvos-Induced Hepatotoxicity and Mitochondrial/Lysosomal Injury. *Environmental Toxicology, 33*(2), 167-177.

Eftekhari, A., Ahmadian, E., Panahi-Azar, V., Hosseini, H., Tabibiazar, M., & Maleki Dizaj, S. (2018). Hepatoprotective and Free Radical Scavenging Actions of Quercetin Nanoparticles on Aflatoxin B1-Induced Liver Damage: In Vitro/in Vivo Studies. *Artificial Cells, Nanomedicine, and Biotechnology, 46*(2), 411-420.

Eftekhari, A., Dizaj, S. M., Chodari, L., Sunar, S., Hasanzadeh, A., Ahmadian, E., & Hasanzadeh, M. (2018). The Promising Future of Nano-Antioxidant Therapy against Environmental Pollutants Induced-Toxicities. *Biomedicine & Pharmacotherapy, 103*, 1018-1027.

Elmadfa, I., & Meyer, A. L. (2008). Body Composition, Changing Physiological Functions and Nutrient Requirements of the Elderly. *Annals of Nutrition and Metabolism, 52(suppl 1)*(Suppl. 1), 2-5.

Enes, R. F., Tomé, A. C., Cavaleiro, J. A., Amorati, R., Fumo, M. G., Pedulli, G. F., & Valgimigli, L. (2006). Synthesis and Antioxidant Activity of [60] Fullerene–Bht Conjugates. *Chemistry–A European Journal, 12*(17), 4646-4653.

Erica, S., Daniel, A., & Silvana, A. (2011). Artificial Nanoparticle Antioxidants. In *Oxidative Stress: Diagnostics, Prevention, and Therapy* (Vol. 1083, pp. 235-253). Washington, DC, USA,: American Chemical Society.doi:10.1021/bk-2011-1083.ch008

10.1021/bk-2011-1083.ch008

Eriksson, P., Tal, A. A., Skallberg, A., Brommesson, C., Hu, Z., Boyd, R. D., . . . Uvdal, K. (2018). Cerium Oxide Nanoparticles with Antioxidant Capabilities and Gadolinium Integration for Mri Contrast Enhancement. *Scientific Reports, 8*(1), 6999.

Esumi, K., Takei, N., & Yoshimura, T. (2003). Antioxidant-Potentiality of Gold–Chitosan Nanocomposites. *Colloids and Surfaces B: Biointerfaces, 32*(2), 117-123.

Fan, J., Yin, J.-J., Ning, B., Wu, X., Hu, Y., Ferrari, M., . . . Nie, G. (2011). Direct Evidence for Catalase and Peroxidase Activities of Ferritin–Platinum Nanoparticles. *Biomaterials, 32*(6), 1611-1618.

Fleuriet, A., & Macheix, J.-J. (2003). Phenolic Acids in Fruits and Vegetables. *Flavonoids in health and disease*, 1.

Francisco, M., Teresa, C., María, C., Ramón, P., Rolando, R., Pedro, F., . . . Carmen, M. (2011). Synthesis and Characterization of Monodisperse Magnetite Hollow Microspheres. *Soft Nanosci. Lett., 1*, 25-32

Gangwar, M., Gautam, M. K., Sharma, A. K., Tripathi, Y. B., Goel, R. K., & Nath, G. (2014). Antioxidant Capacity and Radical Scavenging Effect of Polyphenol Rich Mallotus Philippenensis Fruit Extract on Human Erythrocytes: An in Vitro Study. *The Scientific World Journal, 2014*, 279451.

Gao, J., Gu, H., & Xu, B. (2009). Multifunctional Magnetic Nanoparticles: Design, Synthesis, and Biomedical Applications. *Accounts of Chemical Research, 42*(8), 1097-1107.

Gauthami, R., Vinitha, U. G., Philip Anthony, S., & Sundaram Muthuraman, M. (2021). Cissampelous Pairera Mediated Synthesis of Silver Nanoparticles and It's Invitro Antioxidant, Antibacterial and Antidiabetic Activities. *Materials Today: Proceedings, 47*, 853-857.

Ge, C., Fang, G., Shen, X., Chong, Y., Wamer, W. G., Gao, X., . . . Yin, J.-J. (2016). Facet Energy Versus Enzyme-Like Activities: The Unexpected Protection of

Palladium Nanocrystals against Oxidative Damage. *ACS Nano, 10*(11), 10436-10445.

Ge, L., Li, Q., Wang, M., Ouyang, J., Li, X., & Xing, M. M. (2014). Nanosilver Particles in Medical Applications: Synthesis, Performance, and Toxicity. *International Journal of Nanomedicine, 9*, 2399.

Geisinger, E., & Isberg, R. R. (2017). Interplay between Antibiotic Resistance and Virulence During Disease Promoted by Multidrug-Resistant Bacteria. *The Journal of infectious diseases, 215*(suppl_1), S9-S17.

German, J. B. (1999). Food Processing and Lipid Oxidation. *Adv Exp Med Biol, 459*, 23-50.

Gil, D., Rodriguez, J., Ward, B., Vertegel, A., Ivanov, V., & Reukov, V. (2017). Antioxidant Activity of Sod and Catalase Conjugated with Nanocrystalline Ceria. *Bioengineering, 4*(1), 18.

Ginting, B., Maulana, I., & Karnila, I. (2020). Biosynthesis Copper Nanoparticles Using Blumea Balsamifera Leaf Extracts: Characterization of Its Antioxidant and Cytotoxicity Activities. *Surfaces and Interfaces, 21*, 100799.

Gormaz, J. G., Quintremil, S., & Rodrigo, R. (2015). Cardiovascular Disease: A Target for the Pharmacological Effects of Quercetin. *Curr. Top. Med. Chem. (Sharjah, United Arab Emirates), 15*(17), 1735-1742.

Guajardo-Pacheco, M. J., Morales-Sánchez, J. E., González-Hernández, J., & Ruiz, F. (2010). Synthesis of Copper Nanoparticles Using Soybeans as a Chelant Agent. *Materials Letters, 64*(12), 1361-1364.

Guo, J., Wang, R., Tjiu, W. W., Pan, J., & Liu, T. (2012). Synthesis of Fe Nanoparticles@Graphene Composites for Environmental Applications. *Journal of Hazardous Materials, 225-226*, 63-73.

Gupta, A. K., & Gupta, M. (2005). Synthesis and Surface Engineering of Iron Oxide Nanoparticles for Biomedical Applications. *Biomaterials, 26*(18), 3995-4021.

Halliwell, B. (1995). *How to Characterize an Antioxidant: An Update.* Paper presented at the Biochemical Society Symposium.

Hans, M. L., & Lowman, A. M. (2002). Biodegradable Nanoparticles for Drug Delivery and Targeting. *Current Opinion in Solid State and Materials Science, 6*(4), 319-327.

Harman, D. (1956). Aging: A Theory Based on Free Radical and Radiation Chemistry. *Journal of Gerontology, 11*(3), 298-300.

Harshiny, M., Iswarya, C. N., & Matheswaran, M. (2015). Biogenic Synthesis of Iron Nanoparticles Using Amaranthus Dubius Leaf Extract as a Reducing Agent. *Powder Technology, 286*, 744-749.

Hasanzadeh, M., Mokhtari, F., Shadjou, N., Eftekhari, A., Mokhtarzadeh, A., Jouyban-Gharamaleki, V., & Mahboob, S. (2017). Poly Arginine-Graphene Quantum Dots as a Biocompatible and Non-Toxic Nanocomposite: Layer-by-Layer Electrochemical Preparation, Characterization and Non-Invasive Malondialdehyde Sensory Application in Exhaled Breath Condensate. *Materials Science and Engineering: C, 75*, 247-258.

Hasanzadeh, M., Tagi, S., Solhi, E., Mokhtarzadeh, A., Shadjou, N., Eftekhari, A., & Mahboob, S. (2018). An Innovative Immunosensor for Ultrasensitive Detection of Breast Cancer Specific Carbohydrate (Ca 15-3) in Unprocessed Human Plasma and Mcf-7 Breast Cancer Cell Lysates Using Gold Nanospear Electrochemically Assembled onto Thiolated Graphene Quantum Dots. *International Journal of Biological Macromolecules, 114*, 1008-1017.

Hawkins, M. J., Soon-Shiong, P., & Desai, N. (2008). Protein Nanoparticles as Drug Carriers in Clinical Medicine. *Advanced Drug Delivery Reviews, 60*(8), 876-885.

He, W., Zhou, Y.-T., Wamer, W. G., Hu, X., Wu, X., Zheng, Z., . . . Yin, J.-J. (2013). Intrinsic Catalytic Activity of Au Nanoparticles with Respect to Hydrogen Peroxide Decomposition and Superoxide Scavenging. *Biomaterials, 34*(3), 765-773.

He, Y. (2007). A Novel Solid-Stabilized Emulsion Approach to Cuo Nanostructured Microspheres. *Materials Research Bulletin, 42*(1), 190-195.

Hemmati, S., Ahmeda, A., Salehabadi, Y., Zangeneh, A., & Zangeneh, M. M. (2020). Synthesis, Characterization, and Evaluation of Cytotoxicity, Antioxidant, Antifungal, Antibacterial, and Cutaneous Wound Healing Effects of Copper Nanoparticles Using the Aqueous Extract of Strawberry Fruit and L-Ascorbic Acid. *Polyhedron, 180*, 114425.

Herlekar, M., Barve, S., & Kumar, R. (2014). Plant-Mediated Green Synthesis of Iron Nanoparticles. *Journal of Nanoparticles, 2014*, 140614.

Hirst, S. M., Karakoti, A., Singh, S., Self, W., Tyler, R., Seal, S., & Reilly, C. M. (2013). Bio-Distribution and in Vivo Antioxidant Effects of Cerium Oxide Nanoparticles in Mice. *Environmental Toxicology, 28*(2), 107-118.

Hoskins, C., Min, Y., Gueorguieva, M., McDougall, C., Volovick, A., Prentice, P., . . . Wang, L. (2012). Hybrid Gold-Iron Oxide Nanoparticles as a Multifunctional Platform for Biomedical Application. *Journal of Nanobiotechnology, 10*(1), 1-12.

Hosny, M., Fawzy, M., Abdelfatah, A. M., Fawzy, E. E., & Eltaweil, A. S. (2021). Comparative Study on the Potentialities of Two Halophytic Species in the Green Synthesis of Gold Nanoparticles and Their Anticancer, Antioxidant and Catalytic Efficiencies. *Advanced Powder Technology, 32*(9), 3220-3233.

Hu, B., Liu, X., Zhang, C., & Zeng, X. (2017). Food Macromolecule Based Nanodelivery Systems for Enhancing the Bioavailability of Polyphenols. *Journal of Food and Drug Analysis, 25*(1), 3-15.

Huang, Y., Liu, C., Pu, F., Liu, Z., Ren, J., & Qu, X. (2017). A Go–Se Nanocomposite as an Antioxidant Nanozyme for Cytoprotection. *Chemical communications, 53*(21), 3082-3085.

Huber, D. L. (2005). Synthesis, Properties, and Applications of Iron Nanoparticles. *Small, 1*(5), 482-501.

Ingold, K. U., & Pratt, D. A. (2014). Advances in Radical-Trapping Antioxidant Chemistry in the 21st Century: A Kinetics and Mechanisms Perspective. *Chemical Reviews, 114*(18), 9022-9046.

Islam, M. T. (2017). Oxidative Stress and Mitochondrial Dysfunction-Linked Neurodegenerative Disorders. *Neurological Research, 39*(1), 73-82.

Iyengar, S. J., Joy, M., Ghosh, C. K., Dey, S., Kotnala, R. K., & Ghosh, S. (2014). Magnetic, X-Ray and Mossbauer Studies on Magnetite/Maghemite Core-Shell Nanostructures Fabricated through an Aqueous Route. *RSC Adv., 4*(110), 64919-64929.

Jacob, R. (1996). Three Eras of Vitamin C Discovery. *Sub-cellular biochemistry, 25*, 1-16.

Jiang, L., Lin, J., Taggart, C. C., Bengoechea, J. A., & Scott, C. J. (2018). Nanodelivery Strategies for the Treatment of Multidrug-Resistant Bacterial Infections. *Journal of interdisciplinary nanomedicine, 3*(3), 111-121.

Joseph, A., Wood, T., Chen, C.-C., Corry, K., Snyder, J. M., Juul, S. E., . . . Nance, E. (2018). Curcumin-Loaded Polymeric Nanoparticles for Neuroprotection in Neonatal Rats with Hypoxic-Ischemic Encephalopathy. *Nano Research, 11*(10), 5670-5688.

Ju, E., Dong, K., Chen, Z., Liu, Z., Liu, C., Huang, Y., . . . Qu, X. (2016). Copper (Ii)–Graphitic Carbon Nitride Triggered Synergy: Improved Ros Generation and Reduced Glutathione Levels for Enhanced Photodynamic Therapy. *Angewandte Chemie International Edition, 55*(38), 11467-11471.

Ju, K.-Y., Lee, Y., Lee, S., Park, S. B., & Lee, J.-K. (2011). Bioinspired Polymerization of Dopamine to Generate Melanin-Like Nanoparticles Having an Excellent Free-Radical-Scavenging Property. *Biomacromolecules, 12*(3), 625-632.

Kadir, F., Kassim, N. B. M., Abdulla, M. A., Kamalidehghan, B., Ahmadipour, F., & Yehye, W. (2014). Pass-Predicted Hepatoprotective Activity of Caesalpinia Sappan in Thioacetamide-Induced Liver Fibrosis in Rats. *The Scientific World Journal, in press*.

Kajita, M., Hikosaka, K., Iitsuka, M., Kanayama, A., Toshima, N., & Miyamoto, Y. (2007). Platinum Nanoparticle Is a Useful Scavenger of Superoxide Anion and Hydrogen Peroxide. *Free Radical Research, 41*(6), 615-626.

Kalaiyarasan, T., Bharti, V. K., & Chaurasia, O. (2017). One Pot Green Preparation of Seabuckthorn Silver Nanoparticles (Sbt@ Agnps) Featuring High Stability and

Longevity, Antibacterial, Antioxidant Potential: A Nano Disinfectant Future Perspective. *RSC Advances, 7*(81), 51130-51141.

Kalashnikova, I., Mazar, J., Neal, C. J., Rosado, A. L., Das, S., Westmoreland, T. J., & Seal, S. (2017). Nanoparticle Delivery of Curcumin Induces Cellular Hypoxia and Ros-Mediated Apoptosis Via Modulation of Bcl-2/Bax in Human Neuroblastoma. *Nanoscale, 9*(29), 10375-10387.

Kareem, H. S., Ariffin, A., Nordin, N., Heidelberg, T., Abdul-Aziz, A., Kong, K. W., & Yehye, W. A. (2015). Correlation of Antioxidant Activities with Theoretical Studies for New Hydrazone Compounds Bearing a 3, 4, 5-Trimethoxy Benzyl Moiety. *European Journal of Medicinal Chemistry, 103*, 497-505.

Khalil, I., Yehye, W. A., Etxeberria, A. E., Alhadi, A. A., Dezfooli, S. M., Julkapli, N. B. M., . . . Seyfoddin, A. (2020). Nanoantioxidants: Recent Trends in Antioxidant Delivery Applications. *Antioxidants, 9*(1), 24.

Khan, F., Niaz, K., Maqbool, F., Ismail Hassan, F., Abdollahi, M., Nagulapalli Venkata, K. C., . . . Bishayee, A. (2016). Molecular Targets Underlying the Anticancer Effects of Quercetin: An Update. *Nutrients, 8*(9), 529.

Khan, M. I., & Giridhar, P. (2011). Dietary Antioxidants: The Insurer of Health. *Everyman's Sci, 46*(4), 214-218.

Khan, S., Shah, Z. H., Riaz, S., Ahmad, N., Islam, S., Raza, M. A., & Naseem, S. (2020). Antimicrobial Activity of Citric Acid Functionalized Iron Oxide Nanoparticles - Superparamagnetic Effect. *Ceram. Int., 46*(8_Part_A), 10942-10951.

Khan, W., Khan, N., Jamila, N., Masood, R., Minhaz, A., Amin, F., . . . Nishan, U. (2021). Antioxidant, Antibacterial, and Catalytic Performance of Biosynthesized Silver Nanoparticles of Rhus Javanica, Rumex Hastatus, and Callistemon Viminalis. *Saudi Journal of Biological Sciences*.

Khuda, F., Ul Haq, Z., Ilahi, I., Ullah, R., Khan, A., Fouad, H., . . . El-Saber Batiha, G. (2021). Synthesis of Gold Nanoparticles Using Sambucus Wightiana Extract and Investigation of Its Antimicrobial, Anti-Inflammatory, Antioxidant and Analgesic Activities. *Arabian Journal of Chemistry, 14*(10), 103343.

Kim, C. K., Kim, T., Choi, I.-Y., Soh, M., Kim, D., Kim, Y.-J., . . . Hyeon, T. (2012). Ceria Nanoparticles That Can Protect against Ischemic Stroke. *Angew. Chem., Int. Ed., 51*(44), 11039-11043.

Kim, H. J., Kim, D.-G., Yoon, H., Choi, Y.-S., Yoon, J., & Lee, J.-C. (2015). Polyphenol/Feiii Complex Coated Membranes Having Multifunctional Properties Prepared by a One-Step Fast Assembly. *Advanced Materials Interfaces, 2*(14), 1500298.

Kim, J., Takahashi, M., Shimizu, T., Shirasawa, T., Kajita, M., Kanayama, A., & Miyamoto, Y. (2008). Effects of a Potent Antioxidant, Platinum Nanoparticle, on the Lifespan of Caenorhabditis Elegans. *Mechanisms of Ageing and Development, 129*(6), 322-331.

Knight, J. A. (1998). Free Radicals: Their History and Current Status in Aging and Disease. *Annals of Clinical & Laboratory Science, 28*(6), 331-346.

Kogan, M. J., Olmedo, I., Hosta, L., Guerrero, A. R., Cruz, L. J., & Albericio, F. (2007). Peptides and Metallic Nanoparticles for Biomedical Applications. *Nanomedicine: Nanotechnology, Biology, and Medicine, 2*(3), 287-306.

Kojima, N., Shiraishi, Y., Hisamatsu, F., Miyamoto, A., & Kajita, M. (2008). JP2008156440A.

Kong, Y., Paray, B. A., Al-Sadoon, M. K., & Fahad Albeshr, M. (2021). Novel Green Synthesis, Chemical Characterization, Toxicity, Colorectal Carcinoma, Antioxidant, Anti-Diabetic, and Anticholinergic Properties of Silver Nanoparticles: A Chemopharmacological Study. *Arabian Journal of Chemistry, 14*(6), 103193.

Korschelt, K., Ragg, R., Metzger, C. S., Kluenker, M., Oster, M., Barton, B., . . . Mondeshki, M. (2017). Glycine-Functionalized Copper (Ii) Hydroxide Nanoparticles with High Intrinsic Superoxide Dismutase Activity. *Nanoscale, 9*(11), 3952-3960.

Kotcherlakota, R., Barui, A. K., Prashar, S., Fajardo, M., Briones, D., Rodríguez-Diéguez, A., . . . Gómez-Ruiz, S. (2016). Curcumin Loaded Mesoporous Silica: An Effective Drug Delivery System for Cancer Treatment. *Biomaterials Science, 4*(3), 448-459.

Krekel, C. (1999). The Chemistry of Historical Iron Gall Inks: Understanding the Chemistry of Writing Inks Used to Prepare Historical Documents. *Int. J. forensic document examiners, 5*, 54-58.

Kumar, G. S., Kulkarni, A., Khurana, A., Kaur, J., & Tikoo, K. (2014). Selenium Nanoparticles Involve Hsp-70 and Sirt1 in Preventing the Progression of Type 1 Diabetic Nephropathy. *Chemico-Biological Interactions, 223*, 125-133.

Kumar, H., Bhardwaj, K., Kuča, K., Kalia, A., Nepovimova, E., Verma, R., & Kumar, D. (2020). Flower-Based Green Synthesis of Metallic Nanoparticles: Applications Beyond Fragrance. *Nanomaterials, 10*(4), 766.

Kumar, S. R., Priyatharshni, S., Babu, V. N., Mangalaraj, D., Viswanathan, C., Kannan, S., & Ponpandian, N. (2014). Quercetin Conjugated Superparamagnetic Magnetite Nanoparticles for in-Vitro Analysis of Breast Cancer Cell Lines for Chemotherapy Applications. *Journal of Colloid and Interface Science, 436*, 234-242.

Kumari, A., Yadav, S. K., & Yadav, S. C. (2010). Biodegradable Polymeric Nanoparticles Based Drug Delivery Systems. *Colloids and Surfaces B: Biointerfaces, 75*(1), 1-18.

Lacramioara, L., Diaconu, A., Butnaru, M., & Verestiuc, L. (2016). Biocompatible Spions with Superoxid Dismutase/Catalase Immobilized for Cardiovascular Applications. In V. Sontea & I. Tiginyanu (Eds.), *3rd International Conference*

on Nanotechnologies and Biomedical Engineering (Vol. 55, pp. 323-326): Springer Singapore.10.1007/978-981-287-736-9_78

Lagunin, A., Stepanchikova, A., Filimonov, D., & Poroikov, V. (2000). Pass: Prediction of Activity Spectra for Biologically Active Substances. *Bioinformatics, 16*(8), 747-748.

Lam, S. J., O'Brien-Simpson, N. M., Pantarat, N., Sulistio, A., Wong, E. H., Chen, Y.-Y., . . . Reynolds, E. C. (2016). Combating Multidrug-Resistant Gram-Negative Bacteria with Structurally Nanoengineered Antimicrobial Peptide Polymers. *Nature microbiology, 1*(11), 1-11.

Lam, T., Avti, P., Pouliot, P., Maafi, F., Tardif, J.-C., Rhéaume, É., . . . Kakkar, A. (2016). Fabricating Water Dispersible Superparamagnetic Iron Oxide Nanoparticles for Biomedical Applications through Ligand Exchange and Direct Conjugation. *Nanomaterials, 6*(6), 100.

Laurent, S., Forge, D., Port, M., Roch, A., Robic, C., Vander Elst, L., & Muller, R. N. (2008). Magnetic Iron Oxide Nanoparticles: Synthesis, Stabilization, Vectorization, Physicochemical Characterizations, and Biological Applications. *Chemical Reviews, 108*(6), 2064-2110.

Lee, K. D., Nagajyothi, P. C., Sreekanth, T. V. M., & Park, S. (2015). Eco-Friendly Synthesis of Gold Nanoparticles (Aunps) Using Inonotus Obliquus and Their Antibacterial, Antioxidant and Cytotoxic Activities. *Journal of Industrial and Engineering Chemistry, 26*, 67-72.

Lee, S. S., Song, W., Cho, M., Puppala, H. L., Nguyen, P., Zhu, H., . . . Colvin, V. L. (2013). Antioxidant Properties of Cerium Oxide Nanocrystals as a Function of Nanocrystal Diameter and Surface Coating. *ACS Nano, 7*(11), 9693-9703.

Levine, M., Rumsey, S. C., Daruwala, R., Park, J. B., & Wang, Y. (1999). Criteria and Recommendations for Vitamin C Intake. *JAMA, 281*(15), 1415-1423.

Li, J., Liu, W., Wu, X., & Gao, X. (2015). Mechanism of Ph-Switchable Peroxidase and Catalase-Like Activities of Gold, Silver, Platinum and Palladium. *Biomaterials, 48*, 37-44.

Li, L., Ng, T. B., Gao, W., Li, W., Fu, M., Niu, S. M., . . . Liu, F. (2005). Antioxidant Activity of Gallic Acid from Rose Flowers in Senescence Accelerated Mice. *Life Sciences, 77*(2), 230-240.

Li, Y., Lin, R., Wang, L., Huang, J., Wu, H., Cheng, G., . . . Mao, H. (2015). Peg-B-Age Polymer Coated Magnetic Nanoparticle Probes with Facile Functionalization and Anti-Fouling Properties for Reducing Non-Specific Uptake and Improving Biomarker Targeting. *J. Mater. Chem. B, 3*(17), 3591-3603.

Liakos, I. L., Abdellatif, M. H., Innocenti, C., Scarpellini, A., Carzino, R., Brunetti, V., . . . Pompa, P. P. (2016). Antimicrobial Lemongrass Essential Oil—Copper Ferrite Cellulose Acetate Nanocapsules. *Molecules, 21*(4), 520.

Liao, H., Nehl, C. L., & Hafner, J. H. (2006). Biomedical Applications of Plasmon Resonant Metal Nanoparticles.

Liberman, A., Mendez, N., Trogler, W. C., & Kummel, A. C. (2014). Synthesis and Surface Functionalization of Silica Nanoparticles for Nanomedicine. *Surface science reports, 69*(2-3), 132-158.

Liguori, I., Russo, G., Curcio, F., Bulli, G., Aran, L., Della-Morte, D., . . . Bonaduce, D. (2018). Oxidative Stress, Aging, and Diseases. *Clinical interventions in aging, 13*, 757.

Lim, Y., Lim, T., & Tee, J. (2007). Antioxidant Properties of Several Tropical Fruits: A Comparative Study. *Food Chemistry, 103*(3), 1003-1008.

Liu, G. F., Filipović, M., Ivanović-Burmazović, I., Beuerle, F., Witte, P., & Hirsch, A. (2008). High Catalytic Activity of Dendritic C60 Monoadducts in Metal-Free Superoxide Dismutation. *Angewandte Chemie, 120*(21), 4055-4058.

Liu, K., Xiao, X., Wang, J., Chen, C. Y. O., & Hu, H. (2017). Polyphenolic Composition and Antioxidant, Antiproliferative, and Antimicrobial Activities of Mushroom Inonotus Sanghuang. *LWT - Food Science and Technology, 82*, 154-161.

Liu, P., Tang, H., Lu, M., Gao, C., Wang, F., Ding, Y., . . . Yang, M. (2017). Preparation of Nanosilica-Immobilized Antioxidant and the Antioxidative Behavior in Low Density Polyethylene. *Polymer Degradation and Stability, 135*, 1-7.

Liu, Y., Ai, K., Ji, X., Askhatova, D., Du, R., Lu, L., & Shi, J. (2017). Comprehensive Insights into the Multi-Antioxidative Mechanisms of Melanin Nanoparticles and Their Application to Protect Brain from Injury in Ischemic Stroke. *J. Am. Chem. Soc., 139*(2), 856-862.

Liu, Y., Wu, H., Li, M., Yin, J.-J., & Nie, Z. (2014). Ph Dependent Catalytic Activities of Platinum Nanoparticles with Respect to the Decomposition of Hydrogen Peroxide and Scavenging of Superoxide and Singlet Oxygen. *Nanoscale, 6*(20), 11904-11910.

Locatelli, C., Filippin-Monteiro, F. B., Centa, A., & Creczinsky-Pasa, T. B. (2013). *Antioxidant, Antitumoral and Anti-Inflammatory Activities of Gallic Acid* (Vol. Handbook on gallic acid: natural occurrences, antioxidant properties and health implications). New York: Nova Science Publishers.

Lopez-Abarrategui, C., Figueroa-Espi, V., Lugo-Alvarez, M. B., Pereira, C. D., Garay, H., Barbosa, J. A., . . . Reguera, E. (2016). The Intrinsic Antimicrobial Activity of Citric Acid-Coated Manganese Ferrite Nanoparticles Is Enhanced after Conjugation with the Antifungal Peptide Cm-P5. *International Journal of Nanomedicine, 11*, 3849.

López-Otín, C., Blasco, M. A., Partridge, L., Serrano, M., & Kroemer, G. (2013). The Hallmarks of Aging. *Cell, 153*(6), 1194-1217.

Lu, J., & Holmgren, A. (2014). The Thioredoxin Antioxidant System. *Free Radical Biology and Medicine, 66*, 75-87.

Lucente-Schultz, R. M., Moore, V. C., Leonard, A. D., Price, B. K., Kosynkin, D. V., Lu, M., . . . Tour, J. M. (2009). Antioxidant Single-Walled Carbon Nanotubes. *Journal of the American Chemical Society, 131*(11), 3934-3941.

M, M. H., Joshi, C. G., Danagoudar, A., Poyya, J., Kudva, A. K., & Bl, D. (2017). Biogenic Synthesis of Gold Nanoparticles by Marine Endophytic Fungus-Cladosporium Cladosporioides Isolated from Seaweed and Evaluation of Their Antioxidant and Antimicrobial Properties. *Process Biochemistry, 63*, 137-144.

Ma, H.-l., Qi, X.-r., Maitani, Y., & Nagai, T. (2007). Preparation and Characterization of Superparamagnetic Iron Oxide Nanoparticles Stabilized by Alginate. *International Journal of Pharmaceutics, 333*(1–2), 177-186.

Majeed, M. I., Lu, Q., Yan, W., Li, Z., Hussain, I., Tahir, M. N., . . . Tan, B. (2013). Highly Water-Soluble Magnetic Iron Oxide (Fe3o4) Nanoparticles for Drug Delivery: Enhanced in Vitro Therapeutic Efficacy of Doxorubicin and Mion Conjugates. *J. Mater. Chem. B, 1*(22), 2874-2884.

Manjunath Hulikere, M., & Joshi, C. G. (2019). Characterization, Antioxidant and Antimicrobial Activity of Silver Nanoparticles Synthesized Using Marine Endophytic Fungus- Cladosporium Cladosporioides. *Process Biochemistry, 82*, 199-204.

Markus, J., Mathiyalagan, R., Kim, Y.-J., Abbai, R., Singh, P., Ahn, S., . . . Yang, D. C. (2016). Intracellular Synthesis of Gold Nanoparticles with Antioxidant Activity by Probiotic Lactobacillus Kimchicus Dcy51t Isolated from Korean Kimchi. *Enzyme and Microbial Technology, 95*, 85-93.

Marrazzo, P., & O'Leary, C. (2020). Repositioning Natural Antioxidants for Therapeutic Applications in Tissue Engineering. *Bioengineering, 7*(3), 104.

Marulasiddeshwara, M., Dakshayani, S., Kumar, M. S., Chethana, R., Kumar, P. R., & Devaraja, S. (2017). Facile-One Pot-Green Synthesis, Antibacterial, Antifungal, Antioxidant and Antiplatelet Activities of Lignin Capped Silver Nanoparticles: A Promising Therapeutic Agent. *Materials Science and Engineering: C, 81*, 182-190.

Masoudkabir, F., Sarrafzadegan, N., Gotay, C., Ignaszewski, A., Krahn, A. D., Davis, M. K., . . . Mani, A. (2017). Cardiovascular Disease and Cancer: Evidence for Shared Disease Pathways and Pharmacologic Prevention. *Atherosclerosis, 263*, 343-351.

Massaro, M., Amorati, R., Cavallaro, G., Guernelli, S., Lazzara, G., Milioto, S., . . . Riela, S. (2016). Direct Chemical Grafted Curcumin on Halloysite Nanotubes as Dual-Responsive Prodrug for Pharmacological Applications. *Colloids and surfaces B: biointerfaces, 140*, 505-513.

Massaro, M., Riela, S., Guernelli, S., Parisi, F., Lazzara, G., Baschieri, A., . . . Amorati, R. (2016). A Synergic Nanoantioxidant Based on Covalently Modified Halloysite–Trolox Nanotubes with Intra-Lumen Loaded Quercetin. *Journal of Materials Chemistry B, 4*(13), 2229-2241.

Mattill, H. A. (1947). Antioxidants. *Annual Review of Biochemistry, 16*(1), 177-192.

Medhe, S., Bansal, P., & Srivastava, M. M. (2014). Enhanced Antioxidant Activity of Gold Nanoparticle Embedded 3, 6-Dihydroxyflavone: A Combinational Study. *Applied Nanoscience, 4*(2), 153-161.

Milanezi, F. G., Meireles, L. M., de Christo Scherer, M. M., de Oliveira, J. P., da Silva, A. R., de Araujo, M. L., . . . Scherer, R. (2019). Antioxidant, Antimicrobial and Cytotoxic Activities of Gold Nanoparticles Capped with Quercetin. *Saudi Pharmaceutical Journal, 27*(7), 968-974.

Milinčić, D. D., Popović, D. A., Lević, S. M., Kostić, A. Ž., Tešić, Ž. L., Nedović, V. A., & Pešić, M. B. (2019). Application of Polyphenol-Loaded Nanoparticles in Food Industry. *Nanomaterials, 9*(11), 1629.

Mirzajani, R., & Ahmadi, S. (2015). Melamine Supported Magnetic Iron Oxide Nanoparticles (Fe3o4@Mel) for Spectrophotometric Determination of Malachite Green in Water Samples and Fish Tissues. *Journal of Industrial and Engineering Chemistry, 23*(0), 171-178.

Mittal, A. K., Kumar, S., & Banerjee, U. C. (2014). Quercetin and Gallic Acid Mediated Synthesis of Bimetallic (Silver and Selenium) Nanoparticles and Their Antitumor and Antimicrobial Potential. *Journal of Colloid and Interface Science, 431*, 194-199.

Mobaraki, F., Momeni, M., Taghavizadeh Yazdi, M. E., Meshkat, Z., Silanian Toosi, M., & Hosseini, S. M. (2021). Plant-Derived Synthesis and Characterization of Gold Nanoparticles: Investigation of Its Antioxidant and Anticancer Activity against Human Testicular Embryonic Carcinoma Stem Cells. *Process Biochemistry, 111*, 167-177.

Moghaddam, A. B., Moniri, M., Azizi, S., Rahim, R. A., Ariff, A. B., Saad, W. Z., . . . Mohamad, R. (2017). Biosynthesis of Zno Nanoparticles by a New Pichia Kudriavzevii Yeast Strain and Evaluation of Their Antimicrobial and Antioxidant Activities. *Molecules, 22*(6), 872.

Moglianetti, M., De Luca, E., Pedone, D., Marotta, R., Catelani, T., Sartori, B., . . . Pompa, P. P. (2016). Platinum Nanozymes Recover Cellular Ros Homeostasis in an Oxidative Stress-Mediated Disease Model. *Nanoscale, 8*(6), 3739-3752.

Mohamed, N., Hessen, O. E. A., & Mohammed, H. S. (2021). Thermal Stability, Paramagnetic Properties, Morphology and Antioxidant Activity of Iron Oxide Nanoparticles Synthesized by Chemical and Green Methods. *Inorganic Chemistry Communications, 128*, 108572.

Mohammed, E., & Safwat, G. (2013). Assessment of the Ameliorative Role of Selenium Nanoparticles on the Oxidative Stress of Acetaminophen in Some Tissues of Male Albino Rats. *Beni-Suef University Journal of Basic and Applied Sciences, 2*(2), 80-85.

Morry, J., Ngamcherdtrakul, W., & Yantasee, W. (2017). Oxidative Stress in Cancer and Fibrosis: Opportunity for Therapeutic Intervention with Antioxidant Compounds, Enzymes, and Nanoparticles. *Redox biology, 11*, 240-253.

Motoyoshi, R., Oku, T., Suzuki, A., Kikuchi, K., Kikuchi, S., Jeyadevan, B., & Cuya, J. (2010). Fabrication and Characterization of Cuprous Oxide: Fullerene Solar Cells. *Synthetic Metals, 160*(11), 1219-1222.

Mu, J., Zhang, L., Zhao, M., & Wang, Y. (2013). Co3o4 Nanoparticles as an Efficient Catalase Mimic: Properties, Mechanism and Its Electrocatalytic Sensing Application for Hydrogen Peroxide. *Journal of Molecular Catalysis A: Chemical, 378*, 30-37.

Mu, J., Zhang, L., Zhao, M., & Wang, Y. (2014). Catalase Mimic Property of Co3o4 Nanomaterials with Different Morphology and Its Application as a Calcium Sensor. *Acs Applied Materials & Interfaces, 6*(10), 7090-7098.

Muniyappan, N., Pandeeswaran, M., & Amalraj, A. (2021). Green Synthesis of Gold Nanoparticles Using Curcuma Pseudomontana Isolated Curcumin: Its Characterization, Antimicrobial, Antioxidant and Anti- Inflammatory Activities. *Environmental Chemistry and Ecotoxicology, 3*, 117-124.

Muthukumar, H., & Matheswaran, M. (2015). Amaranthus Spinosus Leaf Extract Mediated Feo Nanoparticles: Physicochemical Traits, Photocatalytic and Antioxidant Activity. *Acs Sustainable Chemistry & Engineering, 3*(12), 3149-3156.

Nasirimoghaddam, S., Zeinali, S., & Sabbaghi, S. (2015). Chitosan Coated Magnetic Nanoparticles as Nano-Adsorbent for Efficient Removal of Mercury Contents from Industrial Aqueous and Oily Samples. *J. Ind. Eng. Chem., 27*(0), 79-87.

Naveena, B. E., & Prakash, S. (2013). Biological Synthesis of Gold Nanoparticles Using Marine Algae Gracilaria Corticata and Its Application as a Potent Antimicrobial and Antioxidant Agent. *Asian J Pharm Clin Res, 6*(2), 179-182.

Nelson, B. C., Johnson, M. E., Walker, M. L., Riley, K. R., & Sims, C. M. (2016). Antioxidant Cerium Oxide Nanoparticles in Biology and Medicine. *Antioxidants, 5*(2), 15.

Netala, V. R., Bethu, M. S., Pushpalatha, B., Baki, V. B., Aishwarya, S., Rao, J. V., & Tartte, V. (2016). Biogenesis of Silver Nanoparticles Using Endophytic Fungus Pestalotiopsis Microspora and Evaluation of Their Antioxidant and Anticancer Activities. *International Journal of Nanomedicine, 11*, 5683.

Netala, V. R., Kotakadi, V. S., Bobbu, P., Gaddam, S. A., & Tartte, V. (2016). Endophytic Fungal Isolate Mediated Biosynthesis of Silver Nanoparticles and Their Free Radical Scavenging Activity and Anti Microbial Studies. *3 Biotech, 6*(2), 132.

Nie, Z., Liu, K. J., Zhong, C.-J., Wang, L.-F., Yang, Y., Tian, Q., & Liu, Y. (2007). Enhanced Radical Scavenging Activity by Antioxidant-Functionalized Gold Nanoparticles: A Novel Inspiration for Development of New Artificial Antioxidants. *Free Radical Biology and Medicine, 43*(9), 1243-1254.

Nita, M., & Grzybowski, A. (2016). The Role of the Reactive Oxygen Species and Oxidative Stress in the Pathomechanism of the Age-Related Ocular Diseases and

Other Pathologies of the Anterior and Posterior Eye Segments in Adults. *Oxidative medicine and cellular longevity, 2016*, 3164734-3164734.

Niu, J., Wang, K., & Kolattukudy, P. E. (2011). Cerium Oxide Nanoparticles Inhibits Oxidative Stress and Nuclear Factor-Kb Activation in H9c2 Cardiomyocytes Exposed to Cigarette Smoke Extract. *Journal of Pharmacology and Experimental Therapeutics, 338*(1), 53-61.

Nosaka, Y., & Nosaka, A. Y. (2017). Generation and Detection of Reactive Oxygen Species in Photocatalysis. *Chemical Reviews, 117*(17), 11302-11336.

Numata, Y., & Tanaka, H. (2011). Quantitative Analysis of Quercetin Using Raman Spectroscopy. *Food Chemistry, 126*(2), 751-755.

Oladipo, I. C., Lateef, A., Elegbede, J. A., Azeez, M. A., Asafa, T. B., Yekeen, T. A., . . . Atanda, O. R. (2017). Enterococcus Species for the One-Pot Biofabrication of Gold Nanoparticles: Characterization and Nanobiotechnological Applications. *Journal of Photochemistry and Photobiology B: Biology, 173*, 250-257.

Padmavathy, N., & Vijayaraghavan, R. (2008). Enhanced Bioactivity of Zno Nanoparticles—an Antimicrobial Study. *Science and Technology of Advanced Materials, 9*(3), 035004.

Padmavathy, N., & Vijayaraghavan, R. (2011). Interaction of Zno Nanoparticles with Microbes—a Physio and Biochemical Assay. *Journal of Biomedical Nanotechnology, 7*(6), 813-822.

Pan, F., Xu, A., Xia, D., Yu, Y., Chen, G., Meyer, M., . . . Fu, J. (2015). Effects of Octahedral Molecular Sieve on Treatment Performance, Microbial Metabolism, and Microbial Community in Expanded Granular Sludge Bed Reactor. *Water Research, 87*, 127-136.

Patrick-Iwuanyanwu, K., Onyeike, E., & Adhikari, A. (2014). Isolation, Identification and Characterization of Gallic Acid Derivatives from Leaves of Tapinanthus Bangwensis. *Journal of Natural Products, 7*, 14-19.

Paul, S., Saikia, J., Samdarshi, S., & Konwar, B. (2009). Investigation of Antioxidant Property of Iron Oxide Particlesby 1′-1′ Diphenylpicryl-Hydrazyle (Dpph) Method. *Journal of Magnetism and Magnetic Materials, 321*(21), 3621-3623.

Periakaruppan, R., Chen, X., Thangaraj, K., Jeyaraj, A., Nguyen, H. H., Yu, Y., . . . Li, X. (2021). Utilization of Tea Resources with the Production of Superparamagnetic Biogenic Iron Oxide Nanoparticles and an Assessment of Their Antioxidant Activities. *Journal of Cleaner Production, 278*, 123962.

Perron, N. R., & Brumaghim, J. L. (2009). A Review of the Antioxidant Mechanisms of Polyphenol Compounds Related to Iron Binding. *Cell Biochemistry and Biophysics, 53*(2), 75-100.

PharmaExpert. (2015). Retrieved from http://www.pharmaexpert.ru/passonline/

Pirmohamed, T., Dowding, J. M., Singh, S., Wasserman, B., Heckert, E., Karakoti, A. S., . . . Self, W. T. (2010). Nanoceria Exhibit Redox State-Dependent Catalase Mimetic Activity. *Chemical communications, 46*(16), 2736-2738.

Pohlmann, A. R., Schaffazick, S. R., Creczynski-Pasa, T. B., & Guterres, S. S. (2010). Preparation of Drug-Loaded Polymeric Nanoparticles and Evaluation of the Antioxidant Activity against Lipid Peroxidation. In *Free Radicals and Antioxidant Protocols* (pp. 109-121): Springer.

Popescu, R. C., Andronescu, E., & Vasile, B. S. (2019). Recent Advances in Magnetite Nanoparticle Functionalization for Nanomedicine. *Nanomaterials, 9*(12), 1791.

Poroikov, V. V., Filimonov, D. A., Ihlenfeldt, W.-D., Gloriozova, T. A., Lagunin, A. A., Borodina, Y. V., . . . Nicklaus, M. C. (2003). Pass Biological Activity Spectrum Predictions in the Enhanced Open Nci Database Browser. *Journal of Chemical Information and Computer Sciences, 43*(1), 228-236.

Poudel, M., Pokharel, R., K.C, S., Awal, S. C., & Pradhananga, R. (2017). Biosynthesis of Silver Nanoparticles Using Ganoderma Lucidum and Assessment of Antioxidant and Antibacterial Activity. *International Journal of Applied Sciences and Biotechnology, 5*(4), 523-531.

Prakash, O., Singh, R. M., Mathur, S. C., & Singh, G. N. (2007). Quantification of Gallic Acid by Hplc and Antioxidant Activity of Amla Fruits. *Journal of Pharmacy Research, 6*(3), 161-162.

Prakash Patil, M., Seong, Y.-A., Kim, J.-O., Bae Seo, Y., & Kim, G.-D. (2021). Synthesis of Silver Nanoparticles Using Aqueous Extract of Cuscuta Japonica Seeds and Their Antibacterial and Antioxidant Activities. *Inorganic Chemistry Communications*, 109035.

Pratt, D. E., & Hudson, B. J. (1990). Natural Antioxidants Not Exploited Commercially. In *Food Antioxidants* (pp. 171-191): Springer.

Prevention, C. f. D. C. a. (2013). *Biggest Threats and Data*. Retrieved from https://www.cdc.gov/drugresistance/biggest-threats.html

Pu, H.-L., Chiang, W.-L., Maiti, B., Liao, Z.-X., Ho, Y.-C., Shim, M. S., . . . Sung, H.-W. (2014). Nanoparticles with Dual Responses to Oxidative Stress and Reduced Ph for Drug Release and Anti-Inflammatory Applications. *ACS Nano, 8*(2), 1213-1221.

Ragg, R., Tahir, M. N., & Tremel, W. (2016). Solids Go Bio: Inorganic Nanoparticles as Enzyme Mimics. *European Journal of Inorganic Chemistry, 2016*(13-14), 1906-1915.

Ragunathan, V., & K, C. (2021). Sequential Microwave-Ultrasound-Assisted Silver Nanoparticles Synthesis: A Swift Approach, Their Antioxidant, Antimicrobial, and in-Silico Studies. *Journal of Molecular Liquids*, 117954.

Raja, K., Balamurugan, V., Selvakumar, S., & Vasanth, K. (2021). Striga Angustifolia Mediated Synthesis of Silver Nanoparticles: Anti-Microbial, Antioxidant and

Anti-Proliferative Activity in Apoptotic P53 Signalling Pathway. *Journal of Drug Delivery Science and Technology*, 102945.

Rajeshkumar, S., Menon, S., Venkat Kumar, S., Tambuwala, M. M., Bakshi, H. A., Mehta, M., . . . Dua, K. (2019). Antibacterial and Antioxidant Potential of Biosynthesized Copper Nanoparticles Mediated through Cissus Arnotiana Plant Extract. *Journal of Photochemistry and Photobiology B: Biology, 197*, 111531.

Rajeshkumar, S., Nandhini, N. T., Manjunath, K., Sivaperumal, P., Krishna Prasad, G., Alotaibi, S. S., & Roopan, S. M. (2021). Environment Friendly Synthesis Copper Oxide Nanoparticles and Its Antioxidant, Antibacterial Activities Using Seaweed (Sargassum Longifolium) Extract. *Journal of Molecular Structure, 1242*, 130724.

Rajeshkumar, S., & Rinitha, G. (2018). Nanostructural Characterization of Antimicrobial and Antioxidant Copper Nanoparticles Synthesized Using Novel Persea Americana Seeds. *OpenNano, 3*, 18-27.

Ramya, S., Shanmugasundaram, T., & Balagurunathan, R. (2015). Biomedical Potential of Actinobacterially Synthesized Selenium Nanoparticles with Special Reference to Anti-Biofilm, Anti-Oxidant, Wound Healing, Cytotoxic and Anti-Viral Activities. *Journal of Trace Elements in Medicine and Biology, 32*, 30-39.

Ricordi, C., Garcia-Contreras, M., & Farnetti, S. (2015). Diet and Inflammation: Possible Effects on Immunity, Chronic Diseases, and Life Span. *Journal of the American College of Nutrition, 34*(sup1), 10-13.

Rizzi, V., Gubitosa, J., Fini, P., Nuzzo, S., Agostiano, A., & Cosma, P. (2021). Snail Slime-Based Gold Nanoparticles: An Interesting Potential Ingredient in Cosmetics as an Antioxidant, Sunscreen, and Tyrosinase Inhibitor. *Journal of Photochemistry and Photobiology B: Biology, 224*, 112309.

Ross, J. A., & Kasum, C. M. (2002). Dietary Flavonoids: Bioavailability, Metabolic Effects, and Safety. *Annual Review of Nutrition, 22*(1), 19-34.

Rudramurthy, G. R., Swamy, M. K., Sinniah, U. R., & Ghasemzadeh, A. (2016). Nanoparticles: Alternatives against Drug-Resistant Pathogenic Microbes. *Molecules, 21*(7), 836.

Sahiner, N., Sagbas, S., & Aktas, N. (2016). Preparation and Characterization of Monodisperse, Mesoporous Natural Poly(Tannic Acid)–Silica Nanoparticle Composites with Antioxidant Properties. *Microporous and Mesoporous Materials, 226*, 316-324.

Sahu, N., Soni, D., Chandrashekhar, B., Sarangi, B. K., Satpute, D., & Pandey, R. A. (2013). Synthesis and Characterization of Silver Nanoparticles Using Cynodon Dactylon Leaves and Assessment of Their Antibacterial Activity. *Bioprocess and Biosystems Engineering, 36*(7), 999-1004.

Saikia, J. P., Paul, S., Konwar, B. K., & Samdarshi, S. K. (2010). Nickel Oxide Nanoparticles: A Novel Antioxidant. *Colloids and Surfaces B: Biointerfaces, 78*(1), 146-148.

Saleh, N., Kim, H.-J., Phenrat, T., Matyjaszewski, K., Tilton, R. D., & Lowry, G. V. (2008). Ionic Strength and Composition Affect the Mobility of Surface-Modified Fe0 Nanoparticles in Water-Saturated Sand Columns. *Environmental Science & Technology, 42*(9), 3349-3355.

Salvador, M., Gutiérrez, G., Noriega, S., Moyano, A., Blanco-López, M. C., & Matos, M. (2021). Microemulsion Synthesis of Superparamagnetic Nanoparticles for Bioapplications. *International Journal of Molecular Sciences, 22*(1), 427.

Samuel, E. L., Marcano, D. C., Berka, V., Bitner, B. R., Wu, G., Potter, A., . . . Tsai, A.-L. (2015). Highly Efficient Conversion of Superoxide to Oxygen Using Hydrophilic Carbon Clusters. *Proceedings of the National Academy of Sciences, 112*(8), 2343-2348.

Samuel, E. L. G., Duong, M. T., Bitner, B. R., Marcano, D. C., Tour, J. M., & Kent, T. A. (2014). Hydrophilic Carbon Clusters as Therapeutic, High-Capacity Antioxidants. *Trends in Biotechnology, 32*(10), 501-505.

Sandhir, R., Yadav, A., Sunkaria, A., & Singhal, N. (2015). Nano-Antioxidants: An Emerging Strategy for Intervention against Neurodegenerative Conditions. *Neurochem. Int., 89*, 209-226.

Santajit, S., & Indrawattana, N. (2016). Mechanisms of Antimicrobial Resistance in Eskape Pathogens. *BioMed research international, 2016*.

Santiago-Rodríguez, L., Lafontaine, M. M., Castro, C., Méndez-Vega, J., Latorre-Esteves, M., Juan, E. J., . . . Rinaldi, C. (2013). Synthesis, Stability, Cellular Uptake, and Blood Circulation Time of Carboxymethyl-Inulin Coated Magnetic Nanoparticles. *Journal of Materials Chemistry B, 1*(22), 2807-2817.

Sarkar, A., & Sil, P. C. (2014). Iron Oxide Nanoparticles Mediated Cytotoxicity Via Pi3k/Akt Pathway: Role of Quercetin. *Food and Chemical Toxicology, 71*, 106-115.

Saygi, K. O., & Cacan, E. (2021). Antioxidant and Cytotoxic Activities of Silver Nanoparticles Synthesized Using Tilia Cordata Flowers Extract. *Materials Today Communications, 27*, 102316.

Schubert, D., Dargusch, R., Raitano, J., & Chan, S.-W. (2006). Cerium and Yttrium Oxide Nanoparticles Are Neuroprotective. *Biochemical and Biophysical Research Communications, 342*(1), 86-91.

Seals, D. R., Justice, J. N., & LaRocca, T. J. (2016). Physiological Geroscience: Targeting Function to Increase Healthspan and Achieve Optimal Longevity. *The Journal of physiology, 594*(8), 2001-2024.

Seo, D.-J., Lee, H.-B., Kim, I.-S., Kim, K.-Y., Park, R.-D., & Jung, W.-J. (2013). Antifungal Activity of Gallic Acid Purified from Terminalia Nigrovenulosa Bark against Fusarium Solani. *Microbial Pathogenesis, 56*, 8-15.

Shah, B. R., Zhang, C., Li, Y., & Li, B. (2016). Bioaccessibility and Antioxidant Activity of Curcumin after Encapsulated by Nano and Pickering Emulsion Based on

Chitosan-Tripolyphosphate Nanoparticles. *Food Research International, 89*, 399-407.

Shah, S. T., Yehye, W. A., Chowdhury, Z. Z., & Simarani, K. (2019). Magnetically Directed Antioxidant and Antimicrobial Agent: Synthesis and Surface Functionalization of Magnetite with Quercetin. *PeerJ, 7*, e7651.

Shah, S. T., Yehye, W. A., Saad, O., Simarani, K., Chowdhury, Z. Z., Alhadi, A. A., & Al-Ani, L. A. (2017). Surface Functionalization of Iron Oxide Nanoparticles with Gallic Acid as Potential Antioxidant and Antimicrobial Agents. *Nanomaterials, 7*(10), 306/301.

Shanmugasundaram, T., Radhakrishnan, M., Gopikrishnan, V., Pazhanimurugan, R., & Balagurunathan, R. (2013). A Study of the Bactericidal, Anti-Biofouling, Cytotoxic and Antioxidant Properties of Actinobacterially Synthesised Silver Nanoparticles. *Colloids and surfaces B: biointerfaces, 111*, 680-687.

Sharma, B., Purkayastha, D. D., Hazra, S., Thajamanbi, M., Bhattacharjee, C. R., Ghosh, N. N., & Rout, J. (2014). Biosynthesis of Fluorescent Gold Nanoparticles Using an Edible Freshwater Red Alga, Lemanea Fluviatilis (L.) C.Ag. And Antioxidant Activity of Biomatrix Loaded Nanoparticles. *Bioprocess and Biosystems Engineering, 37*(12), 2559-2565.

Sharpe, E., Andreescu, D., & Andreescu, S. (2011). Artificial Nanoparticle Antioxidants. *ACS Symposium Series, 1083*(Oxidative Stress), 235-253.

Shebanova, O. N., & Lazor, P. (2003). Raman Study of Magnetite (Fe3o4): Laser-Induced Thermal Effects and Oxidation. *Journal of Raman Spectroscopy, 34*(11), 845-852.

Shi, H., Noguchi, N., & Niki, E. (1999). Comparative Study on Dynamics of Antioxidative Action of A-Tocopheryl Hydroquinone, Ubiquinol, and A-Tocopherol against Lipid Peroxidation. *Free Radical Biology and Medicine, 27*(3), 334-346.

Shreema, K., Mathammal, R., Kalaiselvi, V., Vijayakumar, S., Selvakumar, K., & Senthil, K. (2021). Green Synthesis of Silver Doped Zinc Oxide Nanoparticles Using Fresh Leaf Extract Morinda Citrifoliaand Its Antioxidant Potential. *Materials Today: Proceedings, 47*, 2126-2131.

Silvestri, B., Vitiello, G., Luciani, G., Calcagno, V., Costantini, A., Gallo, M., . . . D'Errico, G. (2017). Probing the Eumelanin–Silica Interface in Chemically Engineered Bulk Hybrid Nanoparticles for Targeted Subcellular Antioxidant Protection. *Acs Applied Materials & Interfaces, 9*(43), 37615-37622.

Singh, K., Chopra, D. S., Singh, D., & Singh, N. (2020). Optimization and Ecofriendly Synthesis of Iron Oxide Nanoparticles as Potential Antioxidant. *Arabian Journal of Chemistry, 13*(12), 9034-9046.

Singh, N., Savanur, M. A., Srivastava, S., D'Silva, P., & Mugesh, G. (2017). A Redox Modulatory Mn3o4 Nanozyme with Multi-Enzyme Activity Provides Efficient Cytoprotection to Human Cells in a Parkinson's Disease Model. *Angewandte Chemie, 129*(45), 14455-14459.

Sivasankar, P., Seedevi, P., Poongodi, S., Sivakumar, M., Murugan, T., Sivakumar, L., . . . Balasubramanian, T. (2018). Characterization, Antimicrobial and Antioxidant Property of Exopolysaccharide Mediated Silver Nanoparticles Synthesized by Streptomyces Violaceus Mm72. *Carbohydrate Polymers, 181*, 752-759.

Slavin, Y. N., Asnis, J., Häfeli, U. O., & Bach, H. (2017). Metal Nanoparticles: Understanding the Mechanisms Behind Antibacterial Activity. *Journal of Nanobiotechnology, 15*, 65.

Sodipo, B. K., & Abdul Aziz, A. (2015). Non-Seeded Synthesis and Characterization of Superparamagnetic Iron Oxide Nanoparticles Incorporated into Silica Nanoparticles Via Ultrasound. *Ultrasonics Sonochemistry, 23*(0), 354-359.

Song, W., Muthana, M., Mukherjee, J., Falconer, R. J., Biggs, C. A., & Zhao, X. (2017). Magnetic-Silk Core–Shell Nanoparticles as Potential Carriers for Targeted Delivery of Curcumin into Human Breast Cancer Cells. *ACS Biomaterials Science & Engineering, 3*(6), 1027-1038.

Soppimath, K. S., Aminabhavi, T. M., Kulkarni, A. R., & Rudzinski, W. E. (2001). Biodegradable Polymeric Nanoparticles as Drug Delivery Devices. *Journal of Controlled Release, 70*(1), 1-20.

Sosa-Acosta, J. R., Silva, J., Fernández-Izquierdo, L., Díaz-Castañón, S., Ortiz, M., Zuaznabar-Gardona, J. C., & Díaz-García, A. (2018). Iron Oxide Nanoparticles (Ionps) with Potential Applications in Plasmid DNA Isolation. *Colloids and Surfaces A: Physicochemical and Engineering Aspects, 545*, 167-178.

Sotiriou, G. A., Blattmann, C. O., & Deligiannakis, Y. (2016a). Nanoantioxidant-Driven Plasmon Enhanced Proton-Coupled Electron Transfer. *Nanoscale, 8.2*, 796-803.

Sotiriou, G. A., Blattmann, C. O., & Deligiannakis, Y. (2016b). Nanoantioxidant-Driven Plasmon Enhanced Proton-Coupled Electron Transfer. *Nanoscale, 8*(2), 796-803.

Souto, E. B., Severino, P., Basso, R., & Santana, M. H. A. (2013). Encapsulation of Antioxidants in Gastrointestinal-Resistant Nanoparticulate Carriers. *Oxidative Stress and Nanotechnology*, 37-46.

Sowani, H., Mohite, P., Munot, H., Shouche, Y., Bapat, T., Kumar, A. R., . . . Zinjarde, S. (2016). Green Synthesis of Gold and Silver Nanoparticles by an Actinomycete Gordonia Amicalis Hs-11: Mechanistic Aspects and Biological Application. *Process Biochemistry, 51*(3), 374-383.

Srihasam, S., Thyagarajan, K., Korivi, M., Lebaka, V. R., & Mallem, S. P. R. (2020). Phytogenic Generation of Nio Nanoparticles Using Stevia Leaf Extract and Evaluation of Their in-Vitro Antioxidant and Antimicrobial Properties. *Biomolecules, 10*(1), 89.

Srinithya, B., Kumar, V. V., Vadivel, V., Pemaiah, B., Anthony, S. P., & Muthuraman, M. S. (2016). Synthesis of Biofunctionalized Agnps Using Medicinally Important Sida Cordifolia Leaf Extract for Enhanced Antioxidant and Anticancer Activities. *Materials Letters, 170*, 101-104.

Sriramulu, M., & Sumathi, S. (2017). Photocatalytic, Antioxidant, Antibacterial and Anti-Inflammatory Activity of Silver Nanoparticles Synthesised Using Forest and Edible Mushroom. *Advances in Natural Sciences: Nanoscience and Nanotechnology, 8*(4), 045012.

Sriranjani, R., Srinithya, B., Vellingiri, V., Brindha, P., Anthony, S. P., Sivasubramanian, A., & Muthuraman, M. S. (2016). Silver Nanoparticle Synthesis Using Clerodendrum Phlomidis Leaf Extract and Preliminary Investigation of Its Antioxidant and Anticancer Activities. *Journal of Molecular Liquids, 220*, 926-930.

Stanely Mainzen Prince, P., Kumar, M. R., & Selvakumari, C. J. (2010). Effects of Gallic Acid on Brain Lipid Peroxide and Lipid Metabolism in Streptozotocin-Induced Diabetic Wistar Rats. *Journal of Biochemical and Molecular Toxicology, 25*(2), 101-107.

Stankic, S., Suman, S., Haque, F., & Vidic, J. (2016). Pure and Multi Metal Oxide Nanoparticles: Synthesis, Antibacterial and Cytotoxic Properties. *Journal of Nanobiotechnology, 14*(1), 1-20.

Stepanchikova, A., Lagunin, A., Filimonov, D., & Poroikov, V. (2003). Prediction of Biological Activity Spectra for Substances: Evaluation on the Diverse Sets of Drug-Like Structures. *Current Medicinal Chemistry, 10*(3), 225-233.

Stepanchikova, A. V., Lagunin, A. A., Filimonov, D. A., & Poroikov, V. V. (2003). Prediction of Biological Activity Spectra for Substances: Evaluation on the Diverse Sets of Drug-Like Structures. *Current Medicinal Chemistry, 10*(3), 225-233.

Sun, D., Li, N., Zhang, W., Yang, E., Mou, Z., Zhao, Z., . . . Wang, W. (2015). Quercetin-Loaded Plga Nanoparticles: A Highly Effective Antibacterial Agent in Vitro and Anti-Infection Application in Vivo. *Journal of Nanoparticle Research, 18*(1), 1-21.

Sun, X., Zhang, H., Wang, J., Dong, M., Jia, P., Bu, T., . . . Wang, L. (2021). Sodium Alginate-Based Nanocomposite Films with Strong Antioxidant and Antibacterial Properties Enhanced by Polyphenol-Rich Kiwi Peel Extracts Bio-Reduced Silver Nanoparticles. *Food Packaging and Shelf Life, 29*, 100741.

Szekeres, M., Illés, E., Janko, C., Farkas, K., Tóth, I. Y., Nesztor, D., . . . Tombácz, E. (2015). Hemocompatibility and Biomedical Potential of Poly(Gallic Acid) Coated Iron Oxide Nanoparticles for Theranostic Use. *J. Nanomed. Nanotechnol. , 6*(252).

Szekeres, M., Toth, I. Y., Illes, E., Hajdu, A., Zupko, I., Farkas, K., . . . Tombacz, E. (2013). Chemical and Colloidal Stability of Carboxylated Core-Shell Magnetite Nanoparticles Designed for Biomedical Applications. *International Journal of Molecular Sciences, 14*(7), 14550-14574, 14525 pp.

Tancredi, P., Botasini, S., Moscoso-Londoño, O., Méndez, E., & Socolovsky, L. (2015). Polymer-Assisted Size Control of Water-Dispersible Iron Oxide Nanoparticles in

Range between 15 and 100 Nm. *Colloids and Surfaces A: Physicochemical and Engineering Aspects, 464*(0), 46-51.

Teerasong, S., Jinnarak, A., Chaneam, S., Wilairat, P., & Nacapricha, D. (2017). Poly (Vinyl Alcohol) Capped Silver Nanoparticles for Antioxidant Assay Based on Seed-Mediated Nanoparticle Growth. *Talanta, 170*, 193-198.

Thomas, R. G., Moon, M. J., Lee, H., Sasikala, A. R. K., Kim, C. S., Park, I.-K., & Jeong, Y. Y. (2015). Hyaluronic Acid Conjugated Superparamagnetic Iron Oxide Nanoparticle for Cancer Diagnosis and Hyperthermia Therapy. *Carbohydrate Polymers, 131*(0), 439-446.

Torres, S. K., Campos, V. L., León, C. G., Rodríguez-Llamazares, S. M., Rojas, S. M., González, M., . . . Mondaca, M. A. (2012). Biosynthesis of Selenium Nanoparticles by Pantoea Agglomerans and Their Antioxidant Activity. *Journal of Nanoparticle Research, 14*(11), 1236.

Torres, T., Roca, A., Morales, M., Ibarra, A., Marquina, C., Ibarra, M., & Goya, G. (2010). *Magnetic Properties and Energy Absorption of Cofe2o4 Nanoparticles for Magnetic Hyperthermia.* Paper presented at the Journal of Physics: Conference Series.

Tortosa, V., Pietropaolo, V., Brandi, V., Macari, G., Pasquadibisceglie, A., & Polticelli, F. (2020). Computational Methods for the Identification of Molecular Targets of Toxic Food Additives. Butylated Hydroxytoluene as a Case Study. *Molecules, 25*(9), 2229.

Toth, I. Y., Szekeres, M., Turcu, R., Saringer, S., Illes, E., Nesztor, D., & Tombacz, E. (2014). Mechanism of in Situ Surface Polymerization of Gallic Acid in an Environmental-Inspired Preparation of Carboxylated Core-Shell Magnetite Nanoparticles. *Langmuir, 30*(51), 15451-15461.

Tudisco, C., Cambria, M. T., Sinatra, F., Bertani, F., Alba, A., Giuffrida, A. E., . . . Condorelli, G. G. (2015). Multifunctional Magnetic Nanoparticles for Enhanced Intracellular Drug Transport. *J. Mater. Chem. B, 3*(20), 4134-4145.

Tułodziecka, A., & Szydłowska-Czerniak, A. (2016). Determination of Total Antioxidant Capacity of Rapeseed and Its by-Products by a Novel Cerium Oxide Nanoparticle-Based Spectrophotometric Method. *Food Analytical Methods, 9*(11), 3053-3062.

Tuzun, B. S., Fafal, T., Tastan, P., Kivcak, B., Yelken, B. O., Kayabasi, C., . . . Gunduz, C. (2020). Structural Characterization, Antioxidant and Cytotoxic Effects of Iron Nanoparticles Synthesized Using Asphodelus Aestivus Brot. Aqueous Extract. *Green Processing and Synthesis, 9*(1), 153-163.

Urso, M. L., & Clarkson, P. M. (2003). Oxidative Stress, Exercise, and Antioxidant Supplementation. *Toxicol., 189*(1-2), 41-54.

Valentao, P., Fernandes, E., Carvalho, F., Andrade, P. B., Seabra, R. M., & de Lourdes Bastos, M. (2002). Antioxidant Activity of Hypericum Androsaemum Infusion: Scavenging Activity against Superoxide Radical, Hydroxyl Radical and Hypochlorous Acid. *Biological and Pharmaceutical Bulletin, 25*(10), 1320-1323.

Valgimigli, L., Baschieri, A., & Amorati, R. (2018). Antioxidant Activity of Nanomaterials. *Journal of Materials Chemistry B, 6*(14), 2036-2051.

Varadan, V. K., Chen, L., & Xie, J. (2008). Biomedical Applications of Magnetic Nanoparticles. *Nanomedicine: design and applications of magnetic nanomaterials, nanosensors and nanosystems*, 129-173.

Varghese, B. A., Nair, R. V. R., Jude, S., Varma, K., Amalraj, A., & Kuttappan, S. (2021). Green Synthesis of Gold Nanoparticles Using Kaempferia Parviflora Rhizome Extract and Their Characterization and Application as an Antimicrobial, Antioxidant and Catalytic Degradation Agent. *Journal of the Taiwan Institute of Chemical Engineers, 126*, 166-172.

Varkey, A. (2010). Antibacterial Properties of Some Metals and Alloys in Combating Coliforms in Contaminated Water. *Scientific Research and Essays, 5*(24), 3834-3839.

Veeraapandian, S., Sawant, S. N., & Doble, M. (2012). Antibacterial and Antioxidant Activity of Protein Capped Silver and Gold Nanoparticles Synthesized with Escherichia Coli. *Journal of Biomedical Nanotechnology, 8*(1), 140-148.

Venkatesan, J., Kim, S.-K., & Shim, M. S. (2016). Antimicrobial, Antioxidant, and Anticancer Activities of Biosynthesized Silver Nanoparticles Using Marine Algae Ecklonia Cava. *Nanomaterials, 6*(12), 235.

Venugopalan, R., Pitchai, S., Devarayan, K., & Swaminathan, V. C. (2020). Biogenic Synthesis of Copper Nanoparticles Using Borreria Hispida (Linn.) Extract and Its Antioxidant Activity. *Materials Today: Proceedings, 33*, 4023-4025.

Verma, A. K. (2014). Anti-Oxidant Activities of Biopolymeric Nanoparticles: Boon or Bane! *Journal of Pharmacy Research Vol, 8*(7), 871-876.

Verma, N. K., Crosbie-Staunton, K., Satti, A., Gallagher, S., Ryan, K. B., Doody, T., . . . Gun'ko, Y. K. (2013). Magnetic Core-Shell Nanoparticles for Drug Delivery by Nebulization. *Journal of Nanobiotechnology, 11*.

Vernekar, A. A., Sinha, D., Srivastava, S., Paramasivam, P. U., D'Silva, P., & Mugesh, G. (2014). An Antioxidant Nanozyme That Uncovers the Cytoprotective Potential of Vanadia Nanowires. *Nature Communications, 5*(1), 1-13.

Viglianisi, C., Di Pilla, V., Menichetti, S., Rotello, V. M., Candiani, G., Malloggi, C., & Amorati, R. (2014). Linking an A-Tocopherol Derivative to Cobalt (0) Nanomagnets: Magnetically Responsive Antioxidants with Superior Radical Trapping Activity and Reduced Cytotoxicity. *Chemistry–A European Journal, 20*(23), 6857-6860.

Vila, A., Sánchez, A., Tobío, M., Calvo, P., & Alonso, M. J. (2002). Design of Biodegradable Particles for Protein Delivery. *Journal of Controlled Release, 78*(1), 15-24.

Vilas, V., Philip, D., & Mathew, J. (2016). Essential Oil Mediated Synthesis of Silver Nanocrystals for Environmental, Anti-Microbial and Antioxidant Applications. *Materials Science and Engineering: C, 61*, 429-436.

Vos, T., Abajobir, A. A., Abate, K. H., Abbafati, C., Abbas, K. M., Abd-Allah, F., . . . Abera, S. F. (2017). Global, Regional, and National Incidence, Prevalence, and Years Lived with Disability for 328 Diseases and Injuries for 195 Countries, 1990–2016: A Systematic Analysis for the Global Burden of Disease Study 2016. *The Lancet, 390*(10100), 1211-1259.

Wang, K., Wu, Y., Li, H., Li, M., Zhang, D., Feng, H., & Fan, H. (2013). Dual-Functionalization Based on Combination of Quercetin Compound and Rare Earth Nanoparticle. *Journal of Rare Earths, 31*(7), 709-714.

Wang, X., Tilley, R. D., & Watkins, J. J. (2014). Simple Ligand Exchange Reactions Enabling Excellent Dispersibility and Stability of Magnetic Nanoparticles in Polar Organic, Aromatic, and Protic Solvents. *Langmuir, 30*(6), 1514-1521.

Wang, Y., Ng, Y. W., Chen, Y., Shuter, B., Yi, J., Ding, J., . . . Feng, S.-S. (2008). Formulation of Superparamagnetic Iron Oxides by Nanoparticles of Biodegradable Polymers for Magnetic Resonance Imaging. *Advanced Functional Materials, 18*(2), 308-318.

Wason, M. S., Colon, J., Das, S., Seal, S., Turkson, J., Zhao, J., & Baker, C. H. (2013). Sensitization of Pancreatic Cancer Cells to Radiation by Cerium Oxide Nanoparticle-Induced Ros Production. *Nanomedicine: Nanotechnology, Biology and Medicine, 9*(4), 558-569.

Watanabe, A., Kajita, M., Kim, J., Kanayama, A., Takahashi, K., Mashino, T., & Miyamoto, Y. (2009). In Vitro Free Radical Scavenging Activity of Platinum Nanoparticles. *Nanotechnology, 20*(45), 455105.

Watts, P., Fearon, P., Hsu, W., Billingham, N., Kroto, H., & Walton, D. (2003). Carbon Nanotubes as Polymer Antioxidants. *Journal of Materials Chemistry, 13*(3), 491-495.

Wei, H., & Wang, E. (2013). Nanomaterials with Enzyme-Like Characteristics (Nanozymes): Next-Generation Artificial Enzymes. *Chemical Society Reviews, 42*(14), 6060-6093.

Williams, D. J., Edwards, D., Hamernig, I., Jian, L., James, A. P., Johnson, S. K., & Tapsell, L. C. (2013). Vegetables Containing Phytochemicals with Potential Anti-Obesity Properties: A Review. *Food Research International, 52*(1), 323-333.

Wu, W., Jiang, C. Z., & Roy, V. A. (2016). Designed Synthesis and Surface Engineering Strategies of Magnetic Iron Oxide Nanoparticles for Biomedical Applications. *Nanoscale, 8*(47), 19421-19474.

Xi, Y., Hu, C., Gao, P., Yang, R., He, X., Wang, X., & Wan, B. (2010). Morphology and Phase Selective Synthesis of Cuxo (X=1, 2) Nanostructures and Their Catalytic Degradation Activity. *Materials Science and Engineering: B, 166*(1), 113-117.

Xie, Y., He, Y., Irwin, P. L., Jin, T., & Shi, X. (2011). Antibacterial Activity and Mechanism of Action of Zinc Oxide Nanoparticles against Campylobacter Jejuni. *Applied and environmental microbiology, 77*(7), 2325-2331.

Yabluchanskiy, A., Ungvari, Z., Csiszar, A., & Tarantini, S. (2018). Advances and Challenges in Geroscience Research: An Update. *Physiology international, 105*(4), 298-308.

Yang, L., Cao, Z., Sajja, H. K., Mao, H., Wang, L., Geng, H., . . . Wang, Y. A. (2008). Development of Receptor Targeted Magnetic Iron Oxide Nanoparticles for Efficient Drug Delivery and Tumor Imaging. *Journal of Biomedical Nanotechnology, 4*(4), 439-449.

Yehye, W. A., Rahman, N. A., Ariffin, A., Abd Hamid, S. B., Alhadi, A. A., Kadir, F. A., & Yaeghoobi, M. (2015). Understanding the Chemistry Behind the Antioxidant Activities Of butylated Hydroxytoluene (Bht): A Review. *European Journal of Medicinal Chemistry, 101*, 295-312.

Yehye, W. A., Rahman, N. A., Ariffin, A., Hamid, S. B. A., Alhadi, A. A., Kadir, F. A., & Yaeghoobi, M. (2015). Understanding the Chemistry Behind the Antioxidant Activities of Butylated Hydroxytoluene (Bht): A Review. *European Journal of Medicinal Chemistry, 101*, 295-312.

Young, I. S., & Woodside, J. V. (2001). Antioxidants in Health and Disease. *Journal of Clinical Pathology, 54*(3), 176.

Yu, J., Zhang, W., Li, Y., Wang, G., Yang, L., Jin, J., . . . Huang, M. (2014). Synthesis, Characterization, Antimicrobial Activity and Mechanism of a Novel Hydroxyapatite Whisker/Nano Zinc Oxide Biomaterial. *Biomedical Materials, 10*(1), 015001.

Zahran, W. E., Elsonbaty, S. M., & Moawed, F. S. (2017). Selenium Nanoparticles with Low-Level Ionizing Radiation Exposure Ameliorate Nicotine-Induced Inflammatory Impairment in Rat Kidney. *Environmental Science and Pollution Research, 24*(24), 19980-19989.

Zangeneh, M. M., Ghaneialvar, H., Akbaribazm, M., Ghanimatdan, M., Abbasi, N., Goorani, S., . . . Zangeneh, A. (2019). Novel Synthesis of Falcaria Vulgaris Leaf Extract Conjugated Copper Nanoparticles with Potent Cytotoxicity, Antioxidant, Antifungal, Antibacterial, and Cutaneous Wound Healing Activities under in Vitro and in Vivo Condition. *Journal of Photochemistry and Photobiology B: Biology, 197*, 111556.

Zhang, H., & Forman, H. J. (2017). 4-Hydroxynonenal-Mediated Signaling and Aging. *Free Radical Biology and Medicine, 111*, 219-225.

Zhu, J., Wang, J., Wang, X., Zhu, J., Yang, Y., Tian, J., . . . Gu, H. (2015). Facile Synthesis of Magnetic Core-Shell Nanocomposites for Mri and Ct Bimodal Imaging. *J. Mater. Chem. B, 3*(34), 6905-6910.

Zoete, V., Daina, A., Bovigny, C., & Michielin, O. (2016). Swisssimilarity: A Web Tool for Low to Ultra High Throughput Ligand-Based Virtual Screening. *Journal of Chemical Information and Modeling, 56*(8), 1399-1404.